Lawrence Berkeley National Laboratory
Recent Work

Title

DETERMINATION OF SPECIFIC SITE OCCUPATIONS IN SINGLE CRYSTALS BY CHANNELLING ENHANCED MICROANALYSIS: PRINCIPLES AND APPLICATIONS

Permalink

https://escholarship.org/uc/item/9mw2n8p8

Author

Krishnan, K.M.

Publication Date

1984-02-01

eScholarship.org Powered by the California Digital Library
University of California

UC-25
LBL-17282

Lawrence Berkeley Laboratory
UNIVERSITY OF CALIFORNIA

Materials & Molecular Research Division

DETERMINATION OF SPECIFIC SITE OCCUPATIONS IN SINGLE CRYSTALS BY CHANNELLING ENHANCED MICROANALYSIS: PRINCIPLES AND APPLICATIONS

K.M. Krishnan
(Ph.D. Thesis)

RECEIVED
LAWRENCE
BERKELEY LABORATORY
MAR 12 1984
LIBRARY AND
DOCUMENTS SECTION

February 1984

For Reference
Not to be taken from this room

Prepared for the U.S. Department of Energy under Contract DE-AC03-76SF00098

LBL-17282

DISCLAIMER

This document was prepared as an account of work sponsored by the United States Government. While this document is believed to contain correct information, neither the United States Government nor any agency thereof, nor the Regents of the University of California, nor any of their employees, makes any warranty, express or implied, or assumes any legal responsibility for the accuracy, completeness, or usefulness of any information, apparatus, product, or process disclosed, or represents that its use would not infringe privately owned rights. Reference herein to any specific commercial product, process, or service by its trade name, trademark, manufacturer, or otherwise, does not necessarily constitute or imply its endorsement, recommendation, or favoring by the United States Government or any agency thereof, or the Regents of the University of California. The views and opinions of authors expressed herein do not necessarily state or reflect those of the United States Government or any agency thereof or the Regents of the University of California.

LBL-17282

DETERMINATION OF SPECIFIC SITE OCCUPATIONS IN SINGLE CRYSTALS BY CHANNELLING ENHANCED MICROANALYSIS: PRINCIPLES AND APPLICATIONS

Kannan M. Krishnan
Ph.D. Thesis

Lawrence Berkeley Laboratory
University of California
Berkeley, California 94720

February 1984

This work was supported by the Director, Office of Energy Research, Office of Basic Energy Sciences, Division of the U.S. Department of Energy under Contract Number DE-AC03-76SF00098.

DETERMINATION OF SPECIFIC SITE OCCUPATIONS IN SINGLE CRYSTALS BY CHANNELLING ENHANCED MICROANALYSIS : PRINCIPLES AND APPLICATIONS

Kannan M. Krishnan

Ph. D.

Materials Science & Mineral Engineering Department

Gareth Thomas

Professor Gareth Thomas

Chairman of Committee

ABSTRACT

A technique that enhances the potential of energy dispersive x-ray microanalysis in materials characterization called "Channelling Enhanced Microanalysis" has been developed. This technique, based on the orientation dependence of electron-induced characteristic x-ray emissions was then used to determine preferential site occupations of elemental additions in magnetic materials.

For the application to a general crystal, a theoretical prediction of the characteristic x-ray production as a function of incident beam orientation is required, as the specific-site sensitive orientations cannot be determined by an inspection of

the crystal structure. Hence, a reciprocal space formulation applying first order perturbation to the inelastic scattered state and an alternative real space formulation considering flux loss from the incident beam have been derived for the characteristic x-ray production in thin crystals. Applying the latter theory, a $\bar{g}=1\bar{2}1$ systematic orientation was predicted to be the particular orientation that is specific-site sensitive for thin film garnets. Experimentally observed data were then refined, using a constrained least squares analysis to give probabilities for the occupations of rare-earth additions in the different crystallographic sites. Thus, it was shown that in these compounds the preference for rare-earth additions is predominantly octahedral occupation with a probability $\geq$ 95%.

For layered crystals the appropriate orientations can be determined by inspection *. However, the analysis requires an a priori knowledge of the distribution of some reference elements along with some implicit assumptions about the crystal structure. A general formalism, with the underlying idea that additional relationships can be generated by performing these experiments at an appropriate number of orientations depending on the stoichiometry of the original compound and which also overcomes some of the limitations of the above analysis was developed. Based on this formalism and by monitoring the characteristic x-ray spectrum as a function of incident beam orientation, it was

---

* J.C.H. Spence & J. Tafto, J. Microscopy, 130, 147 (1983)

determined that 88.5% of the Mn atoms and 85.1% of the Fe atoms occupy sites in the mixed planes in the $Sm_2(Co,TM)_{17}$ compounds.

In general, distributions of elements in specific crystallographic sites for levels of doping equivalent to 10^{-19} atoms/cm^3 with an accuracy of $\pm$ 2-5% can be determined by these techniques.

Finally, calculations of the effect of accleration voltage as an independent parameter on this orientation dependence for $MgAl_2O_4$, predict a non-uniform voltage dependence characterized by an "inversion voltage" with characteristics different from the conventional critical voltage effect.

***

This work was supported by the Director, Office of Energy Research, Office of Basic Energy Sciences, Division of the U. S. Department of Energy under contract number DE-AC03-76SF00098.

TABLE OF CONTENTS

CHAPTER I	INTRODUCTION	1
I.1	Introduction and literature review	2
I.2	Electron microscopy and microanalysis	5
2.1	Transmission electron microscopy	5
2.2	Analytical electron microscopy	7
2.2.1	Conventional x-ray microanalysis	7
2.2.2	Energy dispersive x-ray spectrometry	9
2.2.3	Channelling enhanced microanalysis	11
I.3	Motivation for specific site occupation determinations	13
3.1	$(Y,RE)_3Fe_5O_{12}$ thin films	13
3.2	$Sm_2(Co,TM)_{17}$ compounds	15
I.4	The technique: Physical description	17
I.5	A synopsis of the dissertation	19
CHAPTER II	THEORY OF ELECTRON-INDUCED CHARACTERISTIC X-RAY EMISSIONS	23
II.1	Introduction/Overview	25
II.2	Conventional theory of transmission electron diffraction	27
2.1	Bloch wave methods	27
2.2	Two beam approximation	33

II.3 General theory of the inelastic scattering of fast electrons in crystalline solids.....36

II.4 Characteristic x-ray production in thin crystals....45

II.5 Details of calculations.....53

II.6 Crystallography.....55

6.1 Garnets.....55

6.2 Spinels.....63

II.7 Results of the characteristic x-ray production calculations at 100 KV.....67

II.8 General discussion.....71

II.9 Effect of the acceleration voltage on the orientation dependence of electron-induced characteristic x-ray emissions.....75

9.1 Introduction.....75

9.2 Results of the calculations: "The Inversion Voltage" effect.....76

9.3 Discussions.....81

CHAPTER III EXPERIMENTAL DETERMINATION OF THE SPECIFIC SITE OCCUPATION OF RARE-EARTH ADDITIONS IN THIN OXIDE FILMS BY THE ORIENTATION DEPENDENCE OF CHARACTERISTIC X-RAY EMISSIONS.....85

III.1 Introduction.....86

III.2 Experimental.....87

2.1 Specimen preparation.....87

2.2 Analytical & transmission electron microscopy.....88

III.3 Results.....91

III.4 Analysis.....93

4.1 Least squares refinement.....93

4.2 Error analysis.....96

III.5 Discussion.....96

CHAPTER IV A GENERALIZATION OF ATOM LOCATION BY CHANNELLING ENHANCED MICROANALYSIS.....98

IV.1 Introduction.....99

IV.2 Formulation of the problem and analysis.....100

IV.3 Results and discussions.....107

CHAPTER V SITE OCCUPATION OF TERNARY ELEMENTS IN $Sm_2(Co,TM)_{17}$ COMPOUNDS.....112

V.1 Introduction.....113

V.2 Crystallography of RE_2Co_{17} compounds.....114

V.3 Analysis.....119

V.4 Experimental details.....123

V.5 Results and discussions.....124

CHAPTER VI CONCLUDING DISCUSSION AND SUMMARY.....127

VI.1 Assumptions made in the formulations.....128

VI.2 Resolution that can be achieved.....131

VI.3 Limitations.....132

VI.4 Impact of channelling on analytical & transmission electron microscopy.....134

VI.5 Orientation dependence in electron energy loss spectroscopy.....136

VI.6 Possible extensions in channelling enhanced microanalysis.....138

VI.7 Summary.....141

APPENDIX 1 UNIAXIAL ANISOTROPY IN GARNETS.....147

REFERENCES 152

ACKNOWLEDGEMENTS 159

EPILOGUE 162

CHAPTER I

INTRODUCTION

I.1 Introduction and literature review

I.2 Electron microscopy and microanalysis

2.1 Transmission electron microscopy

2.2 Analytical electron microscopy

2.2.1 Conventional microanalysis

2.2.2 Energy dispersive x-ray spectrometry

2.2.3 Channelling enhanced microanalysis

I.3 Motivation for specific site occupation determinations

3.1 $(Y\ RE)_3Fe_5O_{12}$ thin films

3.2 $Sm_2(Co\ TM)_{17}$ compounds

I.4 The technique: Physical description

I.5 A synopsis of the dissertation

I.1 Introduction and literature review

The anomalous transmission of x-rays, incident on a single crystal oriented close to the Bragg position was first observed by Borrman (1941) and later interpretted by von Laue(1949) in terms of the standing wave patterns set up in the crystal by the incident x-ray beam as it propagates along specific crystal directions. It was argued that the intensity modulation of the primary beam within the crystal is such that it is a maximum on the crystallographic sites for certain incident beam orientations. For these orientations an accompanied increase in anomalous absorption and an enhancement of the secondary emissions arising from highly localized scattering events will result. For other orientations, the intensities are a minimum on these crystallographic sites with a concomitant reduction in absorption and emission products. Similar anomalous transmission effects of the primary beam have been observed in electron diffraction patterns (Honjo, 1953; Honjo & Mihama, 1954) and also used in the interpretation of electron micrographs (Hashimoto, Howie & Whelan, 1960; Hashimoto, Howie & Whelan, 1962).

The primary absorption process for x-rays is the photo-electric effect. The inelastic scattering processes that lead to the attenuation of an electron beam in single crystals are quite different and a proper understanding of the same would involve a

more detailed theory and some calculations (Heidenreich, 1962; Humphreys & Hirsch, 1968; Radi, 1969). Even though the related process of inner shell ionization does not lead to any significant attenuation in electron diffraction, the resultant electron-induced characteristic x-ray emissions are convenient, as they can be used to monitor these attenuations. Hirsch, Howie & Whelan (1962) suggested that these electron-induced characteristic x-ray emissions might also be dependent on the orientation of the incident beam with respect to the crystal, i.e. the "Borrman effect" might apply for the emission product. This was indeed observed by Duncumb (1962). However, the first experimental observation of the orientation dependence of the emission product was made by Knowles (1956) who used an incident neutron beam to excite x-ray emissions. The electron-induced characteristic x-ray emissions were further investigated by Hall (1966) who confirmed that the "Borrman effect" was only of importance for thin crystals ($t \leq 2000$ A°). Finally, Cherns, Howie & Jacobs (1973) have developed a theoretical formalism to describe this phenomenon and have discussed its ramification on conventional x-ray microanalysis in great detail.

Cowley (1964) made the first suggestion that it should be possible to derive structural information from measurements of x-ray fluoroscence radiation given by atoms within a diffracting crystal. The positions of solute atoms in a crystalline lattice were experimentally determined by the nature of their x-ray fluoroscence during a diffraction process by Batterman (1969).

The structural information in diffuse inelastic scattering of electrons has been examined theoretically by Gjonnes & Hoier (1971). More recently, an experimental technique for locating atom positions called " Atom Location by Channelling Enhanced Microanalysis (ALCHEMI) " has been developed by Spence & Tafto (1983) and applied to a number of simple and ideal crystal structures (Tafto, 1982; Tafto & Lilienthal, 1982; Tafto & Spence, 1982a; Tafto & Spence, 1982b). This dissertation complements the work of Tafto et al. by putting it on a firm theoretical foundation and extending it to more complicated crystal structures of technological importance.

In other words, a detailed technique to determine specific site occupations in crystalline solids based on the orientation dependence of characteristic x-ray emissions has been developed and applied to the characterization of magnetic materials, where the magnetic anisotropy, be it magneto-crystalline (e.g. $Sm_2(Co\ TM)_{17}$ compounds; TM - Transition Metal) or growth induced uniaxial (e.g. $(Y\ RE)_3Fe_5O_{12}$ thin films; RE - Rare Earth), is attributed to the preferential occupation of certain elemental additions at specific sites in the crystal structure. This dissertation describes this work and in the process endeavours to (a) emphasize and develop the theoretical formulations that constitute the basis of these techniques (b) point out the appropriate assumptions and limitations (c) demonstrate its versatility in solving practical problems and (d) discuss its potential.

Because of the interdisciplinary nature of this work it would be impossible to review all the relevant background to the satisfaction of every potential reader. Hence, only those materials that have a direct bearing on the larger content of the thesis are presented in this chapter. If additional information is required, the reader is urged to consult standard references in Diffraction physics (Cowley, 1975), Transmission electron microscopy (Thomas & Goringe, 1979; Hirsch, Howie, Nicholson, Pashley & Whelan, 1965), Analytical electron microscopy (Hren, Goldstein & Joy, 1979), Solid state physics (Kittel, 1982; Ziman, 1972), Crystallography (Wykoff, 1960) and Magnetism and magnetic materials (Standley, 1972; Eschenfelder, 1980; Paoletti, 1978; Chikazumi, 1964; Kalvius & Tebble, 1979). However, in this chapter an attempt is made to avoid being partial to any particular scientific parlance and restrict the presentation to the descriptive.

I.2 Electron microscopy and microanalysis

I.2.1 Transmission electron microscopy

The principal products of the scattering of a fast electron by a crystalline solid in the form of a thin film, as observed in a conventional transmission electrom microscope are shown in figure 1.1. The elastic or Bragg scattered electron

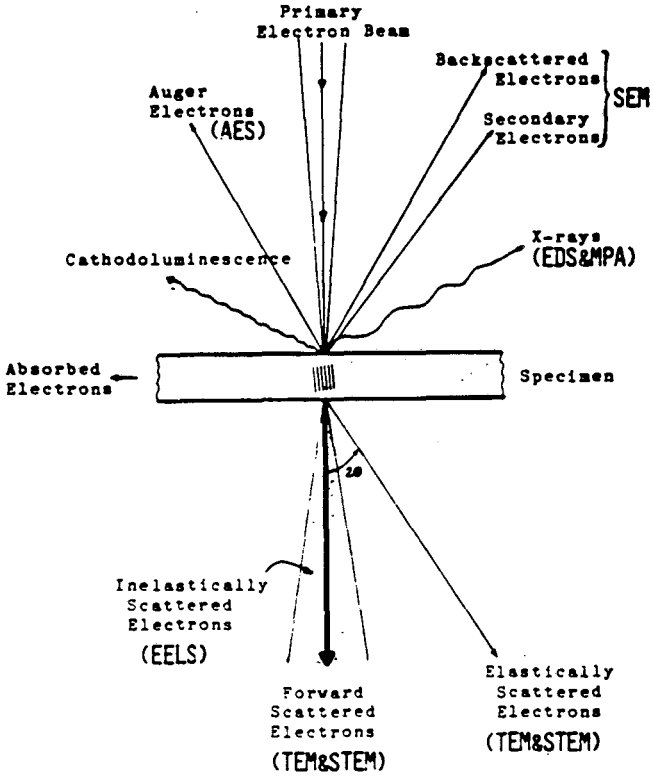

Figure 1.1 Possible products of the interaction of an electron beam with a crystalline specimen.
The electrons that are elastically or inelastically scattered while passing through the sample can be used to form an image of the internal structure of the material. The secondary or backscattered electrons can be collected and displayed to yield information about the topography, composition and crystallography of the sample surface. The crystal structure and the orientations of the material can be determined from the diffraction patterns produced by the transmitted electrons or from the electron channelling patterns produced by the back scattered electrons. The electron-induced characteristic x-ray emissions can be analysed by an energy dispersive detector to give a quantitative microanalysis of the irradiated area. The energy losses in the transmitted beam which correspond to inner-shell ionizations can be detected by a magnetic sector spectrometer and used to identify the elements present. This analytical technique is particularly useful for elements of low atomic number.

XBL 8312-4329

beams are focussed by the objective lens to form a diffraction pattern at its back focal plane. In addition to spots arising from the above, a single crystal electron diffraction pattern also contains a complex pattern of lines due to the subsequent elastic scattering of electrons that have suffered inelastic collisions involving small energy losses. These lines are called Kikuchi (1928) lines. The precise orientation of the incident electron beam with respect to the sample can be readily obtained from the relationship of the Kikuchi pattern to the spot pattern (von Heimendall, Bell & Thomas, 1964) and was one of the two methods used throughout this work.

I.2.2 Analytical electron microscopy

I.2.2.1 Conventional x-ray microanalysis

The energy of the incident fast electrons is significantly greater than the binding energy of the inner atomic shells of the material. Hence some of the incident electrons, in the process of being inelastically scattered, eject an inner shell electron (Fig. 1.2). As the excited atom decays to its ground state it may emit either an x-ray photon or an Auger electron, each having an energy characteristic of the atom (Fig. 1.2). Not all the ionization events result in characteristic x-ray production. Those that do, are shown in the schematic x-ray energy level diagram (Fig. 1.3). The nomenclature used to describe the resultant series of x-ray lines and their

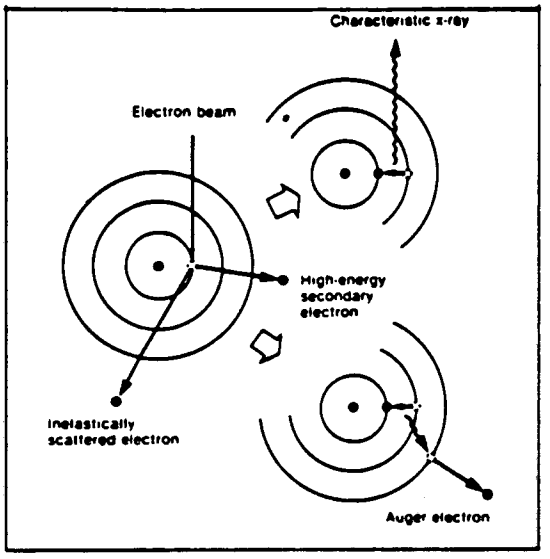

Figure 1.2 An incident fast electron ejects an atomic electron thereby ionizing it and creating a vacancy in the K-shell. An outer L-electron falls into the K-shell leaving a vacancy behind in the L-shell.Either an x-ray photon is created by this transition (characteristic x-ray emission) or an outer electron is ejected (Auger electron).

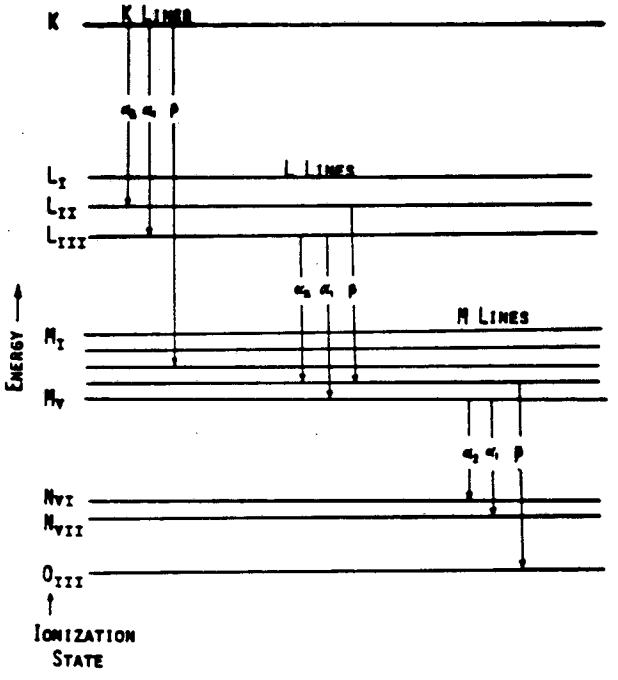

Figure 1.3 Schematic x-ray energy level diagram. The arrows represent transitions of an ionized atom which lead to characteristic x-ray emissions.There is 1 K state,3 L states, 5 M states, etc.

XBL 8312-4330

corresponding ionization states are also shown in the same figure.

The average number of ionizations per incident beam electron with a fixed energy, of a particular element, is amongst other things proportional to the concentration of that particular element in the sample (Castaing, 1951). By monitoring the intensities of any one of the characteristic x-ray lines for the element(s) of interest and resorting to well established methods of quantitative analysis (Hren, Goldstein & Joy, 1979) one can obtain an elemental chemical analysis of the sample. This, we term conventional x-ray microanalysis.

I.2.2.2 Energy dispersive x-ray spectrometry (EDXS)

The acquisition of a typical spectrum is accomplished by an energy dispersive x-ray spectrometer (see Heinrich, Newbury, Myklebust & Fiori, 1981 or Jenkins, Gould & Gedcke, 1981 for a general review of EDXS) which comprises of a lithium drifted silicon Si(Li) detector and its associated electronics. This system is a solid state analog of a conventional proportional counter system but has a far superior energy resolution. In general, the energy dispersive mode of analysis is preferable when high effectiveness of the detector system is more important than high resolution, i.e. the number of photons per primary electron can be 100 to 1000 times stronger in energy dispersive detection. This is because the solid angle subtended by a Si(Li) detector is much larger than that subtended by a

wavelength dispersive x-ray crystal spectrometer and hence the angular collection efficiency is greater. To minimize the electronic noise added to the signal during the process of charge to voltage conversion, the Si(Li) detector along with some parts of the preamplifier is mounted in a light tight vacuum cryostat and operated at liquid nitrogen temperatures (77 K). The x-rays enter the cryostat through a thin beryllium window (8-13 μm thick). Further, the detector typically contains a 0.1 μm thick silicon dead layer, i.e. a region where the electrical resistivity is too low to allow full collection of the electron-hole pairs released by the absorption of an x-ray photon. Hence, low energy x-rays are absorbed in the dead layer and go undetected. Because of these two reasons (Be window and the Si dead layer), energy dispersive x-ray microanalysis (EDXM) is restricted to elements with atomic numbers greater than 11, unless, windowless or thin window detectors are used. For lighter elements, the alternative technique of electron energy-loss spectroscopy (EELS) is generally employed. The physics of EELS is somewhat different from EDXM as you only have a primary ionisation, but some of what is derived and discussed in this dissertation for EDXM is in principle applicable to EELS also. A brief overview of the orientation dependence in EELS is presented in the concluding discussion (Chapter VI).

I.2.2.3 Channelling enhanced microanalysis (CEM)

The characteristic x-ray spectrum produced by the interaction of the fast electron with a crystalline specimen shows significant variation with the orientation of the incident beam. This is best illustrated in figure 1.4. One usually uses a fixed electron source, a fixed detector whose position with respect to the specimen is specified by the take-off angle (ψ) and a thin foil specimen, whose orientation (θ) can be changed precisely by the use of a goniometer, such that the orientation of the incident beam is well determined (Fig. 1.4a). One observes that the characteristic x-ray spectra change with incident beam orientations; there is a change in the intensities of individual peaks but the peak positions themselves do not change as they correspond to fixed atomic transitions. Hence, under certain favourable orientations, the spectra arising from beams channelled between specific planes when compared with those arising from beams blocked by the same set of planes can be used to obtain a chemical microanalysis of those planes. This we term channelling enhanced microanalysis (CEM). For certain crystallographic projections these specific planes can be shown to have a preponderance of a specific site(s) and then this type of microanalysis can be shown to be specific site(s) sensitive.

This is a very rudimentary explanation of this phenomenon. In order to be practically applicable and be developed into a meaningful technique, the following questions have to be asked :

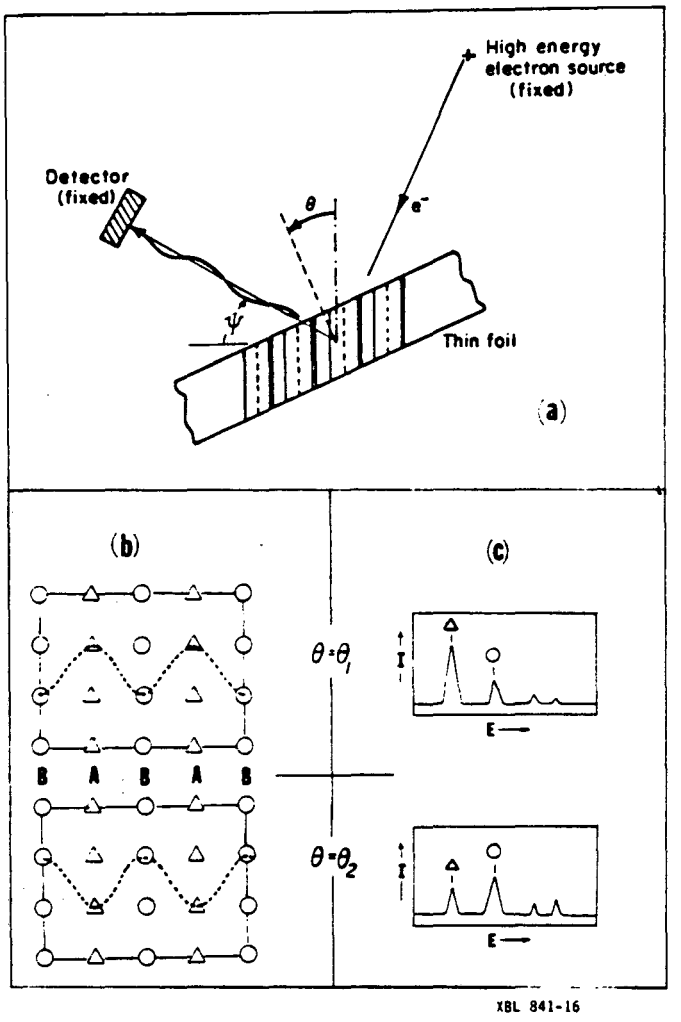

Figure 1.4 Physical principles of channelling enhanced microanalysis.
(a) The experimental arrangement.
(b) The projected crystal structure with the standing wave pattern of the primary beam set up as a result of the dynamical scattering.For a systematic orientation the wave field is two dimensional (i.e. constant in a direction normal to the page). The modulation of the standing wave on specific crystallographic planes is then a function of the incident beam orientation.
(c) The characteristic x-ray emissions are a function of these modulations of the primary beam. For the favourable orientation the Bloch waves are maximized on the A-planes with a concomitant increase for the elements occupying the site △. For the other favourable orientation, the maximization is on the B-planes with a corresponding increase for the elements occupying the sites ○. By monitoring these orientation dependent emission products and resorting to the analyses to be developed in this dissertation, specific site occupations can be quantitatively determined.

(1) How does the characteristic x-ray spectra change with the orientation of the incident electron beam ?

(2) How are the favourable orientations to be determined in the case of crystals with a complicated crystal structure ?

(3) Can this orientation dependence be used to determine quantitatively specific-site occupancies in single crystals ?

The answers to these questions constitute the main body of this thesis. However, before pursuing these questions it would be appropriate to digress a little to present the motivation for the developement of this technique.

I.3 Motivation for specific site occupation determinations

I.3.1 Uniaxial anisotropy of $(Y,RE)_3Fe_5O_{12}$ thin films

These thin film oxides have potential application as information storage devices due to their propensity to harbour small cylindrical magnetic domains or "bubbles" with a direction of magnetization perpendicular to the film surface. This is contrary to thin film behaviour where one would expect the magnetic moments to lie parallel to the surface, as this would satisfy the energy minimization criterion. Therefore, the observed direction of magnetization in these thin films has been attributed to an inbuilt preference termed " uniaxial magnetic anisotropy".

The uniaxial magnetic anisotropy in epitaxially grown garnet films consists of a growth-induced component and a stress-induced component. The latter arises due to magneto-elastic interactions (Hansen, 1978). The former component, as the name implies, originates from the growth process and is explained in terms of the presently accepted "site-preference" model (Callen, 1971a; Rosencwaig, Tabor & Pierce, 1971; Gyorgy, Rosencwaig, Blount, Tabor & Lines, 1971). According to this model the uniaxial anisotropy is attributed to the preferential occupation of the rare-earth (RE) additions in the different crystallographic sites of the garnet lattice. But the results obtained by different investigators (Gyorgy, Sturge & van Uitert, 1974; Akselrad & Callen, 1971) using this model are controversial, if not contradictory. However, it has been observed that there is an order of magnitude reduction and subsequently, ultimate loss of the value of the anisotropy constant (K_u), on annealing (Hegedorn, Tabor & van Uitert, 1973). This observation is an indirect proof for the validity of the site preference model, but specifically which sites are involved is unclear (Nielsen, 1979). (A detailed review of the growth induced uniaxial anisotropy in thin film garnets is given in Appendix 1).

Traditionally, this cation distribution problem has been experimentally determined by one of the following methods : (1) Magnetization (2) Magnetic anisotropy (3) Optical spectroscopy (4)Mossbauer spectroscopy and (5) Spin echo

techniques (see Krishnan, 1978 for further details). These techniques are limited in their application to bulk samples and hence can resolve average distributions only. With the use of a converged probe, the techniques to be developed and described can typically analyse 20-40 nm areas. Hence, local areas of the sample can be studied. This is a significant advantage as the liquid phase epitaxial growth process is a non-equilibrium one and the concentrations and distributions are expected to change as a function of the distance from the substrate-film interface.

I.3.2 Magnetocrystalline anisotropy of $Sm_2(Co\ TM)_{17}$ Compounds

It is well known that the magnetocrystalline anisotropy of RE_2Co_{17} compounds can be appreciably modified by the substitutions of transition metal elements in limited quantities in the Cobalt sites of the lattice (Wallace, Fujii, Satyanarayana & Hirosawa, 1982). For relatively small substitutions of transition metals there is a dramatic increase in the magnitude of the anisotropy ; for example in the $Sm_2Co_{17-x}Zr_x$ system, an increase of x from 0 to 1 causes an increase of the anisotropy field (H_A) from 65 to 110 KOe (Satyanarayana, Fujii & Wallace, 1982). This increase in the magnitude of anisotropy has been attributed, as in the case of thin film garnets, to preferential site occupations of these substitutions in the crystal structure (Inomata, 1981). An alternative theory (Perkins & Strassler, 1977) suggests that the changed electron concentration in the

overall band structure of the compound, as a result of these substitutions,might be responsible for the significant changes in the magnetic properties.

A simple explanation of the effect of substitutions on H_A is that in this crystal structure the "dumbbell" sites have a preferred direction of magnetization perpendicular to the crystallographic c-axis and hence any reduction of this detrimental planar anisotropy (by substituting with an element of anisotropy lower than Co) would enhance the overall axial anisotropy. In general there is very little experimental evidence for the exact site occupations of these substitutions, but for certain elements like Fe, it is reasonably well established (Deportes, Givard, Lemaire, Nagai & Yang, 1976; Perkins & Fisher, 1976; Inomata, 1976) that it tends to occupy the dumbbell (6c) sites in this class of compounds.

A variation of the technique to be developed is particularly suitable to determine the site occupations in these compounds. Apart from the practical significance of this study, these compounds were chosen to illustrate different aspects of the developement of the technique.

* * *

We shall now return to the questions posed in section I.2.2.3 .

I.4 The Technique : Physical description

As a result of the dynamical scattering of an incident plane wave of high energy electrons, a standing wave pattern is set up within the crystal unit cell (Hirsch, Howie, Nicholson, Pashley & Whelan, 1965). The intensity modulation within the crystal is dependent on the incident beam orientation and under favourable conditions will be a maximum on certain crystallographic sites. Hence, highly localized scattering events, like inner shell excitations show a strong orientation dependence (Duncumb, 1962; Cherns, Howie & Jacobs, 1973).

It has also been shown that for certain systematic or "planar channelling" conditions, the characteristic x-ray emissions induced by the channelling or blocking of the incident electrons can provide information on the occupancy of specific crystallographic sites by different elements, provided that an *a priori* knowledge of the distribution of some reference elements in the host lattice is available (Tafto,1979; Spence & Tafto, 1983; Krishnan, Rabenberg, Mishra & Thomas, 1984). In this formulation, either the enumeration of parameters like absorption coefficients,specimen thickness etc. or an a priori knowledge of the dynamical wave function in the crystal is eliminated by a judicious choice of the reference elements. The distribution of the impurity or alloying elements is then determined by an elegant method of ratios of their characteristic x-ray intensities with respect to those of the reference elements

(Spence & Tafto, 1983). This is particularly applicable to crystals with a layered structure(i.e. crystals that in some crystallographic projections can be resolved into alternating layers of parallel non-identical planes [A,B,A,B,....], each plane containing one or more specific crystallographic site) where the appropriate systematic orientation can be determined by mere inspection. For example, the spinel structure compounds can be resolved in the [001] projection into alternating planes of tetrahedral and octahedral sites and hence a $\bar{g}$ = 400 systematic orientation can be easily seen to be appropriate for this kind of experiment.

The above formulation only constitutes a partial answer to the questions posed in section I.2.2.3. If the crystal structure is not a layered one, then it is not obvious by mere inspection which systematic orientation is specific site sensitive. The garnet structure of the liquid phase epitaxially grown thin films, for example, is very complicated and a number of crystallographic projections calculated (Benemma & Giess, 1981) using the ORTEP routine (Johnson, 1965) failed to indicate a systematic orientation that could be specific site sensitive. In such cases, the electron induced characteristic x-ray emission intensities for different site occupations and different incident beam directions have to be calculated. From these calculations the appropriate systematic or planar channelling condition applicable to that particular crystal structure is determined and the experiment performed. On the other hand, in the above

formulation (Spence & Tafto, 1983) applicable to layered structure compounds, the site occupancies are determined by a judicious choice of reference atoms (one for each plane A and B) in the original compound based on some apriori knowledge of their distributions. In many practical alloys/compounds it might not be possible to choose reference elements that are uniquely distributed on one and only one of the two alternating crystallographic planes. Further the alloying concentrations might be large enough to alter the distributions of the constituent elements in the original compound, thereby invalidating the practice of using the original compounds as internal reference standards.

I.5 A synopsis of the dissertation

Figure 1.5 is a set of hypothetical two-dimensional crystal structures that can be used to summarize the contents of this thesis.

Figure 1.5A corresponds to the structure to which the technique of atom location by channellling enhanced microanalysis, ALCHEMI (Spence & Tafto, 1983) can be routinely applied. The crystal structure is a layered one. The distribution of the reference atoms is known. The appropriate systematic or planar channelling condition can be determined by mere inspection. The analysis, then, is straight forward and well defined.

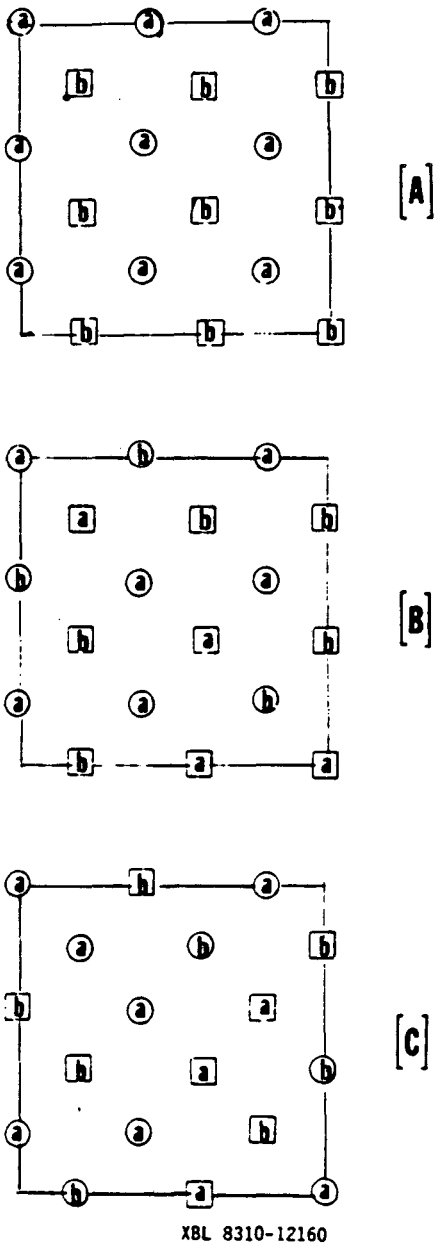

Figure 1.5 Hypothetical two-dimensional figures illustrating the classification of crystal structures in this thesis.
□,○ refer to the crystallographic sites of interest. The distribution of the site determine whether the crystal structure is layered (figs. A & B) or not (fig. C).
a, b are the reference elements. If their distributions are known apriori, the simple ratio technique (A) or a generalization of the same (B) should be used. If not (C) the characteristic x-ray emissions have to be calculated and refined using a least squares refinement to determine site occupancies.

Figure 1.5B corresponds to the structure which is one degree removed in complication. The crystal structure is a layered one but the distribution of the reference atoms is such that they are not uniquely distributed on one and only one of the two alternating crystallographic planes. Further, if the alloying concentrations are large enough, then the original concentrations cannot be used as internal reference standards. In such cases a more comprehensive analysis is required. In Chapter IV, such a generalization of ALCHEMI, that requires only an exact idea of which site(s) a particular element can occupy, whether it is a reference element or alloying addition and not their actual distribution, is presented. The problem is formulated differently and incorporates the stoichiometry of the original compound. This is then applied to the problem of specific site occupations of transition metal additions in Sm_2Co_{17} compounds (Chapter V).

Figure 1.5C corresponds to the most general problem. The crystal structure is not a layered one. Neither the distributions of the reference elements are known nor can the appropriate orientation be determined by inspection. Using a theory of electron induced characteristic x-ray emissions in thin crystals that has been developed (Chapter II), the variation of the intensities of the emission product with incident beam orientation and different site occupancies in such crystals (garnets) are calculated. These calculated intensities are used not only to predict specific site sensitive orientations but also to refine experimentally observed data employing a constrained least squares

analysis to give probabilities for the occupation of RE additions in the different crystallographic sites of the garnet lattice (Chapter III).

Apart from the above the effect of acceleration voltage as an independent parameter on this orientation dependence is calculated. An analogous "inversion voltage" is predicted. Its ramifications on channelling enhanced microanalysis is discussed and its relation to the conventional critical voltage is investigated (Chapter II).

This dissertation concludes with a general discussion (Chapter VI). Some of the assumptions are examined, the limitations are elaborated upon, other applications are enumerated and possible extensions of this work are discussed.

CHAPTER II

THEORY OF ELECTRON-INDUCED CHARACTERISTIC X-RAY EMISSIONS

II.1 Introduction/Overview

II.2 Conventional theory of transmission electron diffraction

- 2.1 Bloch wave methods
- 2.2 Two beam approximation

II.3 General theory of the inelastic scattering of fast electrons in crystalline solids

II.4 Characteristic x-ray production in thin crystals

II.5 Details of calculations

II.6 Crystallography

- 6.1 Garnets
- 6.2 Spinels

II.7 Results of the characteristic x-ray production calculations at 100 KV

II.8 General discussion

II.9 Effect of the acceleration voltage on the orientation dependence of electron-induced characteristic x-ray emissions

9.1 Introduction

9.2 Results of the calculations : " The Inversion Voltage"

9.3 Discussions

II.1 Introduction/Overview

As pointed out in the last chapter, the application of the technique of atom location by channelling enhanced microanalysis or ALCHEMI as formulated by Spence & Tafto (1983) to the study of site occupations in crystalline solids apart from being limited to certain types of layered-structure compounds is also subject to some radical assumptions pertaining to the distribution of the constituent elements. Technologically relevant materials like garnets, on the other hand, have more complicated structures and distributions. In such cases, it is not possible by mere inspection of the crystal structure to predict appropriate orientations where the "Borrman effect" of the emission products would give information leading to the determination of specific site occupations. What is required, then, is a theoretical formulation to calculate intensities of electron induced characteristic x-ray emissions as a function of incident beam orientation, such that the appropriate experimental conditions can be predicted.

We begin this chapter by describing the elastic scattering of fast electrons in crystalline solids. The theory of transmission electron diffraction in the Bloch wave formulation is outlined. Following that a detailed inelastic scattering theory incorporating the effects of elastic scattering is described. The total rate of inelastic-scattering or the integrated cross-section, in a reciprocal space formulation,

representative of the rate of characteristic x-ray production, is then expressed on the basis of the above description. An alternative real space description of the phenomenon of electron-induced characteristic x-ray emissions based on the assumption that the scattering processes leading to these emissions are highly localized, is presented. It is then argued that this simpler description is representative of the actual physical process. Pertinent details of the crystallography of garnets and spinels along with those of the calculations are then presented. The agreement of the results of the calculations of the orientation dependence of the x-ray emissions in spinels with experimental observations has been used as a measure of the validity of the theoretical formulation. Following this, characteristic x-ray intensities for different site substitutions of rare earth additions in a garnet structure and for different systematic excitation conditions were calculated. The $\bar{g}=1\bar{2}1$ systematic condition is then predicted to be the particular crystallographic orientation for which the "Borrman effect" of the emission product is specific site sensitive for these compounds.

For the sake of completeness, the orientation dependence of characteristic x-ray emissions in spinels ($MgAl_2O_4$) at higher acceleration voltages were also calculated. A voltage dependence of the orientation dependence, termed as the "inversion voltage", was predicted. The chapter concludes with a discussion of the nature of this inversion voltage and its

relation to the conventional critical voltage effect.

II.2 Conventional theory of transmission electron diffraction

In this section, some of the salient features of the conventional theory of transmission electron diffraction is reviewed. Emphasis will be on the mathematical formulations (and their physical interpretations) that are of relevance to the developement of a theory of electron-induced characteristic x-ray emissions in thin crystals. Detailed background may be found in the well established literature in this subject (Bethe, 1928; Howie & Whelan, 1961; Hahsimoto, Howie & Whelan, 1962; Sturkey, 1962; Fujimoto, 1959; Niehrs, 1959a; Niehrs, 1959b).

II.2.1 Bloch wave methods

The high energy electron diffraction in a thin foil with the incident beam oriented parallel to the foil normal is described. In this orientation, termed as the Laue case, only scattering by reciprocal lattice vectors in the zero order layer is considered to be important.

The scattering of an electron, represented by the wave function $\Psi(\underline{r})$, in a periodic crystal potential $V(\underline{r})$, expanded in a Fourier series as

$$V(\underline{r}) = \sum_{g} v_g \exp(i\, \underline{g} \cdot \underline{r}) \qquad (2.1)$$

satisfies the Schrodinger equation

$$-\frac{\hbar^2}{2m}\nabla^2\psi(\bar{r}) + eV(\bar{r})\psi(\bar{r}) = E\psi(\bar{r}) \qquad (2.2)$$

Assuming that the solution is a Bloch wave of the form

$$\psi(\bar{r}) = b(\bar{k},\bar{r}) = \sum_g C_g(\underline{k}) \exp[i(\bar{k} + \bar{g})\cdot\bar{r}] \qquad (2.3)$$

and substituting it in the Schrodinger equation (2.2), we get

$$(K^2 - k_z^2)C_g(\bar{k}) - (2k_x\bar{g} + \bar{g}^2)C_g(\bar{k}) + \sum_h U_{g-h}C_h(\bar{k}) = 0 \qquad (2.4)$$

where U is defined as $2meV(\bar{r})/\hbar^2$.

Resorting to the normal high energy approximation

$$(K^2 - k_z^2) = -2K(k_z - K) = -2\gamma K \qquad (2.5)$$

where K is the z-component of the free space wavevector, equation (2.4) can be rewritten as an eigenvalue equation of the form

$$\underline{\underline{A}}_{gh}\,\underline{C}_h = \gamma\,\underline{C}_h \qquad (2.6)$$

where $\underline{A}_{gh}$ in matrix form is

$$A_{gh} = 2\pi \begin{bmatrix} s_o & 1/2\xi_{-g} & 1/2\xi_{-h} \\ 1/2\xi_g & s_g & 1/2\xi_{g-h} \\ 1/2\xi_h & 1/2\xi_{h-g} & s_h \end{bmatrix} \tag{2.7}$$

Here the excitation errors/deviation parameters s_g (defined as the distances from the Bragg spots to the Ewald sphere in a direction perpendicular to the foil) are given by

$$S_g = -\left(\frac{2k_x g + g^2}{4\pi K}\right) \tag{2.8}$$

and

$$\xi_{g-h} = \frac{2\pi K}{U_{g-h}} \tag{2.9}$$

are the extinction distances.

For n beams, there will be n eigenvalues with corresponding eigenvectors. These eigenvalues are the allowed wave vectors in the crystal for an electron of a fixed energy. The variation of k_z as a function of k_x is called the dispersion surface.

The complete wave function in the crystal can then be written as a linear combination of these Bloch waves

$$\phi(\bar{r}) = \sum_j \psi^{(j)} \sum_g C_g^{(j)} \exp\left[i(\bar{k}^{(j)} + \bar{g}) \cdot \bar{r}\right] \tag{2.10}$$

or in matrix notation as

$$\underline{\phi}(\bar{r}) = \left\{\exp\left(i\bar{g} \cdot \bar{r}\right)\right\} \underline{\underline{C}} \left\{\exp\left(i\bar{k} \cdot \bar{r}\right)\right\}_D \underline{\psi} \tag{2.11}$$

Since $\underline{\underline{A}}$ is a Hermitian, i.e. $\underline{\underline{A}} = (\underline{\underline{A}}^T)^*$, the eigenvalues are real and the eigenvector matrix satisfies

$$\underline{\underline{C}}^{-1} = \underline{\underline{C}}^T, \quad \underline{\underline{C}}^T\underline{\underline{C}}^{-1} = \underline{\underline{I}} \quad \& \; \underline{\underline{C}}^T\underline{\underline{C}} = \underline{\underline{I}} \tag{2.12}$$

For non-centrosymmetric crystals the eigenvector matrix satisfies

$$\underline{\underline{C}}^{-1} = \underline{\underline{C}}^{T^*} \quad \& \quad \underline{\underline{C}}^{T^*}\,\underline{\underline{C}} = \underline{\underline{I}} \tag{2.12a}$$

In other words, the Bloch wave amplitudes satisfy the orthonormality relations

$$\sum_i C_g^{(i)*} C_h^{(i)} = \delta_{g,h} \tag{2.13a}$$

$$\sum_g C_g^{(i)*} C_g^{(j)} = \delta_{i,j} \tag{2.13b}$$

The boundary conditions at the upper surface is either

$$\underline{\underline{C}}\ \underline{\psi} = \underline{\phi}(o) \tag{2.14}$$

or

$$\underline{\psi} = \underline{\underline{C}}^{-1}\ \underline{\phi}(o) = \underline{\underline{C}}^{T}\ \underline{\phi}(o) \tag{2.14a}$$

For non-centrosymmetric crystals the boundary condition would be

$$\underline{\underline{C}}^{T*}\ \underline{\phi}(o) = \underline{\psi} \tag{2.14b}$$

This along with the relation $\underline{\phi}(o) = \delta_{o,g}$, gives

$$\psi^{(j)} = C_o^{(j)} \tag{2.15}$$

for centrosymmetric crystals or

$$\psi^{(j)} = C_o^{(j)*} \tag{2.15a}$$

for non-centrosymmetric crystals, thereby determining the excitation amplitudes.

Hence, the solution at a depth 't' from the top surface can be written as

$$\underline{\phi}(t) = \underline{\underline{C}} \left\{ \exp(i\gamma t) \right\}_D \underline{\underline{C}}^{-1} \underline{\phi}(o) \tag{2.16}$$

or alternatively in summation notation as

$$\phi_g(t) = \sum_j C_g^{(j)} \exp\left[i(\bar{k}_x + \bar{g}) \cdot \bar{x}\right] \exp(ik_z^{(j)} z) \, C_o^{(j)*} \, \phi_o(o) \tag{2.17}$$

for a non-centrosymmetric crystal.

II.2.2 Two beam approximation

The properties of the dynamical diffraction can be conveniently illustrated by considering the two beam solution; an approximation that assumes that only one set of Bragg planes associated with the reciprocal lattice vector $\bar{g}$ is near the reflecting position. The matrix $\underline{\underline{A}}$ is then given by

$$\underline{\underline{A}} = 2\pi \begin{bmatrix} 0 & 1/2\xi_g \\ 1/2\xi_g & s_g \end{bmatrix} \tag{2.18}$$

and the eigenvalues are $\pi[s \pm \sqrt{(s^2 + 1/2\,\xi_g^2)}]$. The corresponding dispersion surface has a hyperbolic form (Figure 2.1) and consists of two branches belonging to two different energy bands with a minimum separation of $1/\xi_g$ at the Brillouin zone boundary. Following Humphreys and Fisher (1971), the Bloch waves are numbered in the order of decreasing wave vector. The Bloch wave coefficients associated with a point $D^{(i)}$ on the i^{th} branch can be expressed as

$$C_o^{(1)} = -C_g^{(2)} = \sin(\beta/2) \tag{2.19a}$$

$$C_o^{(2)} = C_g^{(1)} = \cos(\beta/2) \tag{2.19b}$$

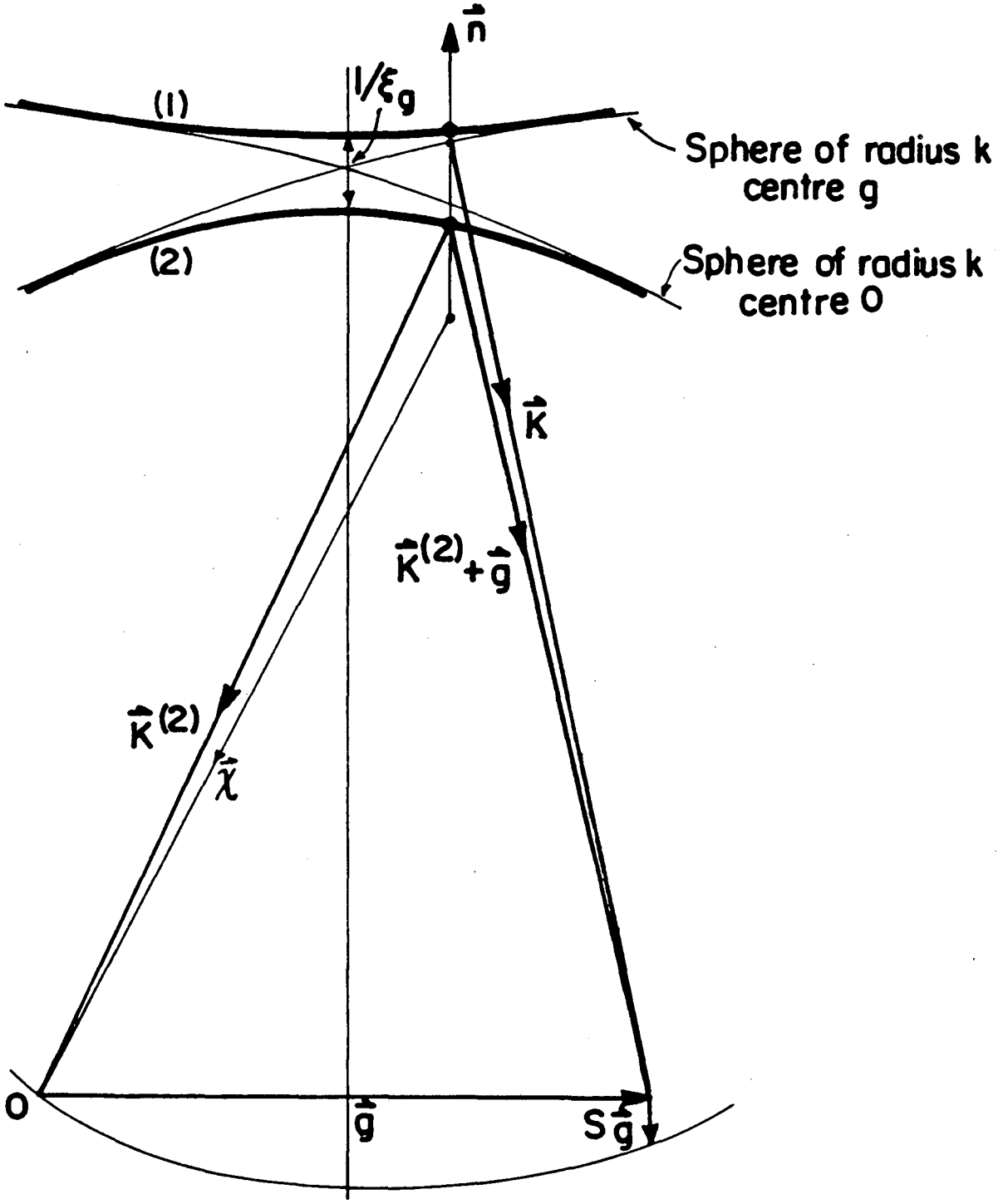

XBL841-6508

Figure 2.1 The dispersion surface in the two beam approximation. The minimum separation between the two waves occurs at the Brillouin zone boundary and is equal to the extinction distance ξ_g. The incident wave vector $\vec{\chi}$ and the wave vector corresponding to one of the waves excited in the crystal $k^{(2)}$ ($K^{(1)}$ not shown for clarity) are also shown. $\vec{n}$ represents a unit vector normal to the crystal surface.

where $\mathrm{Cot}(\beta) = s\,\xi_g = w$.

The amplitude at any depth 't' can then be expressed as

$$\phi_o(t) = \cos\left(\frac{\pi t}{\xi_g}\sqrt{1+w^2}\right) - i\cos\beta\,\sin\left(\frac{\pi t}{\xi_g}\sqrt{1+w^2}\right) \tag{2.20}$$

and

$$\phi_g(t) = i\sin\beta\,\sin\left(\frac{\pi t}{\xi_g}\sqrt{1+w^2}\right) \tag{2.21}$$

and the intensity is

$$|\phi_g|^2 = 1 - |\phi_o|^2 = \frac{\sin^2\left(\frac{\pi t}{\xi_g}\sqrt{1+w^2}\right)}{(1+w^2)} \tag{2.22}$$

From the above, it can be seen that for fixed orientations, the intensity shows oscillations with thickness (thickness fringes) or alternatively for fixed thicknesses the intensity shows oscillations with orientation (rocking curves).

***

In the next section, a general theory of inelastic

scattering of electrons in perfect crystals, where the fast electrons are described by Bloch waves, will be presented. The inelastic transitions will be shown to be dependent on the matrix elements between these Bloch waves and hence some of their properties outlined in this section will be particularly useful in the ensuing descriptions.

II.3 General theory of the inelastic scattering of fast electrons in crystalline solids.

Following Yoshioka (1957), we assume that the the system of the incident fast electron plus the crystal satisfy the Schrodinger equation

$$\left\{\frac{-\hbar^2}{2m}\nabla^2 + H_C + H'\right\}\Phi = E\Phi \qquad (2.23)$$

where $-\hbar^2/(2m)\ \nabla^2$ represent the kinetic energy of the incident electron, H_c the energy of the crystal and H' the interaction energy between the electrons and the crystal.

The interaction Hamiltonian is given by

$$H' = \sum_p \frac{e^2}{|\bar{r} - \bar{r}_p|} - \sum_q \frac{Z_q e^2}{|\bar{r} - \bar{R}_q|} \qquad (2.24)$$

where $\underline{r}$ is the coordinate of the incident electron, $\underline{r}_p$ the coordinate of the p^{th} electron in the crystal and $\underline{R}_q$ the coordinate of the q^{th} nucleus with charge $Z_q e$ in the crystal.

The wave function of the system $\Phi(\underline{r},\underline{r}_j)$, depends on $\underline{r}$ (the coordinate of the incident electron) and $\underline{r}_j$ j=1....N (the coordinates of the electrons and the ions in the crystal). If "exchange" effects between the incident fast electron and the crystal electrons can be neglected, then the wave function of the system can be expanded in the form

$$\Phi(\bar{r}, \bar{r}_1,\ldots, \bar{r}_N) = \sum_n \mathcal{A}_n(\bar{r}_1, \bar{r}_2,\ldots, \bar{r}_N)\, \phi_n(\bar{r}) \qquad (2.25)$$

where $\mathcal{A}_n(\underline{r}_1.....\underline{r}_N)$ is the wave function representing the n^{th} excited state of the crystal of energy ε_n ($\varepsilon_0 = 0$) such that

$$H_c\, \mathcal{A}_n = \varepsilon_n\, \mathcal{A}_n \qquad (2.26)$$

$\phi_n(\underline{r})$ in equation (2.25) describes the inelastically scattered wave of energy $E_n = E - \varepsilon_n$ that excites the crystal from the normal state to the excited state n and $\phi_0(\underline{r})$ describes the elastically scattered wave of energy $E_0=E$.

Substituting from equations (2.25) and (2.26) into equation (2.23), multiplying by $\mathcal{A}_n^*$ and integrating over the crystal electron coordinates $\underline{r}_j$, i.e. $\underline{r}_1.....\underline{r}_N$, we obtain a set of coupled equations for the ϕ_n

$$\left\{ \frac{-\hbar^2}{2m} \nabla^2 + H_{nn} - E_n \right\} \phi_n = - \sum_{m \neq n} H_{nm} \phi_m \qquad (2.27)$$

where

$$H_{nm}(\bar{r}) = \int \mathcal{A}_n^* H' \mathcal{A}_m d\tau \; ; \quad d\tau = d\bar{r}_1, \ldots, d\bar{r}_n \qquad (2.28)$$

The right hand side terms of equation (2.27), comprising of the off-diagonal elements H_{nm}, represent the inelastic scattering involving transitions from ϕ_m to ϕ_n. If these terms are neglected, this formulation would reduce to the Bethe (1928) theory of electron diffraction , i.e. the same theory as in section (II.2). The diagonal elements H_{nn} represent the lattice potential causing Bragg diffraction when the crystal is in its n^{th} excited state. Yoshioka (1957) neglected the terms H_{nn} for $n \neq 0$; i.e. the diffraction of the inelastically scattered waves ϕ_n was ignored. On the other hand, Howie (1963) has accounted for this possibility but makes the assumption that as far Bragg diffraction is concerned, the excited crystal is similar to the unexcited one and hence

$$H_{nn}(\bar{r}) = H_{oo}(\bar{r}) = V(\bar{r}) = \frac{2m}{\hbar^2} \sum_g U_g \exp(i\bar{g}\cdot\bar{r}) \qquad (2.29)$$

where the summation extends over reciprocal lattice vectors $\bar{g}$.

As the crystal wavefunctions satisfy the translational symmetry condition, we have

$$\mathcal{A}_n(\underline{r}_1+\underline{t}, \underline{r}_2+\underline{t}, \ldots, \underline{r}_N+\underline{t}) =$$

$$\exp(i\underline{Q}_n \cdot \underline{t})\, \mathcal{A}_n(\underline{r}_1, \underline{r}_2, \ldots, \underline{r}_N) \tag{2.30}$$

which holds for any lattice translation $\underline{t}$. Hence, it can easily be shown (Howie, 1963) from equation(2.28) that $H_{nm}(\underline{r})$ also satisfy Bloch's theorem, i.e.

$$H_{nm}(\bar{r}) = \exp(-i\underline{q}_{nm} \cdot \bar{r}) \sum_g H_g^{nm} \exp(i\bar{g} \cdot \bar{r}) \tag{2.31}$$

provided that

$H'(\underline{r}, \underline{r}_1, \ldots \underline{r}_N)$ is only a function of $(\underline{r}-\underline{r}_1), (\underline{r}-\underline{r}_2) \ldots (\underline{r}-\underline{r}_N)$. $H_{nm}(\underline{r})$ is thus characterized by a set of Fourier coefficients H_g^{nm} (for the various reciprocal lattice vectors $\bar{g}$) and by a vector $\bar{q}_{nm} = \bar{Q}_n - \bar{Q}_m$ corresponding to the change in wave vector of the crystal electrons (representing some crystal excitation that is created in the transition $m \rightarrow n$).

We try a solution of equation 2.27 of the form

$$\phi_n(\underline{r}) = \psi_n(z)\, B(\underline{k}_n, \underline{r}) \tag{2.32}$$

i.e., a Bloch wave of wave vector $\underline{k}_n$, whose amplitude is depth dependent. A further restriction of small angle scattering is

imposed, such that all reciprocal lattice vectors $\underline{g}$ constituting the Bloch wave $B(\underline{k}_n,\underline{r})$ lie only in the x,y plane. Substituting this fast electron wave function (2.32) in equation (2.27), neglecting the small term $(d^2\Psi_n/dz^2)$, multiplying throughout by the complex conjugate $B^*(\underline{k}_n,\underline{r})$ and integrating over the x,y directions gives the amplitude $\Psi_n(z)$ of the Bloch wave as a function of the depth z as

$$\frac{d\psi_n}{dz} = \sum_{m\neq n} C_{nm}\,\psi_m \qquad (2.33)$$

where

$$C_{nm} = \frac{-\,im}{\hbar^2 (k_n)_z} \exp\,(i\delta k_{nm} z) \sum_{h,g} C_g^*\,(\bar{k}_n)\; H_{g-h}^{nm}\; C_h(\bar{k}_m) \qquad (2.34)$$

and

$$\delta k_{nm} = (k_m)_z - (k_n)_z + (Q_m)_z - (Q_n)_z \qquad (2.35)$$

is the "resonance error" due to the difference between the change in the wave vector of the fast electron and the wave vector of the crystal excitation created.

The coefficients, C_g are obtained from the expansion of the Bloch functions

$$B(\underline{k},\underline{r}) = \sum_{g} C_g(k) \exp\,[i(\underline{k} + \underline{g}) \cdot \underline{r})] \tag{2.36}$$

These expressions can be generalized and rearranged (Humphreys & Whelan, 1969) as follows

$$\phi_n(\bar{r}) = \sum_{i} \psi_n^{(i)}(z) \; B^{(i)}(k_n^{(i)}, \bar{r}) \tag{2.37}$$

$$\frac{d\psi_n^{(i)}(z)}{dz} = \sum_{m\neq n} \sum_{j} S_{nm}^{(i)(j)} \exp\,[i\delta k_{nm}^{(i)(j)} z]\; \psi_m^{(j)}(z) \tag{2.38}$$

where

$$S_{nm}^{(i)(j)} = \frac{-im}{\hbar^2 (k_n^{(i)})_z} \sum_{h,g} C_g^{(i)*}(k_n^{(i)})\; H_{g-h}^{nm}\; C_h^{(j)}\,(k_m^{(j)}) \tag{2.39}$$

and

$$\delta k_{nm}^{(i)(j)} = (k_m^{(j)})_z - (k_n^{(i)})_z - (q_{nm}^{(i)(j)})_z \tag{2.40}$$

Transitions corresponding to a change in the branch index (i) or (j) of the fast electron are called intERbranch transitions and those where they remain the same are called intRAbranch (Figure 2.2). For single electron scattering $H_o >> H_g$,

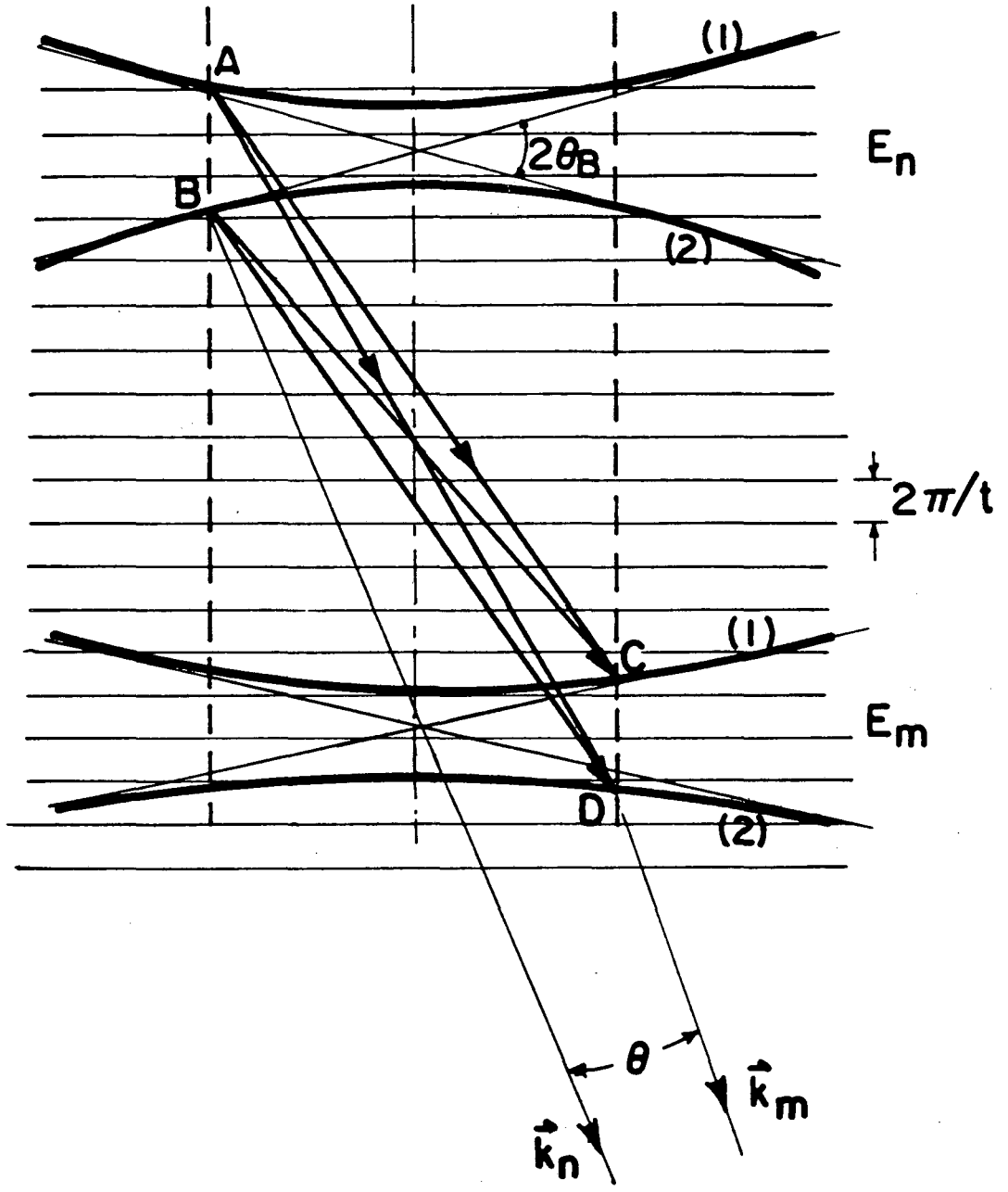

XBL 841-6507

Figure 2.2 Scattering transitions involving two dispersion surfaces of energies E_n (incident electrons) and E_m (inelastically scattered electrons). The line AB represents the incident state and CD the scattered state. AC & BD are intRAbranch transitions and AD & BC are intERbranch transitions. For the periodic boundary conditions, the allowed wave vectors for the crystal are seperated by $2\pi/t$ as indicated by the parallel horizontal lines. For the inelastic intRAbranch transition BD, we have $q_{nm}^2 = K^2 (\theta^2 + \theta_E^2)$ where θ is the angle of scattering and $\theta_E = (E_n - E_m)/2E = 10^{-4}$.

i.e., strongly forward peaked. Using this and the Bloch wave coefficient orthonormality relations, equations (2.13a) & (2.13b), it can be shown that single electron scattering is predominantly intRAbranch. Further, if only first order inelastic scattering is considered, the summation with respect to the excitation states in the above expression can be dropped, leaving only the term corresponding to the excitation from the ground state to the excited state n . The amplitude at the exit surface, for a crystal of thickness t, neglecting absorption, is then given by

$$\psi^{(i)} = \int_0^t \sum_j S^{(i)(j)} \exp\left[i\, \delta k^{(i)(j)} z\right] \quad \psi^{(j)}(0)\, dz \tag{2.41}$$

and $\Psi^{j}(0) = C_0^j$, using the boundary condition for elastically scattered waves.

The intensity scattered to a coordinate $\bar{g}-\bar{q}$ in reciprocal space is then given by

$$I_g^q = \sum_{i,j} \psi^i(t)\psi^j(t) C_g^i\, C_g^j \exp\left[i\,(k^i - k^j)\, t\right] \frac{A}{4\pi^2}\, d\sigma \tag{2.42}$$

where $A/4\pi^2$ is the density of states for the crystal excitation in an infinitesimal region around $\bar{g}-\bar{q}$.

Comparing this method with first order perturbation

theory, Rez (1976) has shown that for a centrosymmetric crystal the differential scattering to a position $\bar{g}-\bar{q}$ in reciprocal space can be written as

$$\frac{dI}{d\Omega} = \frac{Vt}{4\pi^2} \sum_{i'j'} \sum_{ij} C_g^{i'} C_g^{j'} \exp\left[i\,(k^{i'} - k^{j'})t\right] S^{i'j} S^{j'i} C_o^i C_o^j$$

$$\times \frac{k^2}{N_z^2} \sum_{z_n} \sum_{z_m} \exp\left[i\,(k^j - k^{i'} - q_z)z_n\right] \exp\left[-i\,(k^i - k^{j'} - q_z)z_m\right]$$

(2.43)

where the primed indices , for convenience, refer to the scattered states, N_z represents the number of unit cells in the z direction and all other terms have been defined earlier.

If we now sum over the excitation wave vector in equation (2.43) we can calculate the intensity. For mathematical simplicity a periodic boundary condition is resorted to, in which case $q_{x,y,z} = 2\,\pi n_{x,y,z}/L_{x,y,z}$ where n_x, n_y, n_z are integers and L_x, L_y, L_z are the dimensions of the finite crystal. A detailed discussion of the use of periodic boundary conditions is given elsewhere (Born & Huang, 1954). In this particular case $q_z = 2\pi n/t$. Performing the summation over n and m first, assuming that the matrix elements $S^{i'j}(q_z)$ vary slowly over the range of q_z which contributes most to the scattering and utilizing the fact that all single electron scattering are mainly

intRAbranch, the full expression (neglecting absorption) for the differential scattering to a position $\bar{g}-\bar{q}$ is then given by

$$\frac{dI}{d\Omega} = \frac{Vt}{4\pi^2} k^2 \sum_{i'j'} \sum_{ij} C_g^{i'} C_g^{j'} C_o^{i} C_o^{j} S^{i'j} S^{j'i}$$

$$\times \frac{\sin [(k^j - k^i)t] - \sin [(k^{i'} - k^{j'})t]}{[k^j - k^{i'} - k^i + k^{j'}]t} \qquad (2.44)$$

Absorption has been neglected throughout this derivation. However, it has been shown (Rez, 1976) that if absorption effects were to be included, the expressions would remain the same but with complex wave vectors.

II.4 Characteristic x-ray production in thin crystals

We begin by considering explicitly the scattering process involved. In the last section (II.3), an expression for the differential cross-section $dI/d\Omega$ for scattering to a position $\bar{g}-\bar{q}$ in reciprocal space, neglecting absorption, was derived (equation 2.44). The total rate of inelastic scattering or the integrated cross-section, representative of either the rate of characteristic x-ray production or the rate of back-

scattering is obtained by summing equation(2.44) over the reciprocal lattice vectors $\bar{g}$ and integrating $\bar{q}$ in the first Brillouin zone. Inspection of equation(2.44) shows that there is oscillatory dependence on the final state as $\bar{g}$ only appears in the final state Bloch coefficients and

$$\sum_{g} C_g^{i'} C_g^{j'} = \delta_{i',j'} \tag{2.13b}$$

which follows from the orthonormality relations.

The rate of inelastic scattering which is also proportional to the production of characteristic x-rays in thin crystals is then given by

$$\sigma = \sum C_o^i C_o^{i'} U^{ii'} \frac{\mathrm{Sin}\,[t(k^i - k^{i'})]}{(k^i - k^{i'})} \tag{2.45}$$

where

$$U^{ii'} = \sum_{g,h} C_g^i U_{g-h} C_h^{i'} \tag{2.46}$$

and

$$U_{g-h} = \left(\frac{m}{2\pi\hbar^2 k}\right)^2 V \int_{B.Z.} \sum_f \sum_{d,e} C_d^f C_e^f H_{g-d}(q) H_{e-h}(q) d^2q \qquad (2.47)$$

$$= \frac{2m}{\hbar^2 k} P_{g-h} \qquad (2.48)$$

which as pointed out (Rez, 1976) are just the Fourier coefficients of the imaginary part of the crystal potential as given by Radi(1968) where the final states have been assumed to be a Bloch wave. Further, if anomalous absorption is allowed to act on the incident state, the above expression for total inelastic scattering would be modified so as to have a form identical to that given by Cherns, Howie & Jacobs (1973).

Apart from the above, two simple models have been proposed regarding the nature of characteristic x-ray production; the dependent model where the rate of characteristic x-ray production is proportional to the square of the total wave function and the independent model where it is proportional to the sum of the intensities of the individual Bloch waves. In the former model, the x-ray production rate at the coordinate $\underline{r}$ in the unit cell is proportional to

$$|\phi(\bar{r})|^2 = \sum_i \psi^{(i)^2} + \sum_{i \neq j} \psi^{(i)} \psi^{(j)} \exp\left[i(k^i - k^j)z\right] \qquad (2.49)$$

and predicts an oscillatory behaviour with thickness. This

behaviour is predicted earlier also , where we considered explicitly the scattering process. This has been experimentally observed by Cherns, Howie & Jacobs (1973) particularly for thin crystals, $t \leq 10$ nm, even though earlier experiments (Hall, 1966) show a linear dependence with thickness, suggesting the validity of the independent model.

Alternatively, ionizations of inner shell electrons, alters the imaginary part of the crystal potential and this could be calculated from the relevant wave functions (Whelan, 1965a). These calculations would be rather involved, particularly in the case of rare earth elements since exchange effects cannot be neglected. The incorporation of an imaginary crystal potential $iP(\underline{r})$ in the Schrodiner equation, has been shown by Heidenreich (1962) to lead to a rate of electron loss per unit volume at the point $\underline{r}$ proportional to $P(\underline{r}) \, |\phi(\underline{r})|^2$. When an imaginary potential is introduced, the Schrodinger equation is written as

$$\nabla^2 \phi + \frac{2m}{\hbar^2} (E + V + iP) \phi = 0 \qquad (2.50)$$

It follows from equation (2.50) that

$$\phi^* \nabla^2 \phi - \phi \nabla^2 \phi^* = \frac{2m}{\hbar^2} 2i P \phi^* \phi \qquad (2.51)$$

where ϕ^* is the complex conjugate of ϕ.

Since the electron flux is given by

$$S = \frac{\hbar}{2im} \left[\phi^* \text{ Grad } \phi - \phi \text{ Grad } \phi^*\right] \tag{2.52}$$

it can easily be shown that

$$\text{div } \underline{S} = \frac{\hbar}{2im} (\phi^* \nabla^2\phi - \phi \nabla^2\phi^*) = \frac{-2}{\hbar} P(\bar{r}) \phi^*\phi \tag{2.53}$$

and hence the rate of "absorption" of electrons in a volume V is

$$\frac{m}{\hbar k} \int \bar{\nabla}\cdot\bar{S} \, d^3r = \frac{2m}{\hbar^2 k} \int P(\bar{r}) \, |\phi(\bar{r})|^2 \, d^3r \tag{2.54}$$

This could equal the rate of x-ray production if and only if $P(\underline{r})$ is chosen appropriately.

Since the absolute magnitude of the effect is unimportant for our purposes we have assumed this imaginary part of the crystal potential to be a delta function at the mean atomic positions, i.e., a highly localized scattering process.

Therefore, the rate of characteristic x-ray production for the element 'x' given by (equation 2.54)

$$N_x = \int P(\underline{r}) \, |\phi(\underline{r})|^2 \, d^3r \tag{2.55}$$

where the integral extends over the volume of the crystal, can be reduced under the above approximation to

$$N_x = \sum_{RSI} \int_0^t \phi^* \phi \, dz \tag{2.56}$$

Here ϕ is the scattered wave amplitude at any depth z expressed as a linear combination of Bloch waves, for the case of an incident plane wave, in the conventional dynamical theory formulation and the summation is over the relevant crystallographic sites of interest [RSI] where the particular element x is distributed in the unit cell.

The excitation amplitudes ψ^i and the wavevectors k^i of the Bloch waves are perfectly well defined being dependent only on the crystal orientation and the potential. Hence

$$\int_0^t \phi^* \phi \, dz = \sum_{g,h} \exp\,[i(\bar{h} - \bar{g}) \cdot \bar{r}] \sum_{\substack{j\ell \\ j=\ell}} C_o^{(j)*} C_g^{(j)*} C_0^{(\ell)} C_h^{(\ell)} t$$

$$+ \sum_{\substack{j\ell \\ j>\ell}} C_o^{(j)*} C_g^{(j)*} C_o^{(\ell)} C_h^{(\ell)} \frac{\sin\,[(k_z^{(\ell)} - k_z^{(j)})t]}{k_z^{(\ell)} - k_z^{(j)}} \tag{2.57}$$

Dividing throughout by the crystal thickness, t and summing over the specific sites of interest we get the following expression for the site-specific intensity per unit thickness for the characteristic x-ray production

$$N_x = \sum_{RSI} \sum_{g,h} \exp\,[i(\bar{h} - \bar{g})\cdot\bar{r}] \quad \sum_{\substack{j,\ell \\ j=\ell}} C_o^{(j)*} C_g^{(j)*} C_o^{\ell} C_h^{\ell}$$

$$+ \sum_{\substack{j,\ell \\ j>\ell}} C_o^{(j)*} C_g^{(j)*} C_o^{(\ell)} C_h^{(\ell)} \quad \frac{\sin\,[(k^j - k^{\ell})t]}{[(k^j - k^{\ell})t]} \tag{2.58}$$

where C_h^j are the Bloch wave coefficients and k_z^j are the components of the wave vector for the electrons in the crystal. For a centrosymmetric crystal, the Bloch wave elements $C_h^{(j)}$ and the excitation amplitudes $\Psi^{(i)}$ can be taken to be real. This expression (2.57) for the characteristic x-ray production is composed of two parts; a thickness independent term of individual Bloch wave contributions and a thickness dependent term of Bloch wave interference contributions.

The derivations of equations (2.45) and (2.57) for the characteristic x-ray production in thin crystals are identical in so far as they are two different representations of the same physical phenomenon. The reciprocal space formulation leading upto equation (2.45) was derived by applying first order perturbation theory to the inelastically scattered state, i.e. the imaginary part of the crystal potential H' in Yoshioka's equation (2.23) was considered to be small. The real space

formulation, equation (2.57), was derived by considering the flux loss from the incident beam. The consistency of these two formulations have also been discussed by Rez (1979). The crucial step in the argument is that for highly localized inner shell excitations where the inelastic potential is well approximated by a delta function $\delta(\bar{r})$, the Fourier transform P_{gh} is a constant and does not appear explicitly in equations (2.57) and (2.58).

II.5 Details of calculations

The equation (2.58) for the orientation dependence of electron-induced characteristic x-ray emissions derived in the last section, based on the assumption of highly localized inner shell excitations and neglecting absorption, has as its constituents Bloch wave amplitudes derived from the solutions of the elastic scattering process in the conventional dynamical theory formulation. The Bloch wave coefficients are obtained by solving the eigenvalue equation

$$\underline{\underline{A}}_{gh} \; \underline{C}_h = \gamma \underline{C}_h \tag{2.6}$$

where

$$\underline{\underline{A}}_{gh} = 2\pi \begin{bmatrix} S_o & 1/2\xi_{-g} & 1/2\xi_{-h} \\ 1/2\xi_g & S_g & 1/2\xi_{g-h} \\ 1/2\xi_h & 1/2\xi_{h-g} & S_h \end{bmatrix} \tag{2.7}$$

$$S_g = -\left(\frac{2k_x g + g^2}{4\pi K}\right) \tag{2.8}$$

and

$$\xi_{g-h} = \frac{2\pi K}{U_{g-h}} \tag{2.9}$$

The structure factor F_g is given by

$$F_{g_{(h,k,\ell)}} = \sum_i f_{el_i}(\underline{g}) \exp\left[-2\pi i\,(hu_i + kv_i + \ell w_i)\right] \qquad (2.59)$$

where u_i, v_i, w_i are fractional coordinates of the atom 'i'. The electron scattering factors $f_{el}(\bar{g})$ are best approximated in terms of the x-ray scattering factors using the Mott formula as

$$f_{el}(\bar{g}) = \frac{me^2}{2\pi\epsilon_o \hbar^2} \left[\frac{Z - f_{x\text{-}ray}(\bar{g})}{g^2}\right] \qquad (2.60)$$

where $f_{x\text{-}ray}$ is the Fourier transform of the electron density of the atom and is equal to the x-ray scattering factor and Z is the atomic number.

The x-ray scattering factors have been calculated by Doyle & Turner (1968) based on a relativistic Hartree-Fock calculation of free atom wave functions and parametrized into a series of Gausians.

The parametrized values are of the form

$$f_{x\text{-}ray}(\underline{g}) = \sum_{j=1}^{4} A_j \exp\left(-B_j X_g^2\right) \qquad (2.61)$$

where

$$X_g^2 = (\sin\theta_g/\lambda)^2 \qquad (2.62)$$

and

$$(2 \sin \theta_g/\lambda)^2 = (h/a)^2 + (k/b)^2 + (\ell/c)^2 \qquad (2.63)$$

for an orthorhombic crystal.

Here λ is the relativistic wavelength given by

$$\lambda = h/[2m_0eE(1 + eE/2m_0c^2)]^{1/2} \qquad (2.64)$$

$$= 12.26\ E^{-1/2}/[1 + 0.9788 \times 10^{-6}E]^{1/2}\ \text{Å} \qquad (2.65)$$

***

Before the results of the calculations of the orientation dependence of the electron-induced characteristic x-ray emissions are presented and discussed, a digression is made to present the relevant crystallographic datails of the spinel and garnet structures. The reader, familiar with these crystal structures may proceed onto section II.7.

II.6 Crystallography

II.6.1 Garnets

Magnetic garnets are Neel ferrimagnets with an average chemical formula of $\{A_3^{2+}\}[B_2^{3+}](Fe_3)O_{12}$. They belong to the space group I $4_1/a\ 3\ \bar{2}/d$ (O_h^{10}) with a typically large lattice

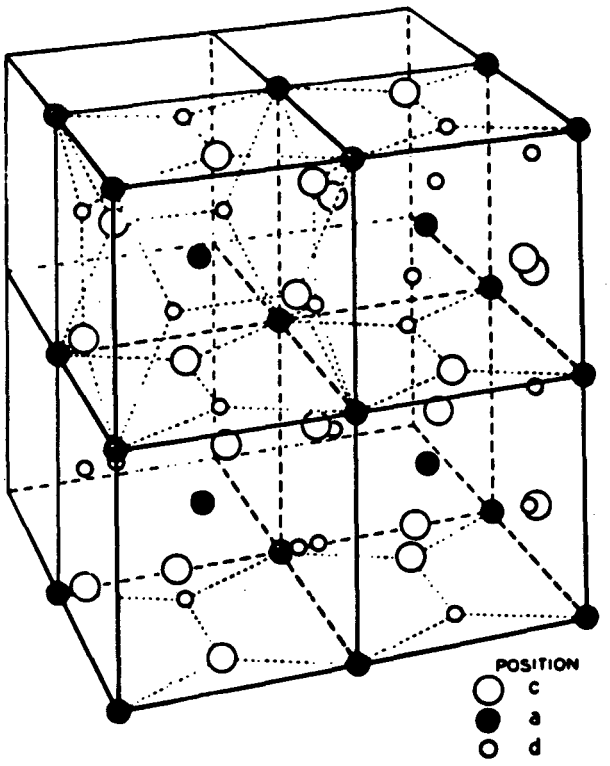

Figure 2.3 Arrangements of the cations in the garnet structure. Only half the unit cell (8 formula units or 160 atoms) is shown. The oxygen ions have been removed for clarity. Note that the octahedral [a] sites form a repeating body centred cubic structure with a lattice parametre $a_0' = a_0/2$.
After Geller & Gilleo (1957).

parameter, $a_0 = 12.376 \pm 0.004$ A° for $Y_3Fe_5O_{12}$ (Geller, 1957). Some of the relevant details of the structure are given in Table 2.1. The detailed ionic positions used in the computation were, however, based on those specified by Wycoff (1960). The prototype magnetic garnet is Yttrium-Iron-Garnet [YIG] or $\{Y_3\}[Fe_2](Fe_3)O_{12}$ with an easy direction of magnetization along the [111] direction, implying that YIG is really rhombohedral (Geller, 1978).

Table 2.1

Description of the magnetic garnet structure

Coord. Polyhedra	Dodecahedron	Octahedron	Tetrahedron	
Point Symmetry	222	3	4	1
Space Grp. Pos.	24c	16a	24d	96h
Ideal Formula	$\{Y_3\}$	$[Fe_2]$	(Fe_3)	O_{12}
Coordinates	(1/4,1/8,0)	(0,0,0)	(1/4,3/8,0)	(x,y,z)

Note: For YIG x=-0.027
y= 0.0569
z= 0.1505

The arrangement of the cations in the {c}, [a] and (d) sites in four of the eight octants of the unit cell is shown in figure 2.3. Bereft of the oxygen ions (which have been removed for clarity) one can represent the garnet structure as a repeating body centred cubic structure of octahedral cations with a lattice parameter of $a_0/2$. The other cations are then distributed along <100> directions of this new unit cell (lattice parameter $a_0' =$

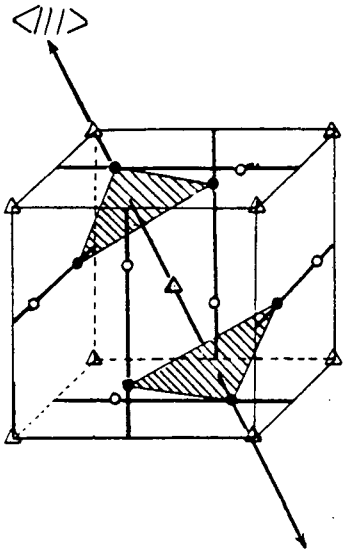

Figure 2.4 Each octant of the garnet unit cell containing one formula unit can be considered to be a BCC unit cell of the octahedral [△] sites. The tetrahedral (○) and dodechedral {●} sites are then distributed alternately along the non-diagonal cube face bisectors of each octant. The distribution of the {c} and (d) sites is such that they form a three-fold axis along the <111> direction.

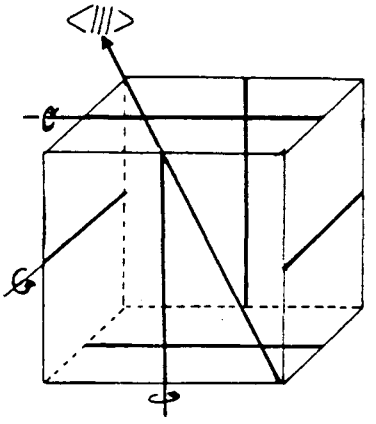

Figure 2.5 Each octant of the unit cell has its own unique three fold axis. However, considering the non-diagonal face bisectors in each octant as two fold rotation axes (with the direction of rotation as shown) and by successful rotation of the octants about these axes the whole unit cell can be generated.

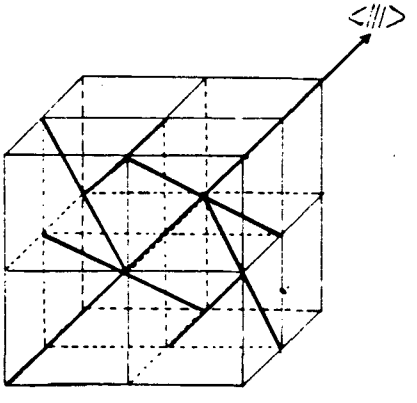

Figure 2.6 The complete unit cell as generated from one octant by the above rotation operations. The three-fold axis in each octant and the single unique <111> three-fold axis of the entire unit cell are also shown.

XBL 841-15

$a_0/2$) such that the {c} and [a] sites are located alternately along these directions with a periodicity of a_0'<100>. The distribution of these cations is such that they form a three fold axis along one of the <100> directions in each octant of the unit cell (figure 2.4). The other three fold axes can be generated by using an arbitary octant as a reference one and by rotating the three fold axis of this reference octant by 180° around one of the rotational face bisectors shown in figure 2.5. The resultant distribution of three fold axes in each unit cell is shown in figure 2.6.

This description gives an idea of how the crystal structure is generated. However, what is required, in order to facilitate the applicability of the experimental technique to be developed, is an idea of whether a normal (defect free) single crystal of this struture can be resolved in some crystallographic projection into alternating planes, each one containing one and only one of the three candidate sites; i.e., whether the crystal structure is layered or not . The [100], [110] and [111] projections of this structure are shown in figures 2.7-2.9 respectively and were generated (Benemma & Giess, 1981) by the ORTEP (Johnson, 1965) computer graphics program. It is not intuitively (or, for that matter, even from close inspection) evident from these projections that the crystal structure is layered. All that, that can be inferred from them, is that it is possible in the [100] projection (figure 2.7) to isolate the octahedral sites from the others, for in this projection, the

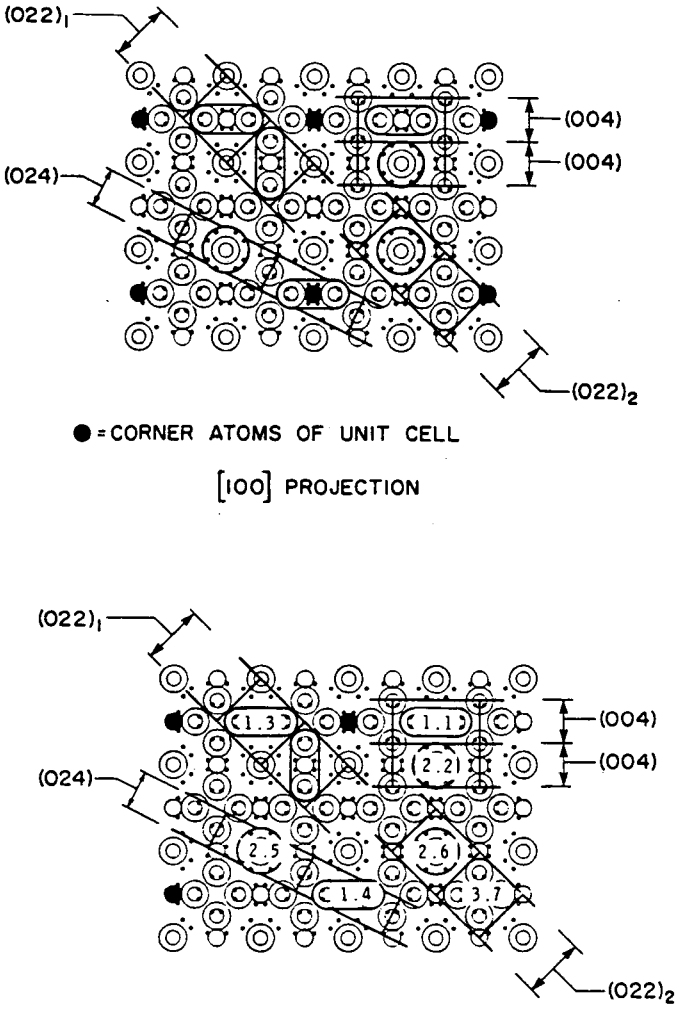

[100] Projection [010] × [001] × [100].

XBL 831-7983

Figure 2.7 [100] projection of the garnet structure. The corner atoms of a unit cell and some of the common crystallographic planes are also indicated. It can be seen that only alternate [008] planes contain octahedral [a] sites. After Bennemma & Giess (1981).

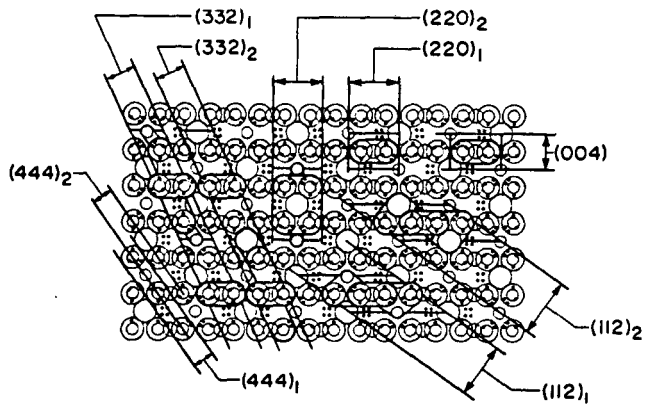

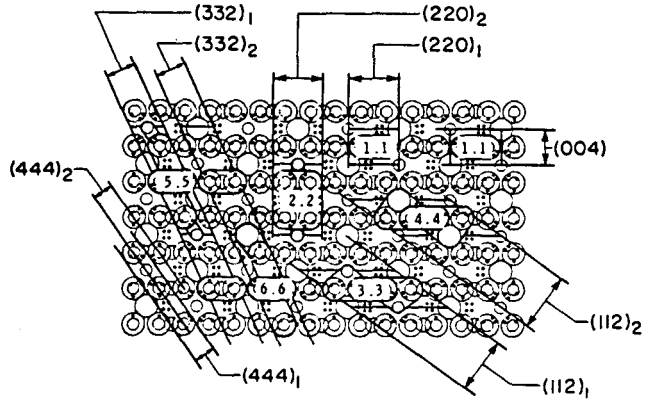

[110] Projection $[\bar{1}10] \times [001] \times [110]$

XBL 831-7985

Figure 2.8 [110] projection of the garnet structure. It is not possible by mere inspection of these projections to conclude that the crystal structure is layered in any of these simple crystallographic planes. After Bennemma & Giess (1981).

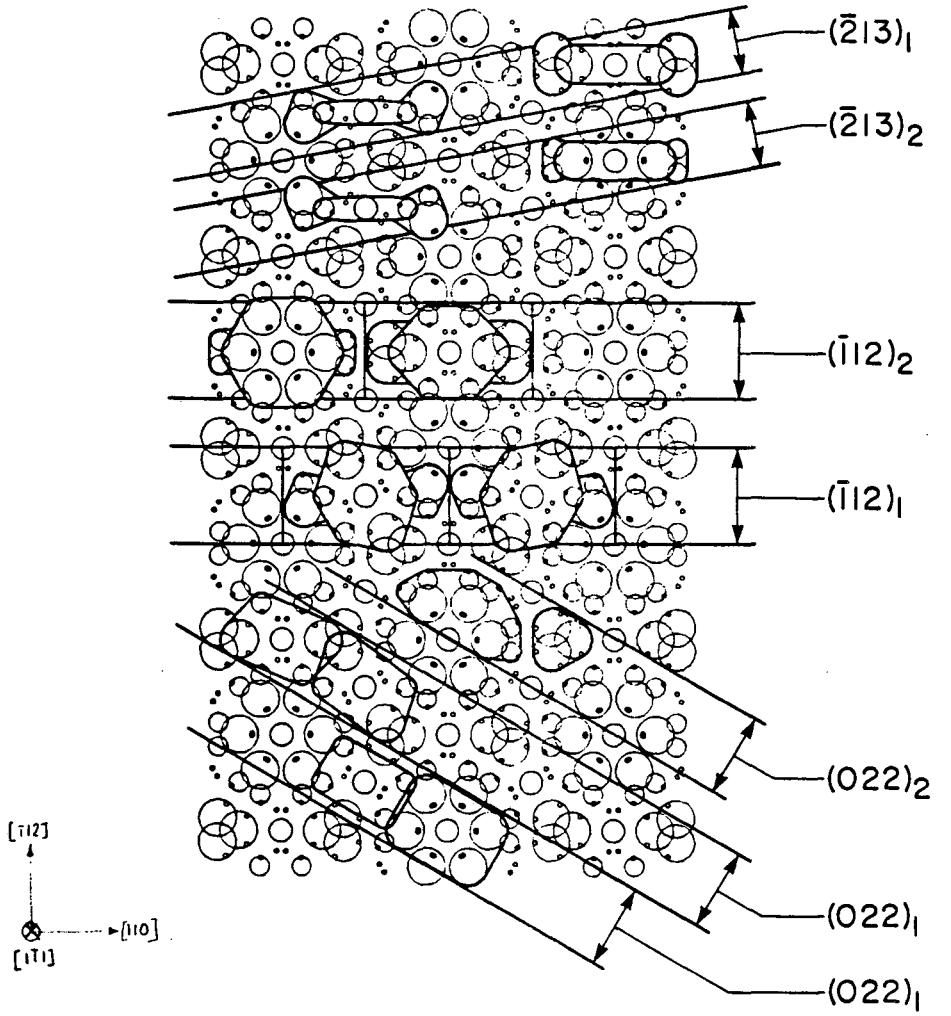

[1$\bar{1}$1] PROJECTION

[1$\bar{1}$1] Projection [110] × [$\bar{1}$12] × [1$\bar{1}$1]

XBL 831-7984

Figure 2.9 [1$\bar{1}$1] projection of the garnet structure. In all these three projections the anions are represented by • for clarity. The cation sites are represented by circles of different diametre depending on the actual size of the crystallographic site. In increasing size they are tetrahedral, octahedral and dodecahedral sites respectively. After Bennemma & Giess (1981).

(008) planes are only alternately endowed with these [a] sites.

II.6.2 Spinels

The mineral spinel $MgAl_2O_4$, like the garnet structure described earlier, has eight formula units per unit cell. However, the oxygen ions in this structure form an almost close packed face-centred cubic arrangement, unlike the garnets, where close packing of the oxygen ions is not possible because of the large ionic radii of the rare earth ions. The cations are distributed in either the tetrahedral or octahedral sites of this close packed structure. Even though there are 64 tetrahedral sites and 32 octahedral sites per unit cell, only 8 and 16 respectively are occupied.

Wycoff (1960) describes the spinel space group as $Fd3m(O_h^7)$. This unit cell can be divided into eight octants of two categories, each having different contents. The distribution of the two types of octants in an unit cell are shown in figure 2.10a and the details of each of the two categories of octants are shown in figure 2.10b. The significance of the oxygen parameter, u is delineated in figure 2.11. The projection of a unit cell of the spinel structure on to cubic face for a perfect structure (u=0.375) is shown in figure 2.12. The coordinates of the ions indicated in figure 2.12 were the ones used in all calculations pertaining to this crystal structure. Finally a [100] projection in perspective of 2x2x2 unit cells is shown in figure 2.13. It is

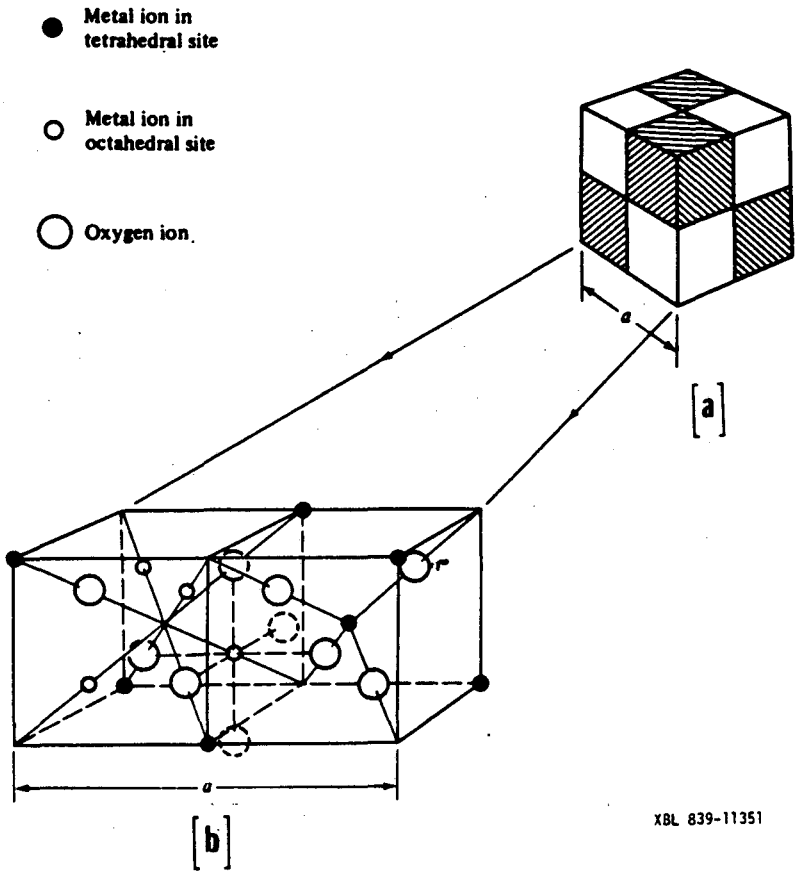

Figure 2.10 The crystal structure of a cubic spinel
(a) The spinel unit cell is made of eight formula units, divided into eight octants. However, there are only two types of octants and they are distributed alternatively as shown (shaded and unshaded).
(b) Contents of two of the lower octants. The octant on the left has tetrahedral sites at four of the eight corners of the octant along with four occupied octahedral sites as shown. The right octant has no occupied octahedral site but has an additional tetrahedral site at the centre of the octant.
After Smit & Wijn (1959).

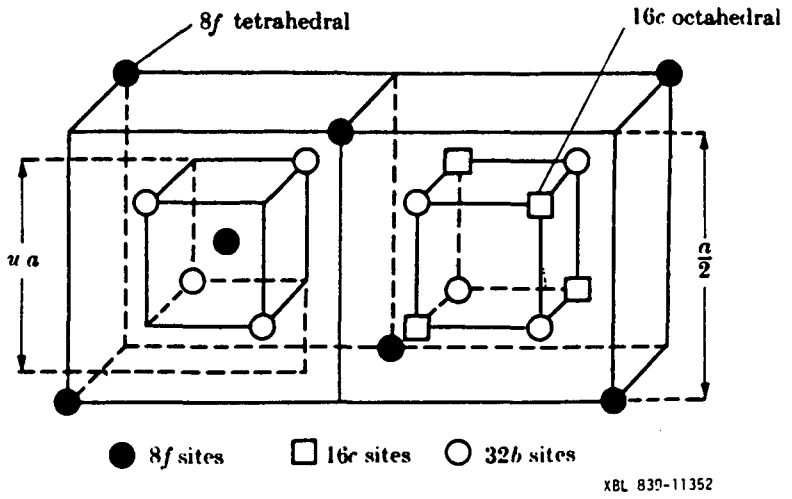

Figure 2.11 Two of the eight octants illustrating the definition of the oxygen parametre,u. For an ideal spinel u=0.375. After Standley (1972).

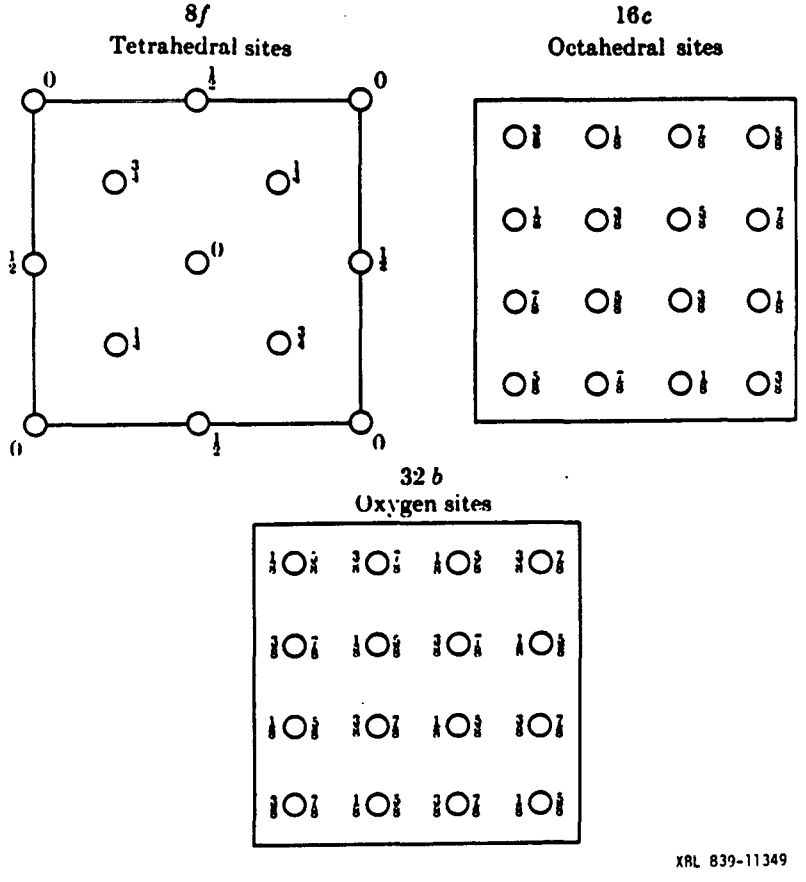

Figure 2.12 [100] projection of the normal spinel unit cell. The coordinate (distances perpendicular to a cube face as a fraction of the lattice parametre) of the occupied tetrahedral and octahedral sites along with those of the oxygen ions, in a normal spinel, that were used in the calculations are indicated. After Standley (1972).

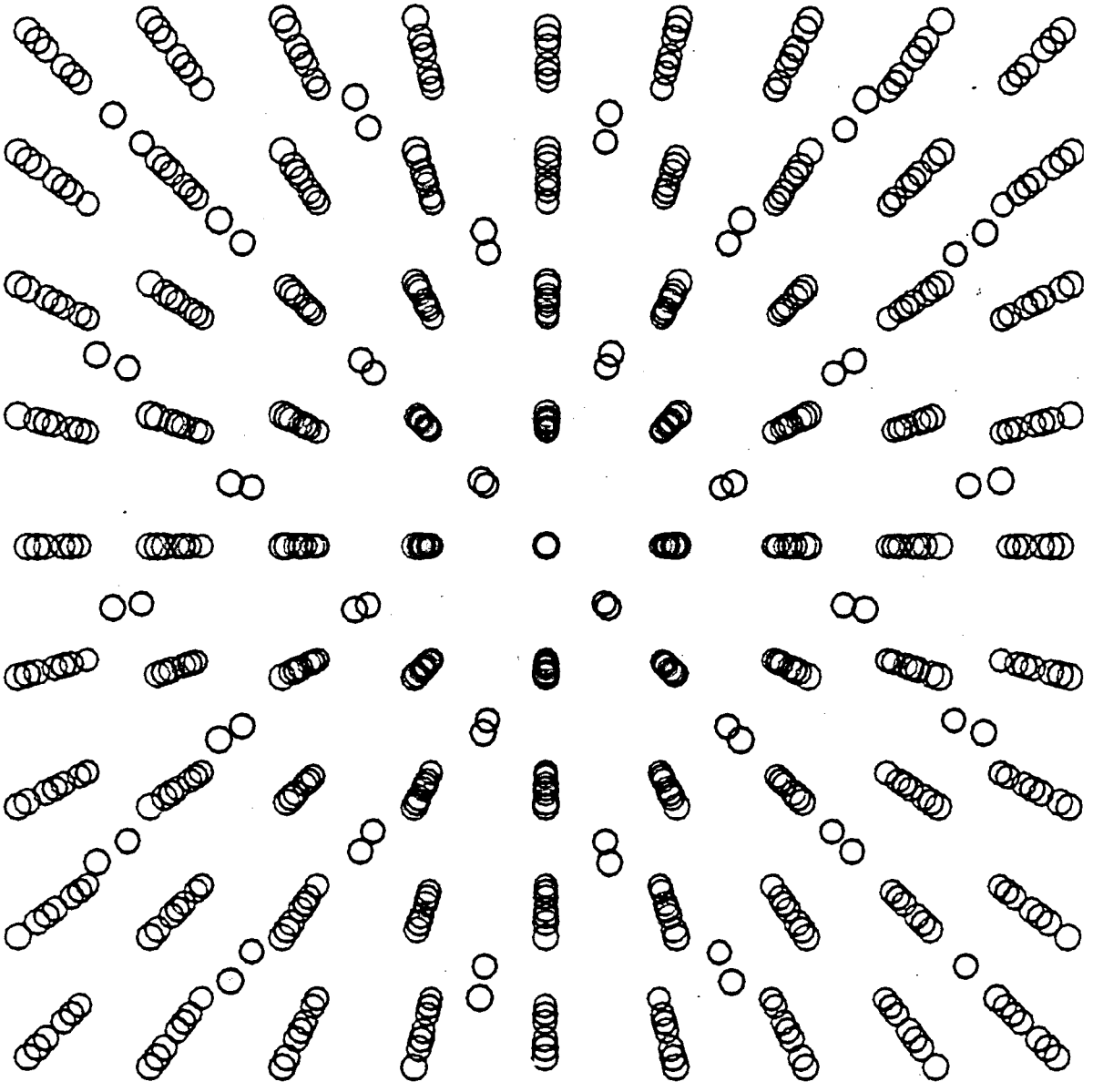

BBC 831-904

Figure 2.13 A [100] projection in perspective of the spinel structure. 2x2x2 unit cells are shown. Blue circles represent oxygen, green circles represent magnesium and red circles represent aluminium. Notice that the structure is layered, i.e. in this projection it can be resolved into alternating [004] planes containing either Mg (tetrahedrally coordinated) or Al (octahedrally coordinated) ions.
(Author's note: illustration originally in color)

evident that in this projection, the crystal structure is a layered one and can be resolved into alternating (004) planes containing exclusively, either the tetrahedrally coordinated Mg atoms or the octahedrally coordinated Al atoms. This fact is particularly beneficial in the demonstration of the experimental technique of channelling enhanced microanalysis.

II.7 Results of the characteristic x-ray production calculations at 100Kv

In this section , the results of the calculation of the orientation dependence of electron-induced characteristic x-ray production at an accelerating voltage of 100KV are presented for two compounds; $MgAl_2O_4$ (spinel) and $Y_3Fe_5O_{12}$ (garnet).

As discussed earlier, the spinel structure in the [100] projection can be resolved into alternating (400) planes of Al_2O_4 with Mg atoms distributed mid-way between them (figure 2.13). Hence, x-ray intensities for Mg and Al distributed in the tetrahedral and octahedral sites (respectively) of a normal spinel were calculated for a 15-beam ($-7\bar{g}$ to $+7\bar{g}$) , $\bar{g}$ = 400 systematic excitation condition and over a range of incident beam orientations. The orientation of the incident beam were specified by varying the values of the excitation error k_x/g which is defined such that $k_x/g=0.5$ for the exact first order Bragg diffraction condition. Figure 2.14 shows the results of the calculations. It can be seen that the standing wave is localized

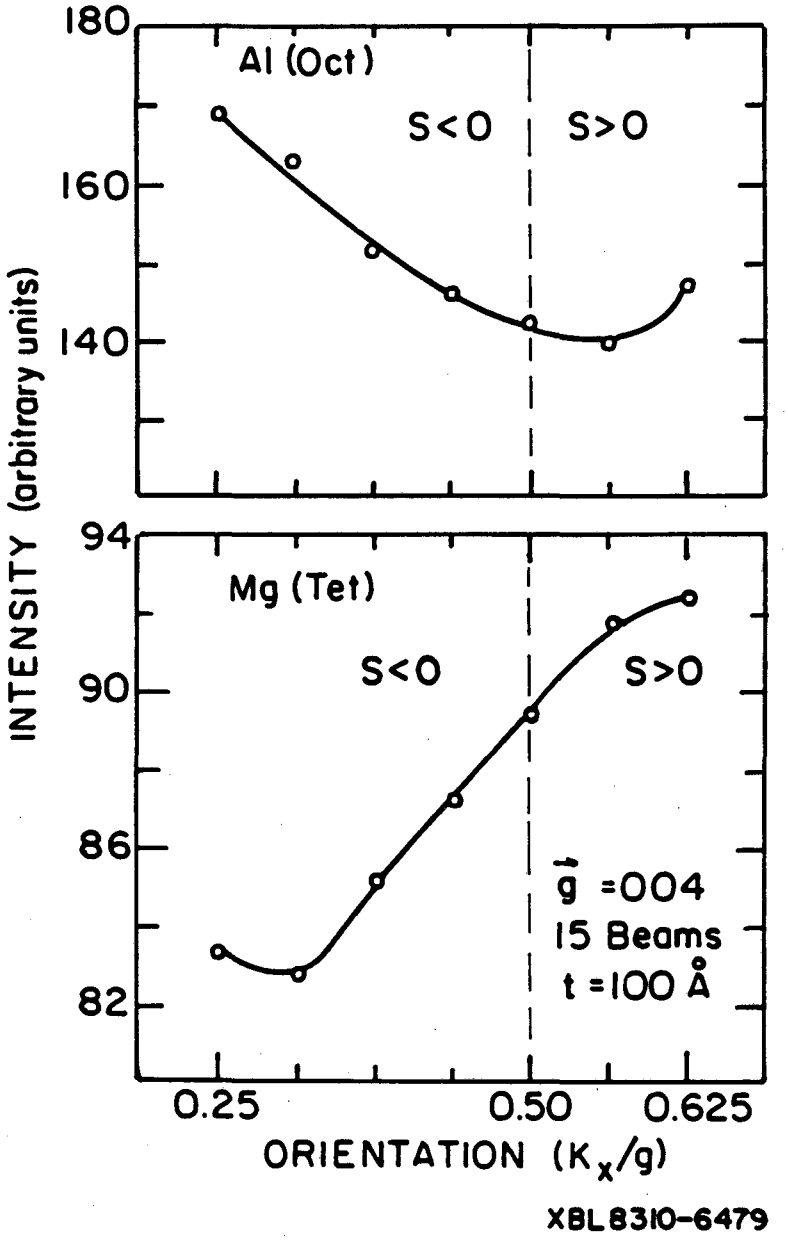

Figure 2.14 Results of the orientation dependent x-ray emissions for spinels. A 15-beam, g=004 systematic excitation condition (-7g to +7g) and a specimen thickness of 100 A° were the conditions used. Note that there is an enhanced emission of the octahedrally coordinated Al for negative excitation error (s<0) of the first order Bragg diffraction condition. The orientation dependence of the tetrahedrally coordinated Mg is reversed, i.e., an enhancement for positive excitation error (s>0) of the first order Bragg reflection.

on the tetrahedrally coordinated Mg atoms for positive excitation errors ($k_x/g > 0.5$) and on the octahedrally coordinated Al atoms for negative excitation errors ($K_x/g < 0.5$) of the first order Bragg diffraction condition with a correspondingly enhanced characteristic x-ray production.

This predicted orientation depedence of the characteristic x-ray emissions is in good agreement with the experimental results of Tafto & Spence (1982a) for spinels. This served as a verification for the validity of the theoretical formulation.

The garnet structure is very much more complicated. It is not possible by mere inspection of the crystal structure to identify crystallographic planes where a particular site is predominant. This has been discussed in the last section.

Therefore, x-ray emission intensities were calculated for complete rare earth occupation in any one of the three crystallographic sites of the prototype compound YIG for different systematic excitation conditions (i.e., $\bar{g} = 00\bar{2}$, $\bar{g} = \bar{2}20$, $\bar{g} = 1\bar{2}1$ etc.) to determine an orientation with specific-site sensitive characteristic x-ray emissions. These 11-beam calculations, for systematic excitation conditions ($-5\bar{g}$ to $+5\bar{g}$) were performed for a range of crystal thicknesses (250A°-2000A°) and for a range of incident beam orientations ($0<k_x/g<2$). The x-ray production was found to be insensitive to crystallographic orientations, irrespective of the site occupation, for excitations of the $\bar{g}=00\bar{2}$ and $g=\bar{2}20$ systematic diffraction conditions. On the

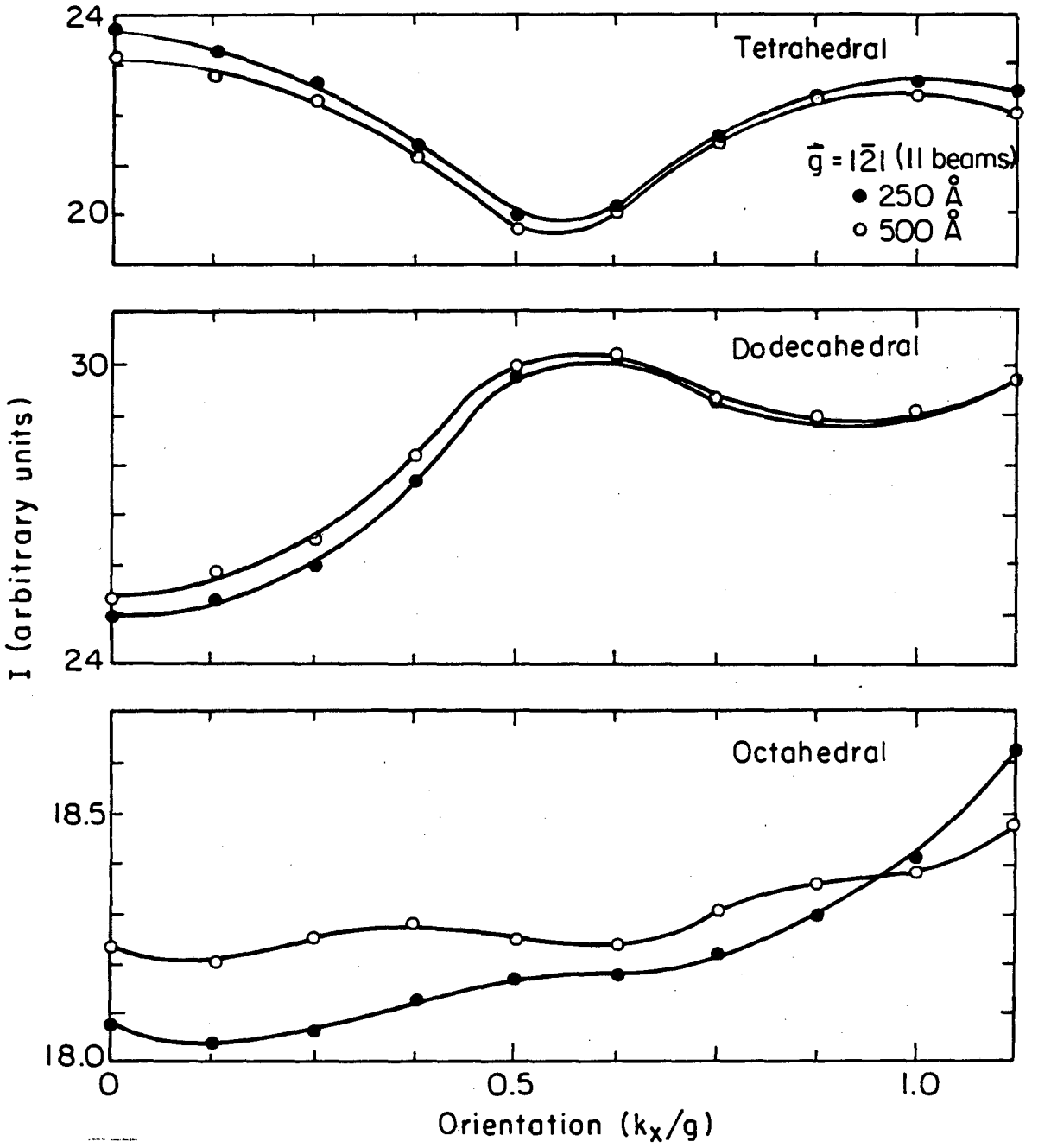

Figure 2.15 Calculated orientation dependence of the characteristic x-ray emissions of the garnet structure. A 11-beam (-5g to +5g), $\bar{g}=1\bar{2}1$ systematic excitation condition and two thicknesses (250 A° & 500 A°) were the conditions used. For these conditions, it can be seen that the emission product is site sensitive, i.e., channelling for tetrahedral site substitutions, blocking for dodecahedral site substitutions and an indifference to orientation (notice change in the scale for intensity) for octahedral site substitutions of the rare earth element.
Similar calculations were made for systematic excitations of other $\bar{g}$ vectors but were found to be such that the emission product is insensitive to either occupations or incident beam orientations.

XBL 831-5156

other hand, strong orientation dependence for the $\bar{g}=1\bar{2}1$ systematic excitation condition were predicted at the exact first order Bragg diffraction conditions ($k_x/g = 0.5$) and for negative and positive excitation errors (figure 2.15), i.e., channelling for dodecahedral site substitutions of the rare earth additions, blocking for tetrahedral substitutions and an insensitivity to orientation for octahedral substitutions.

II.8 General Discussion

It would be prudent at this point to examine the assumptions and limitations of the theoretical (real space) formulation used in the calculation of electron induced characteristic x-ray emissions.

The single most important assumption is that the associated inner shell excitations are highly localized (to the point of being approximated by delta functions at the mean atomic positions) when compared with thermal vibrations. This assumption has been made in light of the following arguments.

Gjonnes and Hoier (1971) have estimated the "radius" of 1s orbitals to be approximately 0.02 A° using electronic band structure calculations, i.e. " the probability density for the 1s electron in a medium or heavy atom is so narrow that any distribution associated with the K-shell will also be narrow". Bourdillon, Self & Stobbs (1981) have used an alternative approach, estimating the time τ over which a virtual photon is

exchanged between a fast electron and the excited particle and converting that (following Howie, 1979) using the uncertainty principle to give an expression for the limiting value of the impact parameter, b. Using a number of radically simplifying arguments they have shown that an expectation value for the impact parameter can be computed as

$$\langle b \rangle = 1.24\,\hbar\, v \,/\, 4.46E_c \qquad (2.66)$$

where E_c is the initial energy for the onset of the transition. The value of the impact parameter, calculated using the above expression for the values of the energy loss relevant to the characteristic x-ray emission for the elements of interest, are shown in Table 2.2.

These values of the impact parameter along with the values obtained from electronic structure calculations suggest that the approximation is indeed a reasonable one.

Table 2.2

Calculated expectation values of

the impact parameter

Emission	E_c(KeV)	<b>(nm)
Al(K_α)	1.486	0.0231
Mg(K_α)	1.253	0.0274
Fe(K_β)	7.019	0.0049
Sm(L_α)	6.656	0.0068
Lu(L_α)	9.281	0.0037
Co(K_α)	6.930	0.0048
Mn(K_α)	5.898	0.0058

A source of inelastic scattering not include in this theory is phonon scattering. This highly localized scattering event with significant contributions to anomalous absorption has been treated by a number of different authors (Takagi, 1958a; Takagi, 1958b; Whelan, 1965b; Hall & Hirsch, 1965). The simplest treatment is to calculate Bragg scattering by modifying the scattering factors as $f(g) \exp[-\alpha(g)]$ where $\alpha(g)$ is the accepted Debye-Waller factor. These thermal vibrations could be incorporated (Cherns, Howie & Jacobs, 1973; Otsuki, 1966) by considering that the region of x-ray production is approximated by a delta function broadened by thermal vibrations such that the

imaginary part of the crystal potential P(r) has Fourier components P_g given by

$$P_g = P_0 \exp(-\alpha g^2) \tag{2.67}$$

Again this would be valid only because the localizations for inner shell excitations is much smaller than the thermal vibration amplitudes. The modified expression for characteristic x-ray emissions would then be

$$N_x = \int |\phi(r)|^2 \sum_g P_g \exp(i\bar{g} \cdot \bar{r})\, d^3r \tag{2.68}$$

where as in equation (2.55) the integral would be over the volume of the crystal.

However, Cherns, Howie & Jacobs (1973) have shown that the reduction of the orientation dependent characteristic x-ray emission due to the thermal vibrations is not significant for temperature rises upto 200 °C when compared with reductions due to the angular spread.

Finally, from the experimental point of view, one of the significant advantages of the use of the orientation dependence of electron induced characteristic x-ray emissions in specific site occupation studies over other accepted techniques, particularly in the studies of magnetic materials, is that this technique could be

potentially applied to study local areas of the specimen. This requires the use of a convergent electron probe. The theory developed here is strictly valid for parallel illumination only. If we want to be rigorous in applying this theory to cases where convergent probes of the order of a few hundred A° are used then it should be suitably modified. This should pose no difficulties and involves resorting to the accepted method (Duval, Duval & Henry, 1974; Duval & Henry, 1974) of averaging over a whole range of incident angles.

II.9 Effect of acceleration voltage on the orientation dependence of characteristic x-ray emissions: The Inversion Voltage effect

II.9.1 Introduction

In an earlier section (II.7) it was shown that the characteristic x-ray emissions for a $MgAl_2O_4$ spinel are indeed dependent on incident beam orientations. Those calculations were done for an acceleration voltage of 100 KV. Since the channelling or blocking is a result of the dynamical scattering of an incident plane wave in a periodic crystal, it is reasonable to expect that this phenomenon might also be dependent on the wave length of the incident electrons. In other words, the acceleration voltage might independently influence this orientation dependence. To verify and understand this analogous phenomena, the effect of

acceleration voltage on the orientation dependence was calculated and in this section those results are presented. The formulation used was the one developed in section (II.4) and calculations were done using equation (2.58).

II.9.2 Results of the calculations: "The Inversion Voltage"

Calculations were done for a 15-beam ($\bar{g}$=400) systematic excitation condition, over a range of incident beam orientations ($0 \leq k_x/g \leq 1.0$) and acceleration voltages (60-400KV). Figure 2.16 describes the variation of the intensities of the characteristic x-ray emissions for positive ($k_x/g \geq 0.5$) and negative ($k_x < 0.5$) excitation errors of the first order Bragg reflection as a function of the acceleration volatge. The ordinate $\mathscr{R}$ is a normalized measure of the orientation dependence and is defined as

$$\mathscr{R} = \frac{R_1 - R_2}{R_1 + R_2} \qquad (2.69)$$

where R_i is the ratio of N_{Al}/N_{Mg} at their corresponding positions of extrema and i takes the value 1 or 2 for negative ($k_x/g < 0.5$) and positive ($k_x/g \geq 0.5$) excitation errors of the first order Bragg reflection, respectively.

A positive value of $\mathscr{R}$ signifies a maxima of the characteristic x-ray intensity of Mg (N_{Mg}) for some orientation with positive excitation errors and a minima for negative excitation errors of the first order Bragg diffraction condition.

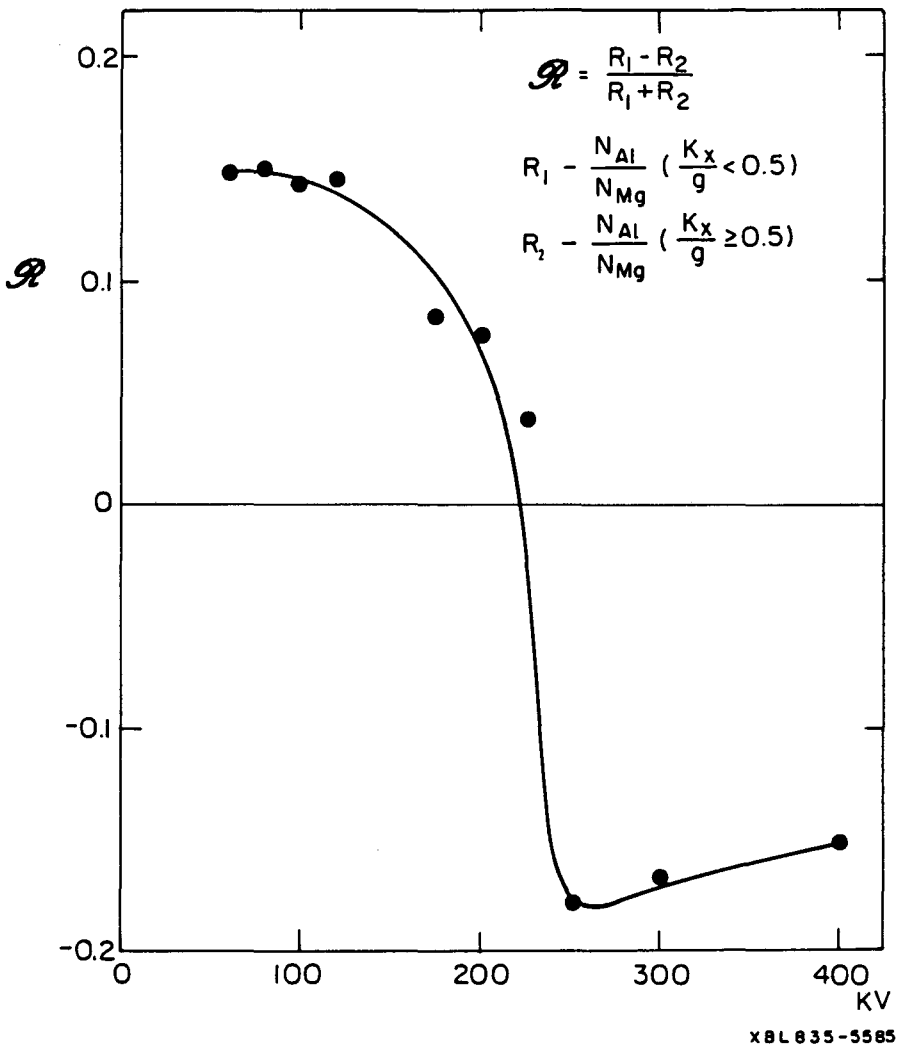

Figure 2.16 Variation of the electron-induced characteristic x-ray emissions with both orientation and acceleration voltage. Calculations were performed for 15 beams, systematic exctation condition (g=400).

It also signifies an exactly opposite behaviour for Al (N_{Al}). This is what one observes at an acceleration voltage of 100 KV and hence these calculations are in agreement with experimental observations.

However, it can be seen that at higher acceleration voltages, this orientation dependence though not particularly enhanced in magnitude exhibits an interesting reversal in character, and in figure 2.16 this is represented by $\mathscr{R}$ taking negative values. The significance of the change in the sign of $\mathscr{R}$ can be best understood by referring to figure 2.17. This is drawn to illustrate the idea and corresponds to a two beam calculation ignoring the Bloch wave interference terms, i.e. an independent model. A change in the sign of $\mathscr{R}$, above some acceleration voltage, which is referred to as the "inversion voltage", implies that the orientation dependence of N_{Al} and N_{Mg} are interchanged (Fig. 2.17). Further, the calculations indicate that the exact orientation (excitation error) of a maximum or a minimum also varies slightly with the acceleration voltage.

In order to isolate the role of the acceleration voltage alone, the variation of the ratios of characteristic x-ray intensities as a function of the acceleration voltage were calculated for a number of different but fixed orientations. They were normalized as before with $R_1 = N_{Al}/N_{Mg}$ at the orientation of interest and $R_2 = N_{Al}/N_{Mg}$ at the symmetric orientation. The results are plotted in figure 2.18. From this plot it can be seen that at the inversion voltage, these normalized ratios of

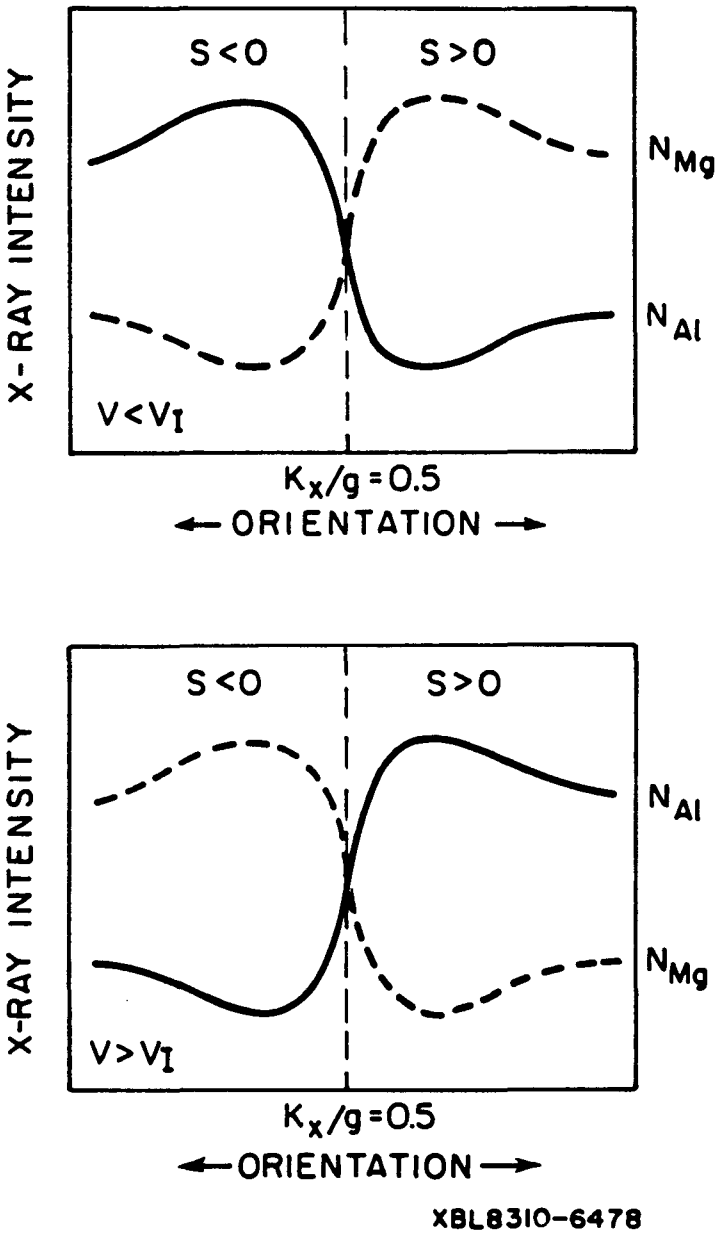

Figure 2.17 Significance of the change in the sign of the normalized parametre $\mathscr{R}$. For values of the acceleration voltage $V>V_I$ the orientation dependence is identical to what has been experimentally observed. For $V>V_I$ the roles are reversed, i.e., increased emission of Al for $s>0$ and an enhancement of the emission of Mg for $s<0$ are observed. The corresponding change in the value of $\mathscr{R}$ would be from a positive to a negative value.

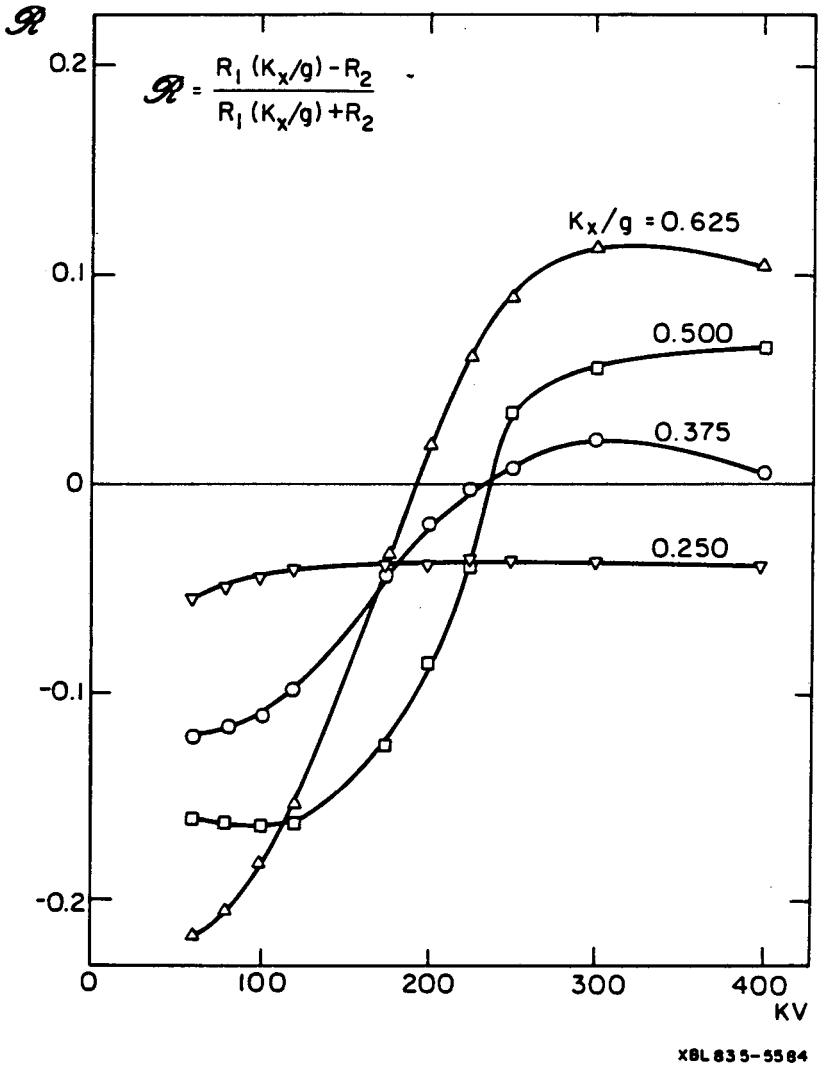

Figure 2.18 Variation of the electron induced characteristic x-ray emissions as a function of the acceleration voltage for fixed excitation errors. Normalization is done with respect to a symmetric orientation.

intensities do indeed undergo a reversal in character at each and every orientation. However, over the range of interest ($0.25 \leq k_x/g < 0.625$) the effect is more pronounced as k_x/g increases.

II.9.3 Discussions

The results of these calculations are very interesting, for they suggest that one can use this voltage dependence to determine qualitatively site occupations in the different crystallographic sites of the constituent elements of a single crystal material. The only requirement is that the inversion voltage be known in advance. Experimental measurements of the intensity of characteristic x-ray emissions at acceleration voltages greater and less than the inversion voltage should be made and from the nature of the change in the sign of the normalized parameter ($\mathscr{R}$), positive to negative or vice versa, the site occupancies can be qualitatively determined.

It is worth discussing the relationship of this "inversion voltage" effect to the conventional "critical voltage" effect. Acording to Lally, Humphreys, Metherrel & Fisher (1972), for a centrosymmetric crystal set at the symmetric Laue position for the second order Bragg reflection ($2\bar{g}$), a change in the symmetries and excitation amplitudes of the Bloch waves is observed, at a particular "critcal voltage" characteristic of the crystal structure and its constituent elements. An alternative

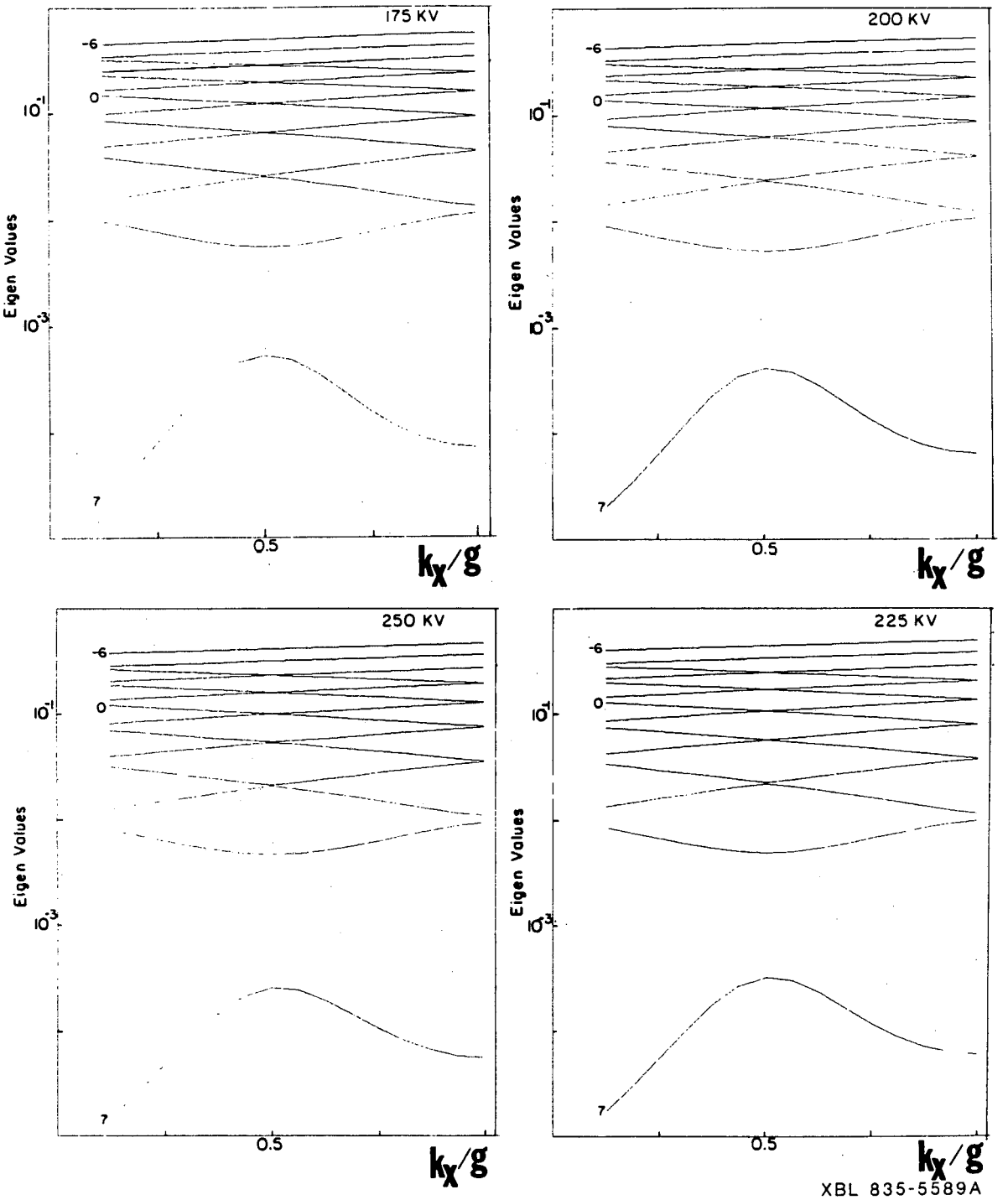

Figure 2.19 Dispersion surfaces [Eigen values of the Bloch waves vs. orientation k_x/g] for different acceleration voltages.

way of interpretting this is that at the critical voltage, the eigenvalues of the Bloch waves become degenerate. In figure 2.19, the dispersion surfaces calculated at 25 KV intervals over the range of interest, with the thickness (t) modified at each voltage such that λt is a constant, have been plotted. These dispersion surfaces indicate that for this particular case of the crystal oriented at the first order Bragg reflection ($1\bar{g}$) condition, exact or with positive or negative excitation errors, no observable degeneracy in the Eigenvalues of the Bloch waves are present. This indicates that the nature of this sensitivity of electron-induced characteristic x-ray emissions to the acceleration voltage, which is termed here as the "inversion voltage", is different from the conventional critical voltage effect. Another point of departure is that the critical voltage effects are observed at the second order Bragg diffraction condition and at much higher acceleration voltages (approximately 800-1000 KV) for such compounds with low atomic number elements. This effect, on the other hand, is predicted at an orientation corresponding to the first order Bragg reflection conditions and at much lower acceleration voltages (between 175 and 250 KV). However, a change in the acceleration voltage or the incident beam orientation (specimen tilt) should have similar effects in so far as they independently change the diagonal elements of the dynamical scattering matrix. Further calculations along with a careful scrutiny of the corresponding scattering matrix elements to look for any systematic dependence, different from that which

characterizes the critical voltage and an experimental verification of this phenomenon of the inversion voltage are in progress to understand this anamoly.

CHAPTER III

EXPERIMENTAL DETERMINATION OF THE SPECIFIC SITE OCCUPATIONS OF RARE EARTH ADDITIONS IN THIN OXIDE FILMS BY THE ORIENTATION DEPENDENCE OF CHARACTERISTIC X-RAY EMISSIONS

III.1 Introduction

III.2 Experimental

2.1 Specimen preparation

2.2 Analytical transmission electron microscopy

III.3 Results

III.4 Analysis

4.1 Least squares refinement

4.2 Error analysis

III.5 Discussion

III.1 Introduction

The controversial theories that are used to explain the growth induced uniaxial anisotropy in liquid phase epitaxially grown garnet films have been alluded to in Chapter I. The details are reviewed in Appendix 1. However, there is one consensus: this phenomenon is definitely determined by site occupancies (a conclusion based on annealing experiments) even though the question," Which sites are involved?" is not satisfactorily answered. This is the larger motivation for this work and a complete answer to this question of site occupations and their relationship to uniaxial anisotropy in these compounds would constitute an entire dissertation in itself. Therefore, we are restricted in our goals to demonstrate the applicability of the technique developed thus far, to this specific problem, as the garnet structure is sufficiently complicated and cannot be resolved by mere inspection into alternating planes containing certain specific sites in any crystallographic projection. The results of the calculations described in the last chapter indicate that the orientation dependence of characteristic x-ray emissions in this structure are indeed specific site sensitive for a $\bar{g}=1\bar{2}1$ systematic excitation condition.

The characteristic x-ray emissions for a $\bar{g}=1\bar{2}1$ systematic excitation condition and at those specific site sensitive orientations of the incident electron beam specified by the theory were experimentally measured. The data was then

refined employing a constrained least squares analysis to give probabilities for the occupation of rare earth additions in the different crystallographic sites of the garnet lattice. The details of this exercise and an analysis of the results concludes this chapter.

III.2 Experimental

III.2.1 Specimen preparation

Samples of nominal melt composition $Y_{1.7}Sm_{.6}Lu_{.7}Fe_5O_{12}$, 0.94 μm thick, grown on GGG substrates by liquid phase epitaxy, at a growth temperature of 969°C and a growth rate of 1.76 μm/min, were studied. Details of the preparation of these samples (liquid phase epitaxial growth), which were supplied by Bell Labs, are given elsewhere (Mathews, 1975).

Thin foils of these samples for observation in a transmission electron microscope (TEM) equipped with an energy dispersive x-ray (EDX) detector were prepared by the routine ion milling technique. However, some minor changes in the case of these LPE grown thin films were introduced. Ultrasonically cut disks of 3mm diameter were mechanically thinned to a thickness of 35-50 microns (determined by optical microscopy) and then milled with argon ions from the side of the substrate only. An accleration voltage of 6-8 KV, a specimen current of approximately 20 microamps and an incidence angle of 18° were the

normal milling conditions. This gave a very thin electron transparent region of the film. However, some surface pitting and damage were observed at this stage and were eliminated by cleaning the specimen in an ion-milling machine using Ne (a lower atomic weight inert gas) ions at reduced acceleration voltages. In fact this problem could altogether be avoided by using the latter as the milling medium, even though this is a considerably slower and time consuming process.

The garnet films grown on the substrates are subjected to residual strains because of the slight mismatch of the cooling rates between the film and substrate. On ion milling, the lack of the substrate support caused many of the films to buckle rendering them useless for TEM observations. This persistent limitation of the specimen preparation technique could not be avoided by any systematic procedure,but could only be circumvented by preparing a large number of specimens.

III.2.2 Analytical & Transmission Electron Microscopy

Experiments were performed on a Philips 400ST analytical transmission electron microscope fitted with a LaB_6 filament and an EDAX energy dispersive analyser. The detector configuration was such that the maximum x-ray collection was achieved for a take-off angle of 20° (a specimen tilt of 10° towards the detector). A low background double tilt specimen holder to reduce x-ray background were used in all experiments.

Stray x-ray generation was further minimized by using gridless self supporting specimens. The specimen thicknesses were estimated by CBED to be approximately 50nm. The incident beam divergence was a few milliradians and the probe diameter was 50-100 nm. The latter is determined by the level of contamination. The characteristic x-ray emissions were collected at different orientations of the collimated electron beam based on the calculations described earlier. A strong $\bar{g}=1\bar{2}1$ systematic row was excited and spectra collected at six different orientations of the incident electron beam :

(1) Symmetric orientation; $k_x/g = 0$

(2) First order Bragg diffraction with small negative excitation error ($s < 0$); $k_x/g \cong 0.375$

(3) Exact first order Bragg diffraction; $k_x/g = 0.5$

(4) Small negative deviation from the second order Bragg diffraction; $k_x/g \cong 0.875$

(5) Exact second order Bragg diffraction; $k_x/g = 1.0$

(6) Second order Bragg diffraction with small positive deviation parametre; $k_x/g \cong 1.125$

The specimens were oriented in all experiments using either convergent beam electron diffraction or the Kikuchi line method described earlier.

In order to ensure proper statistics, spectra were collected (at the appropriate orientations) for a total counting time of 600 seconds and a counting rate of ~3000 counts/sec. A hole count was taken at periodic intervals and subtracted along

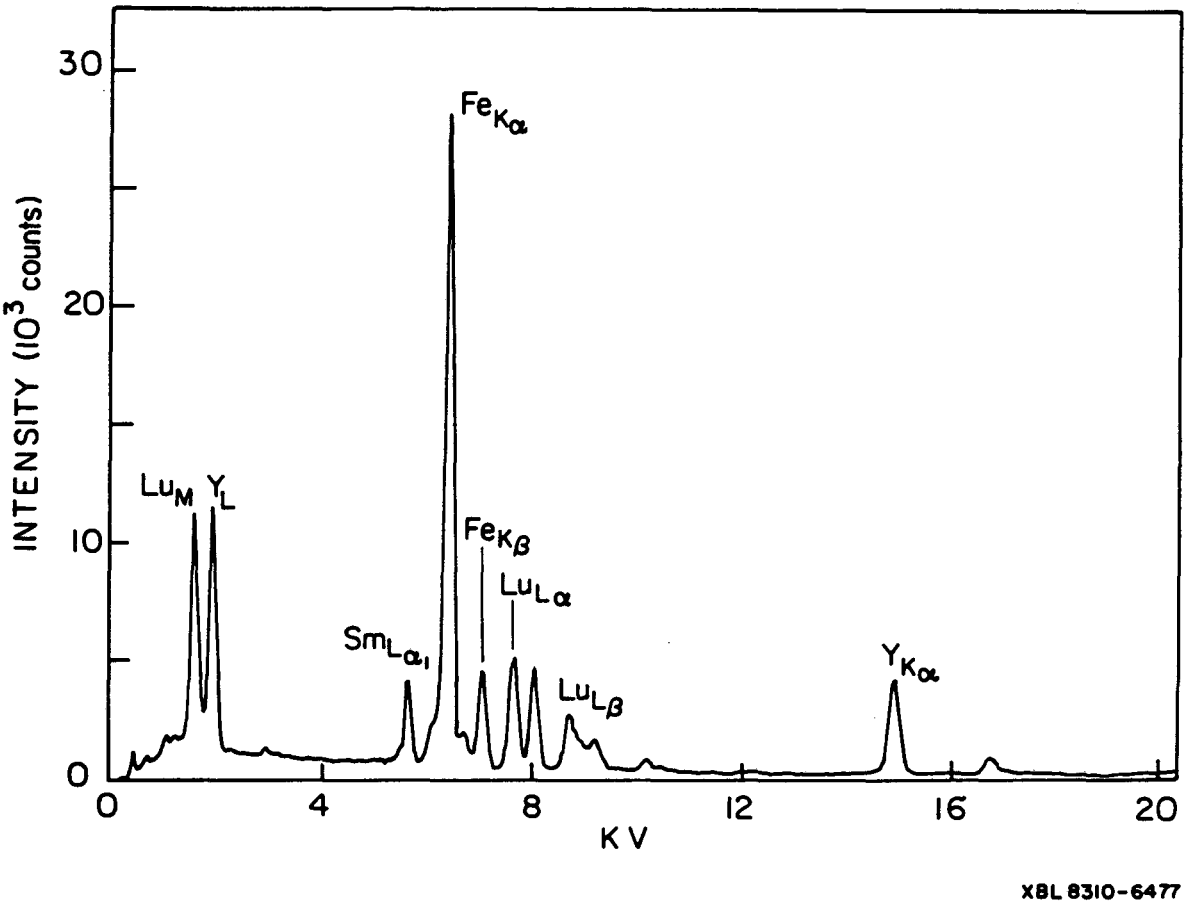

Figure 3.1 A typical energy dispersive x-ray spectra (before background subtraction) with all the characteristic x-ray peaks identified and labeled.

with the continuous background from the spectra. A typical spectra before background subtraction with all the relevant characteristic x-ray peaks identified and labeled is shown in Fig. 3.1.

III.3 Results

The integrated intensities for the two rare earth additions of interest, Sm & Lu, after subtraction of the continuous background, at the orientations mentioned earlier are shown in Table 3.1. Because of the large counting time (600 secs) and the susceptibility of the specimen to damage and contamination, the spectra were collected at a different specimen sampling area for each orientation of the incident electron beam (specimen tilt). Care was taken to ensure that the specimen thickness was not significantly different for the different acquisitions. However, small differences in counting rates or changes due to the small displacements of the probe had to be incorporated in the analysis. This was done by scaling the integrated elemental intensities (Table 3.1) using scaling factors that are actually normalized ratios of the total integrated intensities of the whole spectra (Table 3.2). This gave the normalized integrated elemental intensities for the two rare earth additions (Table 3.3). The standard deviations of the observations are $\sim 0.5\%$ and $\sim 0.65\%$ for $Lu(L_\alpha)$ and $Sm(L_\alpha)$ repectively.

Table 3.1
Integrated Elemental Intensities

k_x/g	0	0.375	0.5	0.875	1.0	1.125
$Lu(L_\alpha)$	57061	51324	61452	50142	60061	59541
$Sm(L_\alpha)$	35839	32761	39785	32073	38277	37546

Table 3.2
Scaling Factors

k_x/g	0	0.375	0.5	0.875	1.0	1.125
Total Counts	1606095	1475254	1788690	1429993	1753256	1688060
Scaling Factor	1.1231	1.0317	1.2508	1.0000	1.2261	1.1805

Table 3.3
Normalized Integrated Elemental Intensities

k_x/g	0	0.375	0.5	0.875	1.0	1.125
$Lu(L_\alpha)$	50807	49747	49130	50142	48985	50437
$Sm(L_\alpha)$	31911	31754	31808	32073	31218	31805

The standard deviations of these observations are 0.5% and 0.65% for $Lu(L_\alpha)$ and $Sm(L_\alpha)$ respectively.

The data is statistically significant but a clear agreement with the theoretical predictions for complete substitutions of the rare earth additions in any particular crystallographic site is not obviously evident. This was interpreted to be due to a mixed distribution of the rare earth additions in all the possible crystallographic sites. The probabilities were then determined by a least squares refinement based on the algorithm of constrained least squares by Lawson & Hanson (1974).

III.4 Analysis

III.4.1 Least squares refinement

The integrated elemental intensity was calculated as a summation over all sites of the product of the theoretical value for complete occupation of each site (calculated earlier section II.7) and a weight factor representing the probability of occupation of that specific site. Mathematically this is expressed as

$$I_\eta^z = K_\eta \sum_\alpha B^z(\eta,\alpha)\ p_\alpha^z \qquad (3.1)$$

where

$B^z(\eta,\alpha)$ - Calculated integrated intensity for the element z at the specific orientation η and the complete

occupation of the specific site α

p_α^z - Weight of occupation of site α by the element z to be determined by the refinement. However the refinement is subject to the constraint $p_\alpha^z \geq 0$, for every α and z.

K_η - Scaling factor for the particular orientation η

I_η^z - Theoretical estimate of the experimentally observed integrated intensity of element z for the specific orientation η.

Then an error term was defined as the difference between the experimentally observed intensity and the theoretical estimate obtained above. For each element of interest, i.e. Sm and Lu, the least squares problem with inequality constraints can be stated as the minimization of a summation over all orientations of the square of this error term, subject to the constraint that all the weights are positive. That is

Minimize

$$\mathfrak{F}^z = \sum_\eta \left(\frac{X_\eta^z}{k_\eta} - \frac{I_\eta^z}{k_\eta} \right)^2 \qquad (3.2)$$

subject to

$$p_\alpha^z \geq 0 \quad \text{for every } \alpha \text{ and } z. \qquad (3.3)$$

Here

X_η^z/K_η - Experimentally observed integrated intensities scaled as described earlier for element z and orientation η.

Introducing the differential operator δ we obtain the following condition for the minimum

$$\delta(\mathcal{F}^z) = 0 \tag{3.4}$$

which gives the following matrix equations

$$\underline{\underline{M}}^z \, \underline{P}^z = \underline{V}^z \tag{3.5}$$

with their components given by

$$V_\alpha^z = \sum_\eta X_\eta^z \, B^z(\eta, \alpha) \tag{3.6}$$

and

$$M_{\alpha,\beta}^z = \sum_\eta B^z(\eta, \alpha) \, B^z(\eta, \beta) \tag{3.7}$$

Hence

$$\underline{P}^z = (\underline{\underline{M}}^z)^{-1} \, \underline{V}^z \tag{3.8}$$

Applying this least squares analysis to the data in Table 3.3 for the observed characteristic x-ray intensities and refining it with respect to the intensities calculated using the theory developed earlier, the weights of the occupation for each of the two rare earth additions were obtained (Table 3.4).

Table 3.4

Relative weights for the site occupancy of the RE additions

	Octahedral	Tetrahedral	Dodecahedral	RNORM
Lu	0.2141±0.02	0.0049±0.0005	***	7.778×10^{-4}
Sm	0.1679±0.0164	***	0.0095±0.0007	4.006×10^{-3}

III.4.2 Error analysis

Let the error in the observed spectra be $\Delta X_\eta = 3\sigma = 3\sqrt{X_\eta}$ where σ is the standard deviation of the experimental observation. The errors in this analysis were calculated in quadrature. Hence, the components of the right array $\underline{V}^z$ in the matrix equation

$$\underline{\underline{M}}^z \, \underline{P}^z = \underline{V}^z \tag{3.5}$$

would be given by

$$V_\alpha^z \pm \Delta V_\alpha^z = \sum_\eta [X^z B^z(\eta, \alpha)] \pm \sqrt{\sum_\eta 3 \, \Delta X_\eta^z [B^z(\eta, \alpha)]^2} \tag{3.9}$$

The errors in the weights of occupation of the different crystallographic sites for the two RE additions were then determined by carrying out the least squares analysis for the upper and lower bounds of the values of X_η^z, i.e. $X_\eta^z + \Delta X_\eta^z$ and $X_\eta^z - \Delta X_\eta^z$ respectively.

Finally the credibility of the least squares refinement was established by determining the norm in the L_2 sense, i.e. $R = \left\| \underline{\underline{M}} \, \underline{P} - \underline{V} \right\|$ (RNORM in Table 3.4) and ensuring that this was less than some acceptable value ($\leq 10^{-2}$).

III.5 Discussion

A significant though reasonable assumption in this experimental technique is that the x-ray emission process is

highly localized, i.e. it can be approximated by delta functions at the mean atomic positions. The estimate of the inner shell radii by band structure calculations (Gjonnes & Hoier, 1971) and the calculations of an impact parameter (Section II.8, Table 2.2) for the values of energy loss relevant to the characteristic x-ray emissions for the elements of interest (Sm-L_α and Lu-L_α) based on the simple expression of Bourdillon, Self & Stobbs (1981), bear out this approximation.

Within the limitations of the assumptions of the technique, it can be inferred that the substitution of these rare earth additions in the octahedral sites of this crystal structure is highly probable, with a probability $\geq$ 95%. These results are in good agreement with earlier studies (Suchow & Kakta, 1972; Blank, Nielsen & Biolsi, 1976), particularly for the distribution of the small rare-earth ion, Lu^{3+} which can easily be accomodated in the smaller octahedral site.

A determination of the contribution of the distribution of these additions to the magnetic anisotropy demands the exact knowledge of the valence of these cations in addition to the site occupancy. This is beyond the scope of this technique. However, site specific valence determinations can be made from the orientation dependent chemical shift in a transmission electron energy loss spectrum, as demonstrated (Tafto & Krivanek, 1981) for Fe^{2+} and Fe^{3+} ions in a mixed valence spinel (see section VI.5).

CHAPTER IV

A GENERALIZATION OF ATOM LOCATION BY CHANNELLING ENHANCED MICROANALYSIS

IV.1 Introduction

IV.2 Formulation of the problem and analysis

IV.3 Results and discussions

IV.1 Introduction

So far, a theory of electron induced characteristic x-ray emissions, within the limitations of the approximation that the scattering processes are highly localized, has been developed. Using this theory, the emission product for different site substitutions and different incident beam orientations were calculated for a general non-layered crystal structure (i.e. garnet). From the results of these calculations, the appropriate systematic or "planar" channelling condition applicable to that particular crystal structure was determined and the experiment performed. In this way, one of the limitations of the technique of " Atom location by channelling enhanced microanalysis" or ALCHEMI, that is, its restricted applicability to crystals with a layered structure, can be overcome. This approach was discussed in great detail in the last two chapters where the distribution of the rare earth additions in the different crystallographic sites of magnetic garnet films grown by liquid phase epitaxy were determined.

In the case of layered structure compounds, following Spence & Tafto (1983), it is possible to effect a simplification of the analysis. As pointed out in Chapter I, for such compounds, the appropriate systematic row can be decided by mere inspection of the crystal structure. Further, the characteristic x-ray emissions induced by the channelling or blocking of the incident electrons within the crystal, can provide information on

the specific site occupation of alloying or impurity additions, if and only if an apriori knowledge of the distribution of some reference elements is available. An important requirement is that these reference elements be chosen judiciously (one for each of the alternating planes A and B of the layered structure) in the original compound. In many practical alloys/compounds it might not be possible to choose reference atoms that are uniquely distributed on one and only one of the two alternating crystallographic planes. Further, the alloying concentrations might be reasonably large that they alter the distributions of the constituent elements in the original compound, thereby invalidating the practice of using the original distribution as internal reference standards.

In this chapter a generalization of this technique of ALCHEMI (Spence & Tafto, 1983) which overcomes the above limitations as applied to layered structure compounds is presented. The problem is formulated differently by incorporating the stoichiometry of the original compound. Finally, experimental conditions required to solve some specific poblems are also presented.

IV.2 Formulation of the problem and Analysis

It is required to determine the crystallographic distributions (site occupations) in a stoichiometric compound $(Z_i)_{n_j}(X_j)_{m_j}$ where

Z_i- elements of known distributions in the ideal compound before alloying additions; (i=1.....r)

and

X_j- alloying elements, unknown distributions (j=1.....s)

For the crystallographic projection of interest, let the crystal structure be separable into non-identical, alternating, parallel planes (A,B,A,B....). [Note that this formulation is restricted in its applicability to crystals with only two repeating planes]. Now define

M_{Z_i} - total number of available sites for element Z_i per unit cell in the ideal compound.

$f^{A,B}_{Z_i,X_j}$ - fraction of available sites for elements (Z_i,X_j) on planes (A,B) respectively, per unit cell.

C_{Z_i}- concentration of element Z_i on plane B to be determined in the non-ideal case, i.e. after alloying additions.

$(1-C_{Z_i})$- concentration of element Z_i on plane A.

M_{X_j} - total number of available sites per unit cell for element X_j in the alloy.

C_{X_j} - concentration of element X_j on plane B, also to be determined.

$(1-C_{X_j})$ - Concentration of element X_j on plane A.

and

q - number of formula units of $(Z_i)_{n_i}(X_j)_{m_j}$ per unit cell.

From the crystal structure, for complete occupation of all the crystallographic sites on plane B, an occupancy balance can be written

$$\sum_{i=1}^{r} n_i C_{Z_i} + \sum_{j=1}^{s} m_j C_{X_j} = \frac{1}{q} \sum_{i=1}^{r} M_{Z_i} f_Z^B \qquad (4.1)$$

The characteristic x-ray emission intensity (N) for any element Z_i for the incident beam orientation (η) is expressed as a linear sum of the contributions from each of the parallel planes (A,B,A,B,....)

$$N_{Z_i}^{(\eta)} = P_{Z_i} f_{Z_i}^A M_{Z_i} (1 - C_{Z_i}) I_A^{(\eta)} + P_{Z_i} f_{Z_i}^B M_{Z_i} C_{Z_i} I_B^{(\eta)} \qquad (4.2)$$

where $I_{A,B}^{\eta}$ is the effective Bloch wave intensity in planes (A,B) for the orientation (η) and P_{Z_i} is the scaling factor for

element Z_i.

Similarly for the alloying element X_j,

$$N_{X_j}^{(\eta)} = P_{X_j} f_{X_j}^{A} M_{X_j} (1 - C_{X_j}) I_A^{(\eta)} + P_{X_j} f_{X_j}^{B} M_{X_j} C_{X_j} I_B^{(\eta)} \qquad (4.3)$$

Now define a normalized measure of the orientation dependence

$$\mathscr{R}(\eta_1, \eta_k, Z_1, X_j) = \frac{N_{Z_1}^{(\eta_1)} / N_{X_j}^{(\eta_1)}}{N_{Z_1}^{(\eta_k)} / N_{X_j}^{(\eta_k)}} \qquad (4.4)$$

where

η_1 is any fixed orientation;

η_k are the orientations η_2 through η_T (excluding η_1)

η_T is the total number of orientations to be determined by this analysis,

and

Z_1 is any one arbitarily fixed original constituent.

The numerator of this normalized measure $\mathscr{R}$ is a ratio of the counts for one of the original elements to that of an alloying element at an arbitary given fixed incident beam orientation. The denominator is the same ratio, but at any one of the other orientations $\eta_2 \ldots\ldots \eta_T$.

Substituting from (4.2) and (4.3) one obtains

$$\mathscr{R}(\eta_1,\eta_k,Z_1,X_j) = \frac{f^A_{Z_1}(1-C_{Z_1}) + f^B_{Z_1}C_{Z_1}\beta_1}{f^A_{X_j}(1-C_{X_j}) + f^B_{X_j}C_{X_j}\beta_1} \times \frac{f^A_{X_j}(1-C_{X_j}) + f^B_{X_j}C_{X_j}\beta_k}{f^A_{Z_1}(1-C_{Z_1}) + f^B_{Z_1}C_{Z_1}\beta_k} \tag{4.5}$$

where

$$\beta_k = \frac{I_B^{(\eta_k)}}{I_A^{(\eta_k)}} \tag{4.6}$$

The factor $\mathscr{R}(\eta_1, \eta_k, Z_1, X_j)$ is experimentally determined. One can define, for fixed η_1 and Z_1, $s(\eta_T-1)$ such independent factors or equations.

However, for each orientation η_k, the relationship

$$\frac{N^{(\eta_k)}_{Z_i}\ (i\neq 1)}{N^{(\eta_k)}_{Z_1}} = k_{1,i}\ \frac{I_A^{(\eta_k)} f^A_{Z_i}(1-C_{Z_i}) + I_B^{(\eta_k)} C_{Z_i} f^B_{Z_i}}{I_A^{(\eta_k)} f^A_{Z_1}(1-C_{Z_1}) + I_B^{(\eta_k)} C_{Z_1} f_{Z_1}} \tag{4.7}$$

is obtained. This equation (4.7) represents the ratio of the counts of one of the original elements (Z_i) at a given orientation (η_k) to the counts of an arbitarily selected original element (Z_1) at the same orientation. Here

$$k_{1,i} = P_{Z_i} M_{Z_i} / P_{Z_1} M_{Z_1} \tag{4.8}$$

and is the corresponding ratio of the scaling factors multiplied by the total number of available sites per unit cell for the same two elements. This on rearrangement, gives

$$\beta_k = \frac{f^A_{Z_i}(1 - C_{Z_i}) - f^A_{Z_1}(1 - C_{Z_1}) \left[\frac{N^{(\eta_k)}_{Z_i}}{N^{(\eta_k)}_{Z_1}} \right] \frac{1}{k_{1,i}}}{\left[\frac{N^{(\eta_k)}_{Z_i}}{N^{(\eta_k)}_{Z_1}} \right] \frac{1}{k_{1,i}} f^B_{Z_1} C_{Z_1} - f^B_{Z_i} C_{Z_i}} \tag{4.9}$$

Again, for every pair $(Z_1, Z_i)_{i \neq 1}$ one can define η_T equations of the type (4.7), giving rise to a total of $(r-1)\eta_T$ such independent factors or equations.

To determine β_k, it is essential to do an experiment under a non-channelling condition, preferably when the condition $I_A \cong I_B$ is satisfied. As a strong dynamical scattering is a prerequisite for any orientation dependence, this condition can be achieved under a kinemtical diffraction condition, which is characterized by the absence of the strong excitation of any of the lower order diffraction vectors. [It is recognized that even though ideally one would prefer that $I_A = I_B$, only the approximate identity can be established in practice because the structure factors for the two planes f_A and f_B are not equal, i.e. $f_A \neq f_B$]. Then for such a non-channelling (nc)

orientation:

$$\frac{N_{Z_i}^{(nc)}}{N_{Z_1}^{(nc)}} = \frac{P_{Z_i} M_{Z_i} f_{Z_i}^{A} (1 - C_{Z_i}) + P_{Z_i} M_{Z_i} f_{Z_i}^{B} C_{Z_i}}{P_{Z_1} M_{Z_1} f_{Z_1}^{A} (1 - C_{Z_1}) + P_{Z_1} M_{Z_1} f_{Z_1}^{B} C_{Z_1}} \tag{4.10}$$

which implies that

$$k_{1,i} = \frac{N_{Z_i}^{(nc)}}{N_{Z_1}^{(nc)}} \frac{f_{Z_1}^{A} (1 - C_{Z_1}) + f_{Z_1}^{B} C_{Z_1}}{f_{Z_i}^{A} (1 - C_{Z_i}) + f_{Z_i}^{B} C_{Z_i}} \tag{4.11}$$

which can then be substituted in equation 4.9.

Therefore, in the general case, there are 's' unknowns in the concentrations C_{X_j}, 'r' unkowns in the concentrations C_{Z_i} and η_T unknowns in the ratios of Bloch wave intensities $I_B^{\eta_k}/I_A^{\eta_k}$. The number of equations of the type (4.5) and (4.7) along with the occupancy balance equation (4.1) required to unequivocally solve for the above number of unknowns can be generated if and only if η_T satisfies:

$$\eta_T = \frac{2s + r - 1}{s + r - 2} \tag{4.12}$$

IV.3 Results and Discussions

For an original compound of 'r' elements Z_i with 's' alloying elements X_j, the number of orientations η_T at which the characteristic x-ray emission intensities have to be measured in order to unequivocally determine the distribution of the constituent elements after alloying in the different crystallographic sites is given in Table 4.1.

Table 4.1

Number of original components (r)	Number of doping elements (s)	Required number of orientations (η_T)
1	2	4
1	3	3
2	1	3
2	2	non-integer
3	1	2
3	2	2
3	3	2
3	4	2

From Table 4.1 it can be seen that in this generalization, specific site occupations can be determined for almost all practical cases. The [r=2,s=2] case is an exception for which this analysis gives a physically non-realizable result

i.e. a non-integer number of incident beam orientations. However, even this exceptional case can be solved if one of the reference elements is confined to only one of the two alternating planes. This will be discussed in detail in the next chapter. As opposed to the original formulation, where an a priori knowledge of the distribution of two reference elements is required for the analysis (it is also assumed that these distributions also remain unchanged on alloying), in this generalization, all that is required is some knowledge of the most probable site a particular element can occupy, whether it is a reference or alloying addition and not the actual distribution.

The Spence & Tafto (1983) formulation follows from this generalization. Their formulation, as applied to layered structured compounds with two repeating planes [A,B,A,B,...] has at least two reference elements (one for each of the two planes). In the simplest case this would correspond to the r=2 type of crystal structure. The additional constraints that the concentrations and distributions of the original elements remain unchanged on alloying and that the alloying concentrations are very small are also superimposed. This means that the distributions of each of the alloying elements can be considered to be independent of the others; i.e. all the problems then reduce to the [r=2, s=1] case. Therefore the only concentration unknown is C_{X_1}. For η_T orientations, using the arguments outlined earlier, only (η_T-1) factors $\mathscr{R}$ can be experimentally determined. Further, $(r-1)\eta_T$ equations of the type 4.7 can be

defined, which for this particular case (r=2) reduces to η_T. There are/is 's(=1)' unknowns in the concentrations C_{X_j} and η_T unknowns in the ratios of the Bloch wave intensities localized on the two planes. By equating the number of equations to the number of unknowns the following relationship is obtained

$$s + \eta_T = \eta_T - 1 + \eta_T \qquad (4.13)$$

Therefore, these problems [r=2,s=1] can be solved if η_T=2 or the experiments are performed in two different orientations of the incident beam along with one non-channelling orientation. This is in agreement with conventional practice and shows that the ALCHEMI formulation (Spence &Tafto, 1983) can be deduced from this generalization.

The applicability of this technique is subject to the condition that the material has a layered structure, e.g. compounds with a spinel structure, $Sm_2(Co\ TM)_{17}$ compounds, etc. Further, the systematic excitation or "planar channelling" condition is always to be maintained and all tilting to change incident beam orientations is to be done along this systematic direction. Orientations close to the normal to the systematic line and at angles corresponding to a small positive or negative excitation error of low order Bragg reflections are sufficient. Finally it must be pointed that even in this formulation, only distributions on specific planes rather than on specific sites can be determined, unless a specific plane harbours a specific

site in that particular crystallographic projection. In the general case, however, site occupations can be unequivocally determined by performing these experiments using a linearly independent set of diffracting vectors. This will be discussed later.

The advantages and limitations of using the orientation dependence of characteristic x-ray emission in site occupation studies have been discussed elsewhere [Chapter VI and Spence & Tafto, 1983]. It suffices to point out that the limitations of conventional energy dispersive x-ray microanalysis confine this technique to elements heavier than Na, unless windowless or thin film window detectors are employed. The entire analysis presented here rests on the assumption that the scattering processes leading to x-ray emissions are highly localized. This formulation though restricted in its application to certain types of layered structure compounds, has some advantages over the earlier formulation (Chapters II and III). As the technique is formulated in terms of characteristic x-ray intensity ratios, no parameters nor any knowledge of the dynamical wavefunction are required. This, combined with the relative ease with which an energy dispersive spectra can be collected and analysed, makes this generalized technique superior to other conventional ones. Finally, the whole analysis is independent of both thickness and local orientation.

The next chapter discusses an application of this generalized formulation, i.e. the determination of the site

occupancy of transition metal elements in $Sm_2(Co\ TM)_{17}$ compounds.

CHAPTER V

SITE OCCUPATION OF TERNARY ELEMENTS IN $Sm_2(Co,TM)_{17}$ COMPOUNDS

V.1 Introduction

V.2 Crystallography of RE_2Co_{17} compounds

V.3 Analysis

V.4 Experimental details

V.5 Results and discussions

V.1 Introduction

The motivation for undertaking this study is two-fold. It is well known that the magnetocrystalline anisotropy in RE_2Co_{17} compounds can be appreciably improved by the substitution of transition metal elements in limited quantities in the cobalt lattice (Wallace, Fujii, Satyanarayana & Hirosawa, 1982). There is very little experimental evidence for the exact site occupations of these elements, but for certain elements like Fe, it is reasonably well established that it tends to occupy the dumbbell (6c) sites in the RE_2Co_{17} compounds. The generaliztion of atom location by channelling enhanced microanalysis, developed in the last chapter is particularly suitable to determine the site occupations in these compounds, because by strong excitation of the [0002] systematic row one can localize the electron standing wave on either one of the two alternating planes of pure Cobalt or mixed planes of Sm & Co. However, this generalized ratio technique as developed in the last chapter, would not be able to resolve site occupations of exactly two transition metal additions in Sm_2Co_{17} compounds, as this would correspond to a [r=2, s=2] alloy in our earlier definition and hence the required number of orientations would then be a non-integer. But, in this particular case, our a priori knowledge of the distribution of Sm, i.e. its distribution being restricted to alternate [0001] planes only, can be used to our advantage and the site occupation determined. In this chapter we show how this has been

accomplished for the case of a compound of nominal composition $Sm_2(Co_{0.8}Fe_{0.1}Mn_{0.1})_{17}$.

V.2 Crystallography of RE_2Co_{17} compounds

The crystal structure of the class of compounds with a nominal composition RE_2Co_{17} can be derived from that of $RECo_5$. The unit cell of $RECo_5$ is a primitive hexagon and its structure (p6/mmm) is commonly referred to as the $CaCu_5$ structure ($D2_d$). This is shown in figure 5.1 and consists of one formula unit per primitive cell or three formula units per conventional unit cell. It satisfies the criterion for a layered structure as it can be resolved into mixed planes of (RE,Co) alternating with pure Co planes along the [0001] direction.

The RE_2Co_{17} structure can be derived from the $RECo_5$ structure by removing one third of the RE atoms and replacing them by pairs of Co atoms. These pairs are normally aligned along the c-axis and are referred to as dumbbell sites. The two observed forms of the RE_2Co_{17} structure, labelled as the hexagonal ($P6_3/mmc$) and the rhombohedral (R3m) forms (Figures 5.2 & 5.3 respectively), are due to the different ordering of the dumbbell sites. The ordering of the dumbbell sites is such that the former structure can be construed as an ABABAB... stacking of the mixed planes and the latter structure as an ABCABC... stacking of the same planes, analogous to the hcp and fcc structures (Rabenberg, 1983). However, the layered structure is

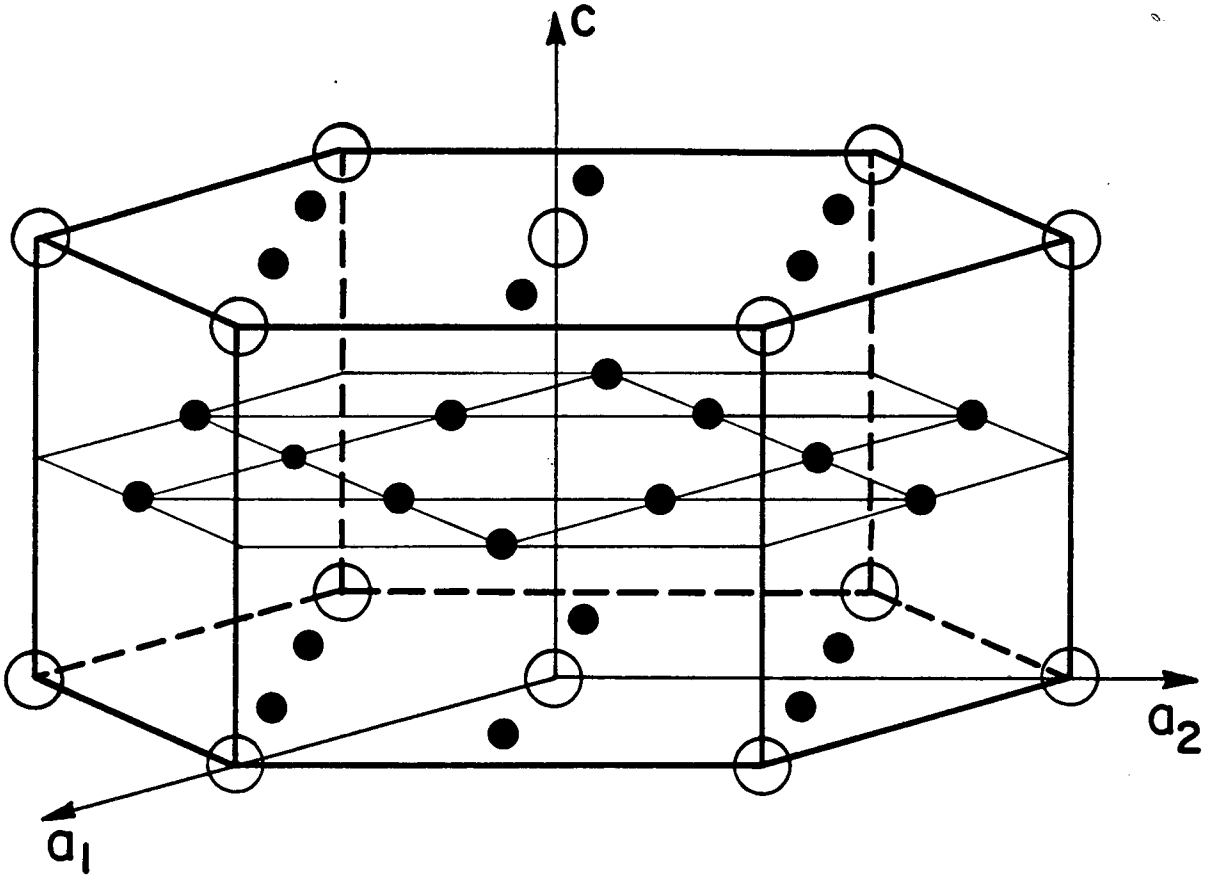

Figure 5.1 A perspective drawing of the $SmCo_5$ conventional unit cell; the basic structural unit of this class of intermetallic compounds. After Rabenberg (1983).

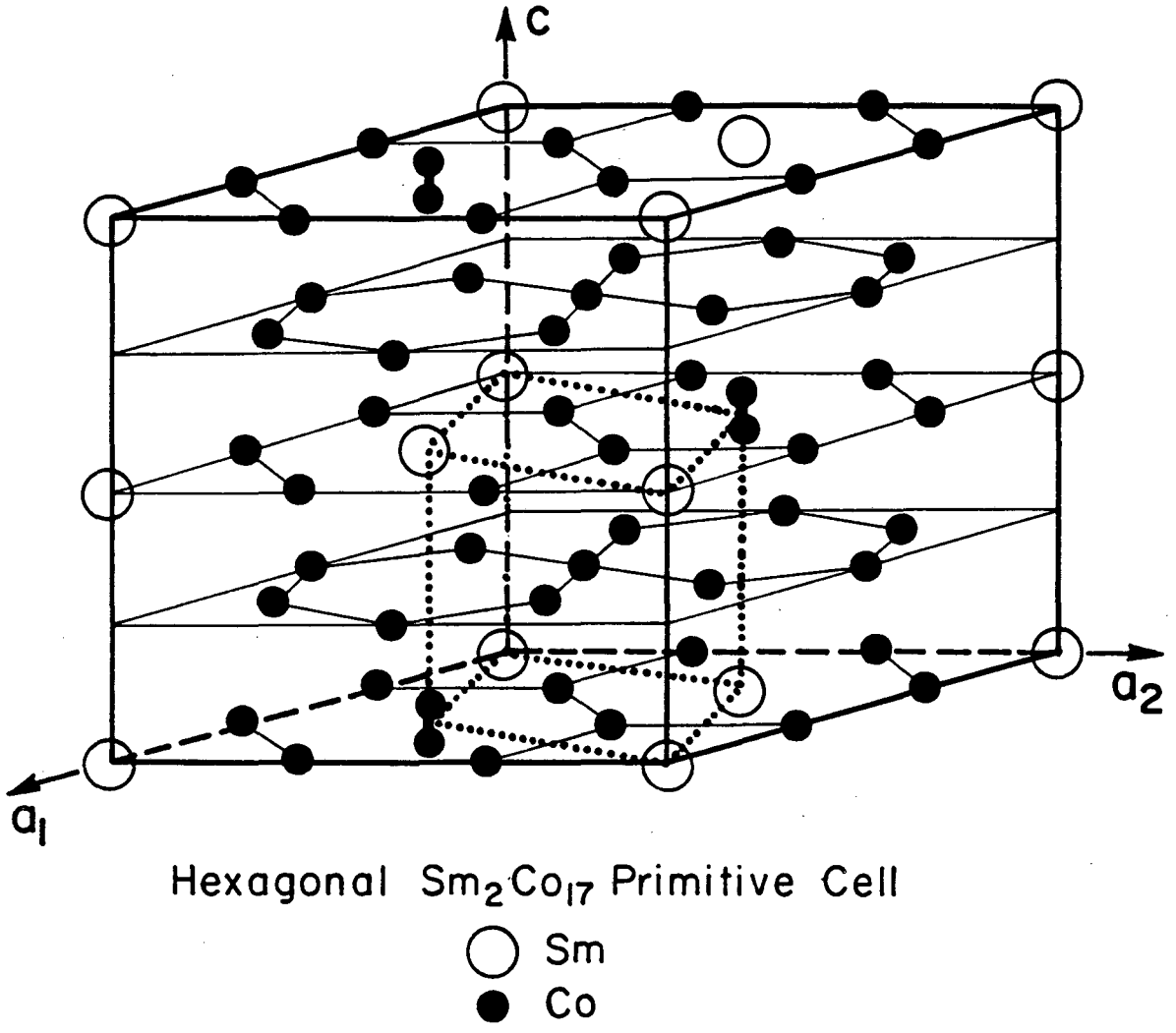

Figure 5.2 Hexagonal Sm_2Co_{17} primitive unit cell along with the corresponding primitive cell of the $SmCo_5$ structure. This perspective drawing illustrates how this structure is formed by the ordered substitution of dumbbell pairs of Co at one third of the Sm sites. After Rabenberg (1983).

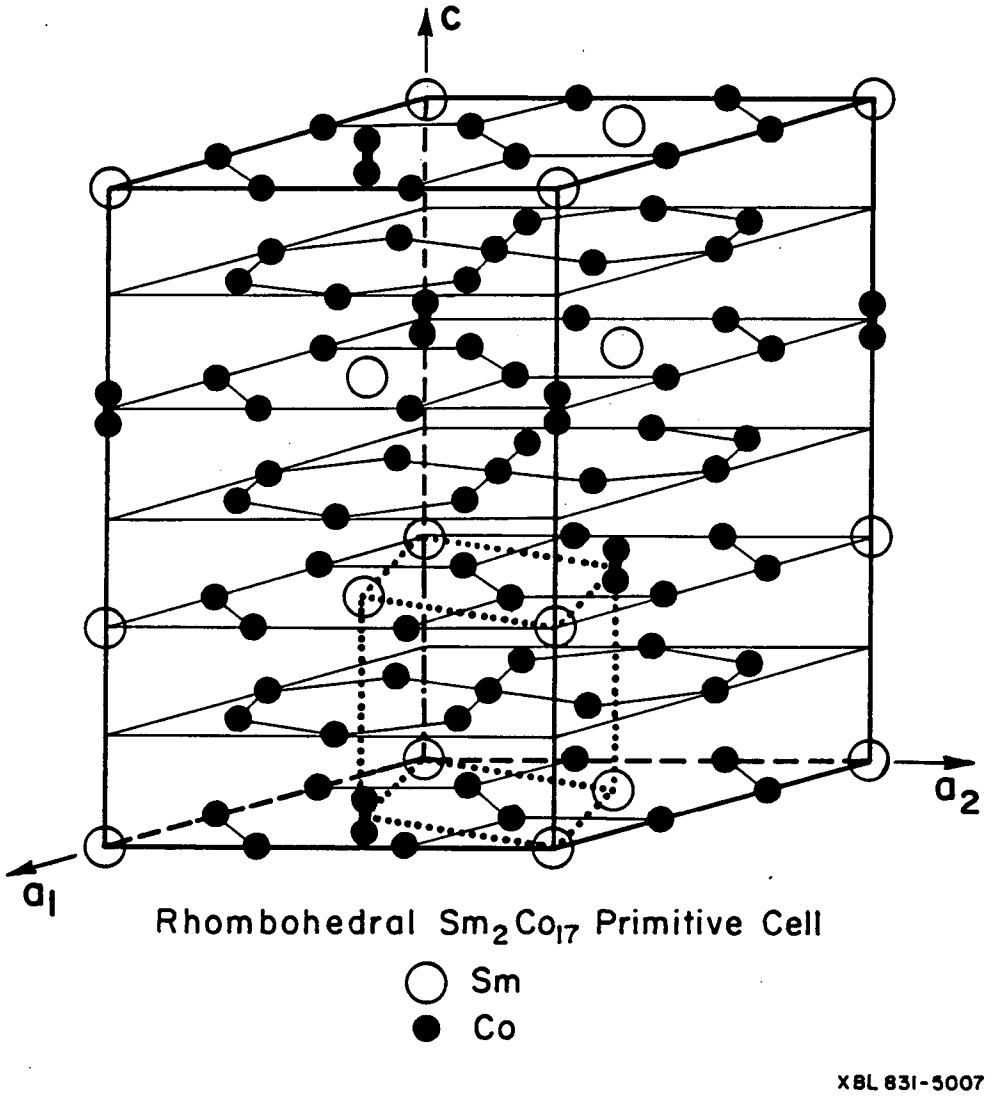

Figure 5.3 Rhombohedral Sm_2Co_{17} primitive unit cell with the corresponding $SmCo_5$ primitive unit cell. This structure is also formed by an ordered substitution of pairs of Co at Sm sites. After Rabenberg (1983).

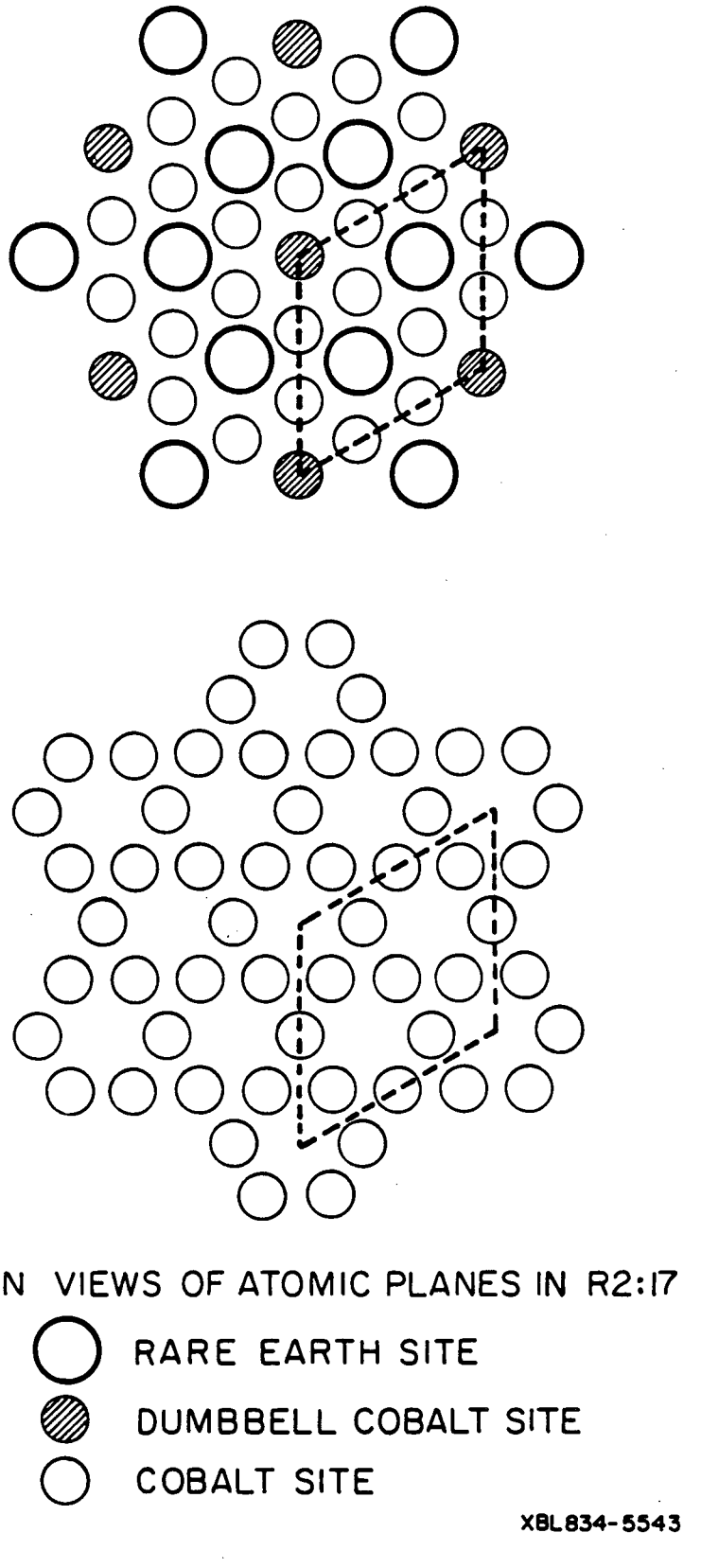

Figure 5.4 Plan view of the atomic planes constituting the layered Sm_2Co_{17} structures. After Rabenberg (1983).

effectively retained in both structures and the alternating planes constituting the layered structure are shown in figure 5.4.

V.3 Analysis

Following equation 4.2, we express the rate of the electron induced characteristic x-ray emissions (N) for a specific element (z) at a particular orientation (η) as

$$N_Z^{(\eta)} = \sum_{A,B,\ldots}^{\text{unit cell}} P_Z m_Z I_A^{(\eta)} f_A^Z C_Z \qquad (5.1)$$

where all the constituents have been described earlier. Since the crystallographic structure in this projection can be resolved into alternating [0001] planes of Co and mixed (Sm,Co) planes, for each orientation of the incident electron beam and for each transition metal Fe or Mn that occupies any Co site (the Sm distribution being fixed) we get two terms for the characteristic x-ray intensity :

$$N_z^{(1)} = P_z m_z I_A^{(1)} f_A^{Co} (1-C_z) + P_z m_z I_B^{(1)} f_B^{Co} C_z \qquad (5.2)$$

and

$$N_z^{(2)} = P_z m_z I_A^{(2)} f_A^{Co} (1-C_z) + P_z m_z I_B^{(2)} f_B^{Co} C_z \qquad (5.3)$$

For the Sm sublattice, equation 5.1 simplifies to

$$N_{Sm}^{(1)} = P_{Sm} m_{Sm} I_A^{(1)} \tag{5.4}$$

and

$$N_{Sm}^{(2)} = P_{Sm} m_{Sm} I_A^{(2)} \tag{5.5}$$

We now define a normalized measure of the orientation dependence as

$$\mathscr{R}\left(\frac{Sm}{Z}\right) = \frac{N_{Sm}^{(1)}/N_Z^{(1)}}{N_{Sm}^{(2)}/N_Z^{(2)}} \tag{5.6}$$

Substituting equations 5.2 through 5.5 in equation 5.6 we get

$$\mathscr{R}\left(\frac{Sm}{Z}\right) = \frac{f_A^{Co}(1 - C_z) + \gamma f_B^{Co} C_Z}{f_A^{Co}(1 - C_Z) + \beta f_B^{Co} C_Z} \tag{5.7}$$

where

$$\beta = I_B^{(1)}/I_A^{(1)} \tag{5.8}$$

$$\gamma = I_B^{(2)}/I_A^{(2)} \tag{5.9}$$

are ratios of the Bloch wave intensities on the two planes for each incident beam orientation. The expression 5.7 can be inverted to give an expression for the concentration of the transition metal elements on the mixed planes in terms of the experimentally observed intensities and the parameters β and γ:

$$C_Z = \frac{\mathscr{R}\left(\frac{Sm}{Z}\right) - 1}{\frac{f_B^{Co}}{f_A^{Co}} \left[\gamma - \beta\mathscr{R}\left(\frac{Sm}{Z}\right)\right] + \left[\mathscr{R}\left(\frac{Sm}{Z}\right) - 1\right]} \qquad (5.10)$$

The parameters γ and β can be evaluated from an experimental spectra at a non channelling condition for which $I_A \simeq I_B$. Then, for such a non-channelling (nc) orientation

$$\frac{N_{Co}^{nc}}{N_{Sm}^{nc}} = k[f_A^{Co}(1 - C_{Co}) + f_B^{Co} C_{Co}] \qquad (5.11)$$

where

$$k = \frac{P_{Co} m_{Co}}{P_{Sm} m_{Sm}} \qquad (5.12)$$

Then from the original orientations (1) & (2) we get

$$\beta = \frac{1}{f_B^{Co} C_{Co}} \left[\frac{1}{k} \frac{N_{Co}^{(1)}}{N_{Sm}^{(1)}} - f_A^{Co} (1 - C_{Co}) \right] \qquad (5.13)$$

and

$$\gamma = \frac{1}{f_B^{Co} C_{Co}} \left[\frac{1}{k} \frac{N_{Co}^{(2)}}{N_{Sm}^{(2)}} - f_A^{Co} (1 - C_{Co}) \right] \qquad (5.14)$$

respectively.

From the crystal structure, the fraction of sites available for the element z on the two planes A and B are known, i.e.

$$f_A^{Co} = 24/51 \qquad (5.15)$$

$$f_B^{Co} = 27/51 \qquad (5.16)$$

From these equtions one can obtain an expression for the concentration of the transition metals on the Co plane, in terms of the concentration of Co on the Co plane (not a fixed value since the level of substitution is significantly large) and the

experimentally observed values of the x-ray intensities N_z^{η}. Finally, since there are three formula units per unit cell, for the particular compound of interest, $Sm_2(Co_{0.8}Fe_{0.1}Mn_{0.1})_{17}$, an occupancy balance for the Co planes gives

$$13.6\ C_{Co} + 1.7\ (\ C_{Fe} + C_{Mn}\ ) = 9 \qquad (5.17)$$

This additional relationship, expressing the concentrations C_z in terms of C_{Co}, gives the required number of equations to complete the analysis.

V.4 Experimental details

Samples of $Sm_2(Co_{0.8}Fe_{0.1}Mn_{0.1})_{17}$ corresponding to a nominal composition of 23.3 wt% Sm, 7.4 wt% Fe, 7.2 wt% Mn and 62.1 wt% Co, obtained from General Motors Research Laboratories, were studied. Specimens for observation in an analytical transmission electron microscope were obtained by sectioning followed by routine ion beam milling. In the microscope, these electron transparent thin foils were oriented such that a strong [0002] systematic row was excited. The characteristic x-ray spectra were collected for a period of 300 seconds (at each orientation) at an average counting rate between 2500-3000 counts per second in three distinct orientations:

1) Positive deviation from the exact $[0006]_{2:17} = [0002]_{1:5}$ Bragg condition.($s>0$)

2) Negative deviation from the exact $[0006]_{2:17} = [0002]_{1:5}$ Bragg condition ($s<0$), and

3) A non-channelling condition in which no strong low-order diffraction vectors were excited.

Other details of the experimental procedure have been discussed earlier (section III.2).

V.5 Results and discussions

The observed characteristic x-ray intensities for the elements of interest, after background subtraction are shown in Table 5.1.

TABLE 5.1

Characteristic X-ray Intensity

(x 10^3 counts in peak)

	$s<0$	$s>0$	non-channelling
$Sm(L_\alpha)$	110.7	87.1	156.9
$Mn(K_\alpha)$	77.5	64.2	105.6
$Fe(K_\beta)$	81.2	68.4	109.8
$Co(K_\alpha)$	654.4	690.7	920.0

Applying the analysis described earlier to the data in Table 5.1, we can determine the distribution of the elements in the alloy $Sm_2(Co_{0.8}Fe_{0.1}Mn_{0.1})_{17}$ as

$$C_{Co} = 0.629$$
$$C_{Fe} = 0.149$$
$$C_{Mn} = 0.115$$

In other words 62.9% of the Co atoms, 14.9% of the Fe atoms and 11.5% of the Mn atoms lie in the Co plane.

The application of this technique to the determination of the distribution of the constituent elements of an $Sm_2(CoTM)_{17}$ alloy, apart from being subject to the general limitations of energy dispersive x-ray analysis and the inherrent assumptions made in the developement of these techniques (section VI.1), is subject to additional assumptions in this specific application. They are:(i) there are no antisite defects and (ii) for RE_2Co_{17} compounds, the dumbbell sites can be considered as part of the mixed planes.

In the course of this analysis it has only been determined that approximately 90% of the Fe and Mn atoms occupy sites on the mixed planes. In this crystallographic projection, the mixed planes contain both the dumbbell sites (6c) and the adjacent (18j) sites. As this technique cannot distinguish crystallographic sites within atomic planes it is not possible to

resolve preferential occupations between these two sites. However since we do know that the concentration of Fe and Mn on the mixed planes is in excess of the number of dumbbell sites, it can be concluded that the 18j sites are favoured over the 18h or 9d sites in the Co planes. The exact site occupancies can be determined by performing a series of experiments for different systematic orientations such that a linearly independent set of diffraction vectors are excited. These diffraction vectors would be determined by the crystal structure and the specific details of the problem, but, it can be said in general, that occupations of a particular site could be determined only if it were possible to find three sets of parallel but unequal planes in the crystal structure and by performing the experiment described in this section for the systematic excitation of each one of these family of planes.

CHAPTER VI

CONCLUDING DISCUSSION AND SUMMARY

VI.1 Assumptions made in the formulations

VI.2 Resolution that can be achieved

VI.3 Limitations

VI.4 Impact of channelling on analytical & transmission electron microscopy

VI.5 Orientation dependence in electron energy loss spectroscopy

VI.6 Possible extensions in channelling enhanced microanalysis

VI.7 Summary

In the course of this dissertation, two different formulations of channelling-enhanced microanalysis to determine specific-site occupations in single crystals have been developed. Two practical applications that are also representative of the two different categories of crystal structures as classified in this thesis have also been presented.

The diversity of the contents of this dissertation has necessiated appropriate discussions during the course of its developement. However, in this chapter an overall discusssion is presented, that should hopefully, tie up loose ends, make up for omissions, address related issues, place this work in proper perspective with respect to similar techniques and suggest possible extensions.

VI.1 Assumptions

The assumption that the scattering processes leading to characteristic x-ray emissions are highly localized is so important that it cannot be over-emphasized.

The channelling of an incident plane wave of electrons in a single crystal is dependent on the incident beam direction. The corresponding characteristic x-ray emission product is a function of the above and the degree of localization of the scattering event. A detailed calculation of the orientation dependent emission product using the Fourier coefficients of the imaginary part of the crystal potential would be very involved.

It is the validity of the approximation that the scattering processes are represented by delta functions at the mean atomic positions, that makes the prediction of incident beam orientations that are specific site sensitive feasible, particularly for complicated crystals(e.g. a garnet structure - not layered and has as many as 160 atoms per unit cell).

The justifications for this assumption have been presented and discussed earlier (section II.8). It has been shown that the "radii" of the K or L shells for the elements of interest are less than the thermal vibration amplitudes. Further plausibility arguments were also presented based on an estimate of the limting value of the impact parameter.

This assumption is equally crucial in the Generalized ALCHEMI formulation (Chapter IV) as applied to layered structure compounds (ratio method). If this were not the case, it would be incorrect to express the characteristic x-ray emissions as a linear sum of the contributions from each of the parallel planes (A,B,A,B,...). Much of the elegance of the ratio technique would have to be sacrificed, for the normalized measure of the orientation dependence would then be a rather invoved and complicated expression.

In the ratio technique the localization is represented by the effective Bloch wave intensities I_A & I_B on the two planes. For the planar channelling or systematic excitation condition that is normally used to separate the candidate sites into alternating non-identical planes, these effective Bloch wave

intensities would then be depth-integrated or thickness-averaged. In other words, a column approximation is resorted to. Hence, for an uniform distribution of reference and alloying elements, one can assume that variations of specimen thickness and local orientation under the electron probe are insignificant, as the local change in diffracting conditions would then have an identical effect on both species of atoms.

The distribution with depth needs further elaboration. In order for the emission product to be proportional to the thickness averaged effective Bloch wave intensities I_A & I_B it is essential that the variation of the distribution of the alloying elements with the depth of the specimen be uniform. It is believed that the cumulative effect of the alloying additions on the depth dependence of the dynamical wave function is unimportant by assuming that its effect would be identical on the characteristic emissions of both the reference elements as well as the alloying additions. As pointed out by Spence & Tafto (1983) the error due to a non-uniform distribution would be a maximum for a sheet of alloying additions parallel to the specimen surface.

Finally, in both the formulations developed here, apart from assuming that the crystals are free of defects it is also assumed that the error due to the absorption of x-rays is not appreciable as the specimens are thin and the tilt angles are very small.

VI.2 Resolution

Within the confines of the above assumptions and the limitations to be described in the next section the techniques developed here are capable of the following resolutions.

Both techniques are capable of resolving adjacent elements in the periodic table and are restricted in spatial resolution to 50nm . Further, trace elemental compositions (0.2-0.3 wt%) can be routinely analysed. With some care, distributions of elements in specific crystallographic sites for levels of doping equivalent to 10^{-19} atoms/cm^3, can be determined. The smallest error in the fraction of the total concentration occupying a particular site is about $\pm$ 2% in the ratio technique, part of which is due to the assumption of highly localized scattering events. In the other formulation where site occupancies are determined by least squares refinements, the error is a compounded one consisting of the inherent approximations of the theoretical formulation, the statistical error in experimentation and the computational error in least squares refinements. Hence, in this case, the smallest error achievable is estimated to be $\pm$5%.

VI.3 Limitations

The techniques that have been described are subject to all the limitations of conventional energy dispersive x-ray microanalysis. In comparison with wavelength dispersive analysis, EDXM is limited in three aspects : resolution, count rate and ability to analyse light elements ($Z \leq 11$). The attainable resolution of energy dispersive detectors has been improving gradually (state of the art in detector resolution = 145 ev FWHM for Mn K_α) but can never compete with a diffracting crystal. However, in practice, obtainable signal intensities in terms of photons per primary electron can be 10^2 to 10^3 times stronger with energy dispersive detection. Further, a number of deconvolution techniques have been developed and used to separate peaks not resolved by the detector itself. Improvements in the count rate handling capability, particularly the prevention of a distortion of the spectra at high count rates have been made. However, in the electron microscope, the continued use of small probes and thin foils, has shifted the emphasis from the ability to handle high count rates to the use of very large detector solid angles to get acceptable results. In other words, the collection efficiency is improved. Finally, use of windowless or ultra-thin window detectors has extended the detection capabilities down to energies above approximately 200ev. Hence, now low atomic number elements can also be analysed.

As these techniques presuppose dynamical scattering, it

is essential that the sample be of sufficient thickness ($t = n\xi_g$, where $n \geq 3$). The channelling effect is of an observable magnitude for crystals of thickness t>100A°. However, there is an upper limit of t<2000A°, corresponding to the attenuation distance of the poorly transmitted Bloch waves. At distances greater than this, the electrons are diffusely scattered through small angles and effectively behave as plane waves in producing further x-rays.

The minimum probe size is limited by the statistics of the impurity distribution. The requirement of uniform distribution places a fundamental limit on the minimum volume that can be analysed. The condition that has to be satisfied (Spence & Tafto, 1983) in order that the dynamical wavefunction is well sampled in depth is given by

$$\xi_g \, n \, A \geq 1 \qquad (6.1)$$

where n(atoms/unit vol) is the uniformly distributed concentration, A is the projected area of the electron probe and ξ_g is the dynamical extinction distance for the reflection $\bar{g}$. This condition has been satisfied in all the studies discussed in this dissertation.

The determination of the site occupations of alloying elements in ionic crystals is not included in these formulations. In such cases an additional relationship imposed by charge conservation, has to be incorporated. This would significantly change the analysis pertaining to the Generalized ALCHEMI technique and hence Table 4.1 will have to be revised. In

general the techniques are also limited to materials that are insensitive to electron radiation.

When compared with other techniques with similar objectives, the two different formulations of channelling enhanced microanalysis developed in this thesis have significant advantages. Unlike Rutherford backscattering, x-ray diffraction or any of the conventional techniques (mentioned earlier) applicable to magnetic materials, CEM is capable of analysing very small areas; a spatial resolution of 50-100 nm are quite routine. Further, adjacent elements in the periodic table can be easily distinguished. In the application to layered structure compounds, there is no need for any adjustable parameters unlike HREM or EXAFS.

VI.4 Impact of channelling on analytical & transmission electron microscopy

The channelling effect or the orientation dependence of characteristic x-ray emissions that has been favourably used to determine specific site occupations can also have a detrimental influence on conventional x-ray microanalysis. For thin crystals, the orientation dependence can be significant and as a result the count rate can be strongly dependent on the crystal orientation and the angular spread of the incident beam. To avoid this, it is essential to tilt the specimen to an orientation such that no strong lower order Bragg diffraction

vectors are excited. This ensures that a non-channelling condition is in effect and the microanalysis would then be representative of the actual sample. However, if this were to be difficult to implement, then it would be necessary to make appropriate corrections employing the theory developed in Chapter II.

For thin crystals it was shown in Chapter II that the independent Bloch wave model was inadequate to describe the characteristic x-ray emissions. Hence the dependent model where the characteristic x-ray emission is proportional to the square of the overall wavefunction was used. A similar modification of the anomalous theory of transmission electron diffraction is required. Normally, the independent Bloch wave model is used. It has been shown (Heidenreich, 1962) that the general solution to the Schrodinger equation with a complex crystal potential can be written in terms of independent Bloch waves, but, with each having a characteristic wave vector with real and imaginary components; i.e. a "damping vector" is introduced. A small modification of the Bloch wave coefficients C_g^i in equation (2.3) would also be required. This could be neglected in thick crystals under the assumption that it is the attenuation which is dominant. In thin crystals this argument does not hold and interference terms similar to the ones used for characteristic x-ray production have to be incorporated. However a consistent solution in terms of the exact Bloch wave cefficients can be obtained by the diagonalisation of a complex non-Hermitian

scattering matrix.

VI.5 Orientation dependence in electron energy loss spectroscopy

Electron energy loss spectroscopy is now an accepted tool for elemental microanalysis with high spatial resolution (Collieux, 1983). Chemical analysis is accomplished by monitoring the core loss signals for all elements using a magnetic sector energy spectrometer and is particularly useful for low atomic number elements ($Z \leq 11$) which exhibit sharp edges of strong intensity in the high energy loss region ($50 < E < 2000$ev). This complements EDXM which is restricted to elements with $Z \geq 12$, using conventional detectors.

What is of relevance to this discussion is the effect of channelling in EELS. A weak dependence on orientation due to the localization of the Bloch waves at specific crystallographic planes on the K-loss of Mg in MgO single crystals was first observed by Tafto & Lempfuhl (1982). Earlier, Craven, Gibson, Howie & Spalding (1978) had concluded that an impact parameter for forward inelastic scattering can be approximated by $L \approx 2\lambda E_o / \Delta E$, i.e. an energy loss $\Delta E = 1500$ev would correspond to an impact parameter $L = 0.4$nm. As the impact parameter decreases with the energy loss, they predicted that it would be impossible to detect localization effects for energy losses lower than 1500ev.

Based on a more detailed study, Tafto & Krivanek(1982a) and Spence, Tafto, Krivanek & Disko (1982) have concluded that the height of the core loss peak in transmission electron energy loss spectra from crystals depend strongly on both the incident beam direction and the degree of localization. By choosing a systematic orientation and placing the detector at various positions along a line normal to the systematic line the diffraction and localization conditions were varied independently. Based on this study, they argue that the "Borrman effect" is pronounced in EELS when compared with characteristic x-ray emissions because of the consideration of elastic diffraction of the inelastically scattered electrons. Further, with a special direction of incidence and collection, Tafto & Krivanek (1981) have demonstrated a combination of channelling and blocking effects. Using a reciprocity argument they suggest that the channelling effect may be squared in EELS as compared to characteristic x-ray emissions by placing the entrance aperture and collector aperture at equivalent positions in the Brillouin zone.

The valence of an atom occupying a particular crystallographic site can also be determined by combining its chemical shift with the orientation dependence of the transmission electron energy loss spectra (Tafto & Krivanek, 1982b). This specific site valence determination technique has been applied to the location of Fe^{2+} and Fe^{3+} ions in mixed valence spinels by monitoring the details of the Fe $L_{2,3}$ edge.

The sharp peaks at the edge threshold splits into two components separated by 2ev, consistent with the chemical shift between Fe^{2+} and Fe^{3+} and following the usual relationship between the chemical shift and the valence state (Agarwal, 1979). A similar splitting could be monitored for the $M_{4,5}$ edge of the rare earth additions whose site occupancies in a garnet structure were determined by the orientation dependence of the characteristic x-ray emissions (Chapters II & III). As one of the motivations for this work was the prediction or the understanding of the growth induced uniaxial anisotropy in these thin films (and for which the specific site valence determination is most relevant) this technique could be of immense value and worthy of further investigation.

VI.6 Possible extensions in channelling enhanced microanalysis

There are innumerable other problems of site occupation determinations in materials characterization to which the techniques of channelling enhanced microanalysis can be applied. However, each problem will have to be tackled separately, beginning by classifying the crystal structure into one of the two categories that have been discussed in this thesis and then proceed with the appropriate analysis. Apart from these a number of intrinsic extensions of this work should also be considered.

In many practical cases, it is important to determine whether a particular alloying addition is distributed at a

specific site in the unit cell. For example, in the $Sm_2(CoTM)_{17}$ compounds it is important to know whether the TM are distributed on the dumbbell sites are not. Even though the crystallographic structure is layered, this compound is such that these dumbbell sites are one of three possible crystallographic sites on the [002] planes. The ratio technique in the Generalized ALCHEMI formulation does not distinguish sites within planes. Since the crystal structure cannot be resolved in any other projection as a layered structure harbouring only the dumbbell sites, the only way of overcoming this limitation is to perform a series of experiments using a linearly independent set of diffracting vectors. Any particular site in a crystal unit cell can be uniquely identified as an intersection of three unequal (non-parallel) planes. If these planes were such that they satisfy the conditions required for employing the ratio technique, then the analysis of experiments performed for each family of planes would allow complete determination of the occupation of that particular site.

Extension of these methods to include interstitial occupation determination should pose no difficulties, for it is possible to find favourable crystallographic planes that contain a particular interstitial site. The analysis would then be identical.

Even though extending these techniques to higher voltages would have all the known ramifications of microanalysis at higher voltages, it has to be done with extreme care. As

predicted by the calculations (section II.9), the effect of the acceleration voltage as an independent parameter shows an interesting "inversion voltage" effect. Alternatively, the inversion voltage itself could be used to determine qualitatively specific site occupations. However, it is important to experimentally verify the inversion voltage behaviour. Preliminary attempts indicate that the experiment has to be performed with extreme circumspection. Apart from ensuring that the beam current is the same at every voltage, one has to make sure that the thickness of the specimen analysed at the different voltages are such that λ t is a constant.

As pointed out earlier, the best resolution in terms of detection that can be resolved by these techniques is about 10^{-19} atoms/cm^3. For many applications, particularly in semiconductor materials, it would be worthwhile to increase these detectability limits. If the limitation is due to a poor signal to background ratio then a possible solution (Wittry, 1976) is to measure the characteristic x-ray and the transmitted electron energy loss spectra simultaneously, i.e. coincidence counting. One could run into problems as not all EELS events can give rise to a detectable EDX event (P.Rez, private communication). If the limitation were to be the overall counting time caused by a pile up of x-ray counts from the matrix, it has been suggested (Tafto, Spence & Fejes, 1983) that it could be avoided by suitable filters to suppress the matrix x-ray counts. These would certainly be worth exploring.

VI.7 Summary

It has been known that the secondary emissions, particularly the characteristic x-ray spectra, produced by the interaction of a fast electron incident on a crystalline specimen shows a significant variation with the orientation of the incident beam. This observation that the "Borrman effect" might be applicable to the secondary emission product, had stimulated considerable speculation about the possibility of deriving structural information (specific site occupations) from measurements of the orientation dependent electron-induced characteristic x-ray intensities. Previous attempts had been marred by difficulties, for the application of this "Borrman effect" as a crystallographic probe requires, in the general case, a knowledge of the dynamical wave function, incorporating inelastic scattering, as well as a stringent calibration of all the instrumentation. Nevertheless, more recently, an experimental technique based on this dependence has been developed by Spence and Tafto (1983). They have demonstrated that for certain layered crystal structures it is possible to effect a simplification of the analysis, provided that an *a priori* knowledge of the distributions of certain reference elements is available. However, in order to be applicable to practical crystal structures and be developed into a more meaningful technique, a systematic treatment is required.

This thesis addressed this developement.

Two different formulations based on the crystal structure to be analysed were presented. The crystal structures were classified either as layered or non-layered. A layered structure was defined as one that in some crystallographic projection can be resolved into alternating, non-identical, parallel planes (A,B,A,B....), each plane containing one or more specific crystallographic site. For such layered structures the appropriate orientations were determined by mere inspection and the site occupations were then obtained by a generalization of the analysis of Spence and Tafto (1983). For a general non-layered crystal structure, on the other hand, a theory of characteristic x-ray production to calculate the secondary emission intensities as a function of the incident beam orientation and specific site occupation was formulated and used not only to determine the appropriate orientations but also to refine the experimental data.

As any theory of the inelastic scattering of fast electrons in crystals has to incorporate the effects of elastic scattering, the theoretical developement began with a brief description of the conventional theory of transmission electron diffraction in the Bloch wave formulation. This was followed by a detailed theory of inelastic scattering pertinent to the calculation of characteristic x-ray emissions. Two different formulations were presented. A reciprocal space formulation was derived by applying first order perturbation theory to the

inelastic scattered state, i.e. by assuming that the imaginary part of the crystal potential to be small. Alternatively, a simpler real space formulation, considering the flux loss from the incident beam was also derived. These two formulations are identical in so far as they decribe the same physical phenomena. Further, for highly localized inner shell excitations, where the inelastic potential is well approximated by a delta function $\delta(r)$ at the mean atomic positions, the Fourier transform P_{gh} is a constant and does not appear explicitly in the final equations. The expression for characteristic x-ray emission, applicable to a general non-centrosymmetric crystal, derived therein , was factorized into two parts; a thickness independent term of individual Bloch wave contributions and a thickness dependent term of Bloch wave interference contributions. The agreement of the results of the calculation of the orientation dependence of the x-ray emissions in spinels ($MgAl_2O_4$) with experimental results was used as a measure of the validity of the real space theoretical formulation. The assumptions and limitations incorporated in this formulation were examined and were shown to be reasonable for inner shell excitations.

A change in the incident beam orientation or the acceleration voltage should have identical effects on the orientation dependence of the emission products. This is because they independently change the diagonal elements of the dynamical scattering matrix. Calculations of the orientation dependence of characteristic x-ray emissions in spinels, at different voltages,

predicted a non-uniform voltage dependence characterized by an analogous "inversion voltage". The characteristics of this inversion voltage were investigated and were shown to be different from the conventional "critical voltage" effect. It was also argued that this voltage dependence could be used independently to qualitatively determine site occupations in crystals provided that the corresponding value of the inversion voltage was known in advance.

The theory developed thus far was then applied to the determination of the specific-site occupations of rare earth additions in epitaxially grown garnet films. These single crystal films have a general non-layered structure. This makes a prediction of the appropriate systematic excitation or "planar channelling" conditions, by an examination of the crystal structure or its projections, rather difficult. Therefore, characteristic x-ray emission intensities for this crystal structure were calculated, based on the real space formulation described earlier, for different incident beam orientations and complete occupation of the rare earth additions in each of the three different crystallographic sites. It was then shown that a $\bar{g} = 1\bar{2}1$ systematic excitation condition is the appropriate one for this crystal structure, i.e. enhanced channelling for dodecahedral site substitutions of the rare earth additions, blocking for tetrahedral site substitutions and an insensitivity to orientation for octahedral substitutions, were predicted. Experimentally obtained data were then refined using a

constrained least squares analysis with respect to the theoretical estimates of the characteristic x-ray intensities, to give probabilities for the occupations of the rare earth additions in the different crystallographic sites. Thus it was shown that in these compounds the preference for rare earth additions is predominantly octahedral occupation with a probability $\geq$ 95%. The credibility of this least square refinement was then established by calculating the norm in the L_2 sense and ensuring that this was less than some acceptable value ($\leq 10^{-2}$).

In the case of crystals with a layered structure, Spence and Tafto (1983) have demonstrated that it is possible to effect a simplification of the above analysis, for, the appropriate specific-site sensitive systematic excitation conditions can be determined by mere inspection of the crystal structure. However, an *a priori* knowledge of the distributions of certain reference elements is required for the analysis. These reference elements are chosen judiciously and are dependent on the crystal structure to be analysed. Further, their analysis assumes that the distributions of these reference elements remain unchanged on alloying or on impurity addition. A generalization of their formulation, requiring only an idea of which sites a particular element can potentially occupy, irrespective of whether it is an alloying addition or reference element, and not their actual distributions has been developed. Using this analysis, experimental conditions required to solve for the

specific site occupations in a whole class of related layered structure compounds were presented. Based on this generalized formulation and by monitoring the characteristic x-ray spectrum as a function of incident beam orientation, it was shown that 88.5 % of the Mn atoms and 85.1 % of the Fe atoms occupy sites in the mixed planes in the $Sm_2(Co,TM)_{17}$ compounds.

This thesis concluded with a general discussion. Some of the assumptions were examined, the limitations were elaborated upon, other applications were enumerated and possible extensions of channelling enhanced microanalysis were discussed.

APPENDIX 1

UNAXIAL ANISOTROPY IN GARNETS

The uniaxial anisotropy in epitaxially grown thin film magnetic garnets consists of two components, a growth induced component and a stress induced component. The latter is well understood in terms of magneto-elastic interactions (Hansen, 1978). The former component as the name implies originates from the growth process and results in the ordering of the magnetic ions along certain growth directions leading to a deviation from the cubic symmetry of the garnet structure.

Of the many models that have been proposed to explain the growth induced anisotropy, the most accepted one has been the site preference model (Callen, 1971a; Rosencwaig, Tabor & Pierce, 1971). This model was proposed for mixed rare earth garnets and is based on the preferential incorporation of the two rare earth ions in the dodecahedral sites.

In the garnet structure, the dodecahedral sites have the nearest neighbour site distributions given in Table A1. If we consider the nearest neighbour tetrahedral (n.n.t) site only, the number of types of dodecahedral sites reduces to 3; i.e. X, Y and Z with n.n.t sites along the three crystallographic axes $\bar{x}$, $\bar{y}$ and $\bar{z}$ respectively. Addition of a rare earth ion (B) to a pure $A_3Fe_5O_{12}$ compound would result in an increase in internal energy by α_1^2 (where $\bar{\alpha} = \alpha_1 \bar{i} + \alpha_2 \bar{j} + \alpha_3 \bar{k}$ is the magnetization

Table A1

Classification of the dodechedral (c) sites in a garnet structure

Type of (c) site	Nearest neighbour tetrahedral site	Nearest neighbour octahedral site	2nd Nearest neighbour tetrahedral site
X_1	200 , $\bar{2}00$	120 , $1\bar{2}0$	$1\bar{1}2$, $11\bar{2}$
		$\bar{1}02$ & $\bar{1}0\bar{2}$	$\bar{1}\bar{2}1$ & $\bar{1}2\bar{1}$
X_2	Neighbours obtained from 'X_1' by inversion		
X_3	Neighbours obtained from 'X_1' by reflection either in the 'XY' or 'XZ' planes.		
X_4	Neighbours obtained from 'X_3' by inversion.		
Y_i, Z_i $i=1, 4$	Neighbours obtained from 'X_i' by cyclic permutation.		

direction), if the ion B occupies an X site. Hence for N_x replacements in the X sites, N_y replacements in the Y sites and N_z replacements in the Z sites the overall increase in energy is given by

$$\varepsilon = C_1 (N_x \alpha_1^2 + N_y \alpha_2^2 + N_z \alpha_3^2) \qquad (A1)$$

resulting in a noncubic anisotropy if the N's are different.

However, the experimentally determined directions of the Eigenaxes of magnetic anisotropy (easy directions) do not coincide with the crystal axis as determined by equation (A1). It was also shown that the results obtained by taking into consideration the n.n.o. sites (Table A1) gives an energy expression isomorphic with equation (A1). Finally by also considering n.n.n.t sites agreement with experiment in the sense of eigenaxes of anisotropy were obtained for films grown along both <110> and <112> directions (Callen, 1971a).

In the above model one crucial assumption was made. The ionic distribution on the various sites was assumed to be determined by the angle between the growth face normal and the pair bond direction (θ). This was quantified by taking scalar products of the growth facet normal [(110), say] with the various neighbour's direction vectors shown in Table A1 (Callen, 1971b). For the X_1 sites mentioned above, this woud give 2 & -2 (n.n.t. sites); 3, -1, -1 & -1 (n.n.o. sites) and 0, 2, -3 & 1 (n.n.n.t. sites) respectively. For the X_3 sites identical products and for

the X_2 sites negatives of the above values are obtained. This was interpreted as $N_{X_1} = N_{X_3}$ and $N_{X_1} \neq N_{X_3}$. Proceeding in this manner, and keeping in mind that $\sum_i N_i = N$, relationships between the distributions in all the other sites were determined (Callen, 1971b).

An alternate model called the pair preference model (Rosencwaig & Tabor, 1971), introduces this angle (θ) as one of the determining parameters in the magnetic contribution of each of the pair bond (i.e. the possible occupancy of a particular site) only. However, both models have been shown (Gyorgy, Rosencwaig, Blount, Tabor & Lines, 1971) to be identical and hence this will not be elaborated upon.

The above models were derived for two rare earth ions on dodecahedral sites; but growth induced anisotropies have been observed in garnets like $Eu_3Fe_{5-x}Ga_xO_{12}$ prepared to preclude the mechanism based on two rare earth ions (Akselrad & Callen, 1971). In this case, an alternate site preference model, with preferential occupation of the tetrahedral sites and identical in procedure to the one described earlier has been proposed.

In the case of $Lu_xY_{3-x}Fe_5O_{12}$ the concentration dependence of the anisotropy constants was also found to obey a site preference model. However, it was found that the uniaxial anisotropy constant K_u is proportional to M_a^3 where M_a is the reduced magnetization in the octahedral site, thereby suggesting an octahedral site preference model (Gyorgy, Sturge & van Uitert, 1974).

Large uniaxial anisotropies have also been observed in the case of YIG (Stacy & Tolksdorf, 1972). Since there are no rare earth substitutions on any of the crystallographic sites the origin of this anisotropy is unclear. One suggested mechanism is the ordering of the oxygen vacancies during the growth process (Stacy & Rooyans, 1971). An oxygen vacancy will produce a large uniaxial crystal field at a neighbouring Fe^{3+} ion. Unfortunately this theory is incompatible with the diffusion of oxygen in garnets at the growth temperatures (Gyorgy, Stacy, van Uitert, Heilner & Grodkiewicz, 1973).

From the above it is obvious that the origins of the growth induced uniaxial anisotropy in garnets is not well understood. However, the anisotropy constant K_u was found to be reduced by an order of magnitude on annealing (Hegedorn, Tabor & van Uitert, 1973). The reduction and ultimate loss of the the growth induced anisotropy on annealing is indirect support for the site preference model, but precisely which sites are involved is not known (Nielsen, 1979).

REFERENCES

B. K. Agarwal, "X-ray Spectroscopy", Springer Verlag, Berlin (1979).

A. Akselrad and H. Callen, Appl. Phys. Lett. 19,464 (1971).

B. W. Batterman, Phys. Rev. Lett. 22, 703 (1969)

P. Bennema and E. A. Giess, "Garnet Structure Drawings", IBM Research Report (1981).

H. A. Bethe, Ann. Phys. Lpz. 87, 55 (1928)

S. L. Blank, J. W. Nielsen and W. A. Biolsi, J. Electrochem. Soc. 123, 845 (1976).

M. Born and K. Huang, "The dynamic theory of crystal lattices", Appendix 4, Clarendon Press, Oxford (1954).

G. Borrman, Phys. Z. 42, 157 (1941)

A. J. Bourdillon, P. G. Self and W. M. Stobbs, Phil. Mag. A44, 1335 (1981).

H. Callen, Appl. Phys. Lett. 18, 311 (1971a).

H. Callen, Mat. Res. Bull. 7, 931 (1971b).

R. Castaing, Ph.D. Thesis, U. Paris, ONERA Publ. #55 (1951).

D. Cherns, A. Howie and M. H. Jacobs, Z. Naturfor. 28A, 565 (1973).

S. Chikazumi, "Physics of Magnetism", Wiley, N.Y. (1964).

C. Collieux, Ann. Rev. of Elec. and Light Optics, In press (1983).

J. M. Cowley, Acta Cryst. 17, 33 (1964).

J. M. Cowley, "Diffraction Physics", North Holland, Amsterdam (1975).

A. J. Craven, J. M. Gibson, A. Howie and D. R. Spalding, Phil. Mag. A38, 519 (1978).

J. Deportes, D. Givard, R. Lemaire, H. Nagai and Y. T. Yang, J. Less-Common Metals, 41,273 (1976).

P. A. Doyle and P. S. Turner, Acta Cryst. A24, 390 (1968).

P. Duncumb, Phil. Mag. 7, 2101 (1962).

H. Duval, P. Duval and L. Henry, J. de Physique 35, L169 (1974).

H. Duval and L. Henry, C. R. Acad. Sci. Paris, 278B, 331 (1974).

A. H. Eschenfelder, "Magnetic Bubble Technology", Springer Verlag, Berlin (1980).

F. Fujimoto, J. Phys. Soc. Jap. 14, 1558 (1959).

S. Geller, Acta Cryst. 10, 243 (1957).

S. Geller,in "Physics of Magnetic Garnets", Int. School of Phys. << Enrico Fermi >>, A. Paoletti, Editor (1978).

S. Geller and M. A. Gilleo, Acta Cryst. 10, 239 (1957).

J. Gjonnes and R. Hoier, Acta Cryst. A27, 166 (1971).

P. C. M. Gubbens, A. M. van der Kraan and H. J. Buschow, Sol. St. Comm. 19, 355(1976).

E. M. Gyorgy, A. Rosencwaig, E. I. Blount, W. J. Tabor and M. E. Lines, Appl. Phys. Lett. 18, 479 (1971).

E. M. Gyorgy, M. D. Sturge, L. G. van Uitert, E. J. Heilner and W. H. Grodkiewicz, J. Appl. Phys. 44, 438 (1973).

E. M. Gyorgy, M. D. Sturge and L. G. van Uitert, AIP Conf. Proc. 18, 70 (1974).

C. R. Hall, Proc. Roy. Soc. A295, 140 (1966).

C. R. Hall and P. B. Hirsch, Proc. Roy. Soc. A268 158 (1965).

P. Hansen, in "Physics of Magnetic Garnets", Int. School of Phys. << Enrico Fermi >>, A. Paoletti, Editor (1978).

H. Hashimoto, A. Howie and M. J. Whelan, Phil. Mag. 5, 967 (1960).

H. Hashimoto, A. Howie and M. J. Whelan, Proc. Roy. Soc. A269, 80 (1962).

F. B. Hegedorn, W. J. Tabor and L. G. van Uitert, J. Appl. Phys. 44, 432 (1973).

R. D. Heidenreich, J. Appl. Phys. 33, 2321 (1962).

K. F. J. Heinrich, D. E. Newbury, R. L. Myklebust and C. E. Fiori "Energy Dispersive X-ray Spectrometry", NBS Publication #604, Washington (1981).

P. B. Hirsch, A. Howie and M. J. Whelan, Phil. Mag. 7, 2095 (1962)

P. B. Hirsch, A. Howie, R. B. Nicholson, D. W. Pashley and M. J. Whelan, "Electron Microscopy of Thin Crystals", Butterworth, London (1965).

G. Honjo, J. Phys. Soc. Jap. 8, 776 (1953).

G. Honjo and K. Mihama, J. Phys. Soc. Jap. 9, 184 (1954).

A. Howie and M.J. Whelan, Proc. Roy. Soc. A267, 217 (1961).

A. Howie, Proc. Roy. Soc. A271, 268 (1963).

A. Howie, J. Microscopy 117,1 (1979).

J. J. Hren, J. I. Goldstein and D. C. Joy, "Introduction to Analytical Electron Microscopy", Plenum, N.Y. (1979).

C. J. Humphreys and P. B. Hirsch, Phil. Mag. 18 115 (1968).

C. J. Humphreys and M. J. Whelan, Phil. Mag. 20, 165 (1969).

C. J. Humphreys and R. M. Fisher, Acta Cryst. A27, 42 (1971).

K. Inomata, Jap. J. Appl. Phys. 15, 821 (1976).

K. Inomata, Phys. Rev. B23, 2076 (1981)

Ms. C. K. Johnson, ORTEP, ORNL Report # 3794, Oak Ridge (1965).

R. Jenkins, R. W. Gould and D. Gedcke, "Quantitative X-ray Spectrometry", p161, Marcel Dekker, N.Y. (1981).

G. M. Kalvius and R. S. Tebble, "Experimental Magnetism", Wiley, N.Y. (1979).

S. Kikuchi, Jap. J. Phys. 5, 83 (1928).

C. Kittel, "Introduction to Solid State Physics", Wiley, N.Y.(1982).

J. W. Knowles, Acta Cryst. 9, 61(1956).

K. M. Krishnan, L. Rabenberg, R. K. Mishra and G. Thomas, J. Appl. Phys., To be published, March (1984).

R. Krishnan, in "Physics of Magnetic Garnets", Int. School of Physics << Enrico Fermi >>, A. Paoletti, Editor (1978).

J. S. Lally, C. J. Humphreys, A. J. F. Metherrel and R. M. Fisher, Phil. Mag. 25, 321 (1972).

C. L. Lawson and R. J. Hanson, "Solving Least Squares Problems", Chapters 23 and 25, Prentice Hall, N.J. (1974).

J. W. Mathews, "Epitaxial Growth", Academic Press, N.Y. (1975).

Ms. H. Niehrs, Z. Naturf. 14a, 504 (1959a).

Ms. H. Niehrs, Z. Phys. 156, 446 (1959b).

J. W. Nielsen, Ann. Rev. Mater. Sci. 9,87 (1979).

Y. H. Otsuki, J. Phys. Soc. Jap. 21,2300 (1966).

A. E. Paldino, E. A. Maguire and R. G. Rubin, J. Am. Cer. Soc. 47,280 (1964).

A. Paoletti, "Physics of Magnetic Garnets", Int. School of Physics << Enrico Fermi >> (1978).

R. S. Perkins and P. Fisher, Sol. St. Comm. 20, 1013 (1976).

R. S. Perkins and S. Strässler, Phys. Rev. B15, 477 (1977).

L. Rabenberg, Ph. D. Thesis, University of California, Berkeley (1983).

G. Radi, Z. Phys. 212, 146 (1968).

G. Radi, Acta Cryst. A26, 41 (1969).

P. Rez, Ph.D. Thesis, Oxford (1976).

P. Rez, Phys. Stat. Sol. 55a, K79 (1979).

A. Rosencwaig, W. J. Tabor and R. D. Pierce, Phys. Rev. Lett. 26, 779 (1971).

A. Rosencwaig and W. J. Tabor, J. Appl. Phys., 42, 1643 (1971).

M. V. Satyanarayana, H. Fujii and W. E. Wallace, J. Appl. Phys. 53, 2374 (1982).

J. Smit and H. P. J. Wijn, "Ferrites", p349, Wiley, N. Y. (1959).

J. C. H. Spence, J. Tafto, O. L. Krivanek and M. M. Disko, Inst. Phys. Conf. Series, 61, 253 (1982).

J. C. H. Spence and J. Tafto, J. Microscopy, 130, 147 (1983).

W. T. Stacy and C. J. M. Rooyans, Sol. Stat. Comm. 9, 2005 (1971).

W. T. Stacy and W. Tolksdorf, AIP Conf. Proc. 5, 185 (1972).

K. J. Standley, "Oxide Magnetic Materials", Clarendon Press, Oxford (1972).

L. Sturkey, Proc. Phys. Soc. 80, 321 (1962).

L. Suchow and M. Kakta, J. Sol. St. Chem. 5, 329 (1972).

J. Tafto, J. Appl. Cryst. 15, 378 (1979).

J. Tafto, J. Appl. Cryst. 18, 452 (1982).

J. Tafto and O. L. Krivanek, EMSA Proceedings (1981).

J. Tafto and O. L. Krivanek, Nucl. Inst. Meth. 194, 153 (1982a).

J. Tafto and O. L. Krivanek, Phys. Rev. Lett. 48, 560 (1982b).

J. Tafto and G. Lempfuhl, Ultramicroscopy. 7, 287 (1982).

J. Tafto and Z. Lilienthal, Acta Cryst. 15, 260 (1982).

J. Tafto and J. C. H. Spence, Ultramicroscopy 9, 243 (1982a).

J. Tafto and J. C. H. Spence, Science 218, 49 (1982b).

J.Tafto, J. C. H. Spence and P. Fejes, J. Appl. Phys. 54, 5014 (1983).

S. Takagi, J. Phys. Soc. Jap. 13, 278 (1958a).

S. Takagi, J. Phys. Soc. Jap. 13, 287 (1958b).

G. Thomas and M. J. Goringe, "Transmission Electron Microscopy of Materials", Wiley, N.Y. (1979).

H. von Heimendall, W. L. Bell and G. Thomas, J. Appl. Phys. 35, 361 (1964).

M. von Laue, Acta Cryst. 2, 106 (1949).

W. E. Wallace, H. Fujii, M. V. Satyanarayana and S. Hirosawa, Proc. VI Inter. Workshop on RE-Cobalt Perm. Mag. and Thin Films, J. Fidler, ed., p57 (1982).

M. J. Whelan, J. Appl. Phys. 36, 2099 (1965a).

M. J. Whelan, J. Appl. Phys. 36, 2103 (1965b).

D. Wittry, Ultramicroscopy, 1, 302 (1976).

R. W. G. Wykoff, "Crystal Structures", Vol. 3, Ch. XII, p 3-5, Interscience, N.Y. (1960).

H. Yoshioka, J. Phys. Soc. Jap. 12(6), 618 (1957).

J. M. Ziman, "Principles of the Theory of Solids", Cambridge (1972).

ACKNOWLEDGEMENTS

To:

Professor Gareth Thomas for his support, encouragement and supervision of this work;

Dr. Peter Rez for many useful discussions, comments on this manuscript, fiery pontifications on the state of academia, important guidance in the early stages of this work and continued friendship (not necessarily in that order);

Professors Didier de Fontaine, Hans-Rudolf Wenk and Ronald Gronsky for their critical review of this manuscript;

Professor David Cockayne for helpful suggestions and comments on portions of this dissertation;

Professor Robert Sinclair and Dr. Alan Pelton for permission and assistance in the usage of the TEM facilities at Stanford;

Dr. Vincent J. Fratello of Bell Labs for providing the garnet samples used in the experiments;

Dr. Raja K. Mishra and Professor Llewellyn Rabenberg for many interesting though not necessarily technical discussions;

Mr. Don J. Jurica who insists that operating an electron microscope and getting a Ph. D. are mutually exclusive entities, but nevertheless tries his best to preserve the instruments in the best working conditions;

Maresi, Vish, Jim, Aniruddha, Vittal, Shankar, John, Rahim, Gustavo, Ayse, Chris, Eduardo and "maybe" Jurek whose enduring company, indulgence, friendship (inspite of this thesis) and commitment to see things in a broader perspective has been a constant source of inspiration;

The perpetrators of the poverty of "alien" graduate students who have helped me develop word-processing skills in the course of typing this manuscript;

The cafes of Berkeley: Mediterraneum, Sufficient Grounds, The Old Mole and The Espresso (affectionately known to those who frequent it as the Depresso) for providing the "conducive" atmosphere in which many of the ideas expressed in this thesis were developed;

I would like to express my sincere acknowledgements.

This work was supported by the Director, Office of Energy Research, Office of Basic Energy Sciences, Division of the U. S. Department of Energy under contract number DE-AC03-76SF00098.

THE PLAY IS OVER

The play is over. The performance committed. Slowly
The theatre, a sagging intestine, empties. In the dressing
rooms
The nimble salesman of hotchpotch mimicry, of rancid
rhetoric
Wash of make-up and sweat. At last
The lights go down which showed up the miserable
Botched job; twilight falls on the
Lovely nothingness of the misused stage. In the empty
Still mildly smelly auditorium sits the honest
Playwright, unappeased, and does his best
To remember.

Poem by Bertolt Brecht

This report was done with support from the Department of Energy. Any conclusions or opinions expressed in this report represent solely those of the author(s) and not necessarily those of The Regents of the University of California, the Lawrence Berkeley Laboratory or the Department of Energy.

Reference to a company or product name does not imply approval or recommendation of the product by the University of California or the U.S. Department of Energy to the exclusion of others that may be suitable.

TECHNICAL INFORMATION DEPARTMENT
LAWRENCE BERKELEY LABORATORY
UNIVERSITY OF CALIFORNIA
BERKELEY, CALIFORNIA 94720